MAGNETIC FIELD AND PRESSURE EFFECTS IN A SATURATED GAS LASER AMPLIFIER

Thesis by

Robert T. Menzies

In Partial Fulfillment of the Requirements

For the Degree of

Doctor of Philosophy

California Institute of Technology

Pasadena, California

1970

(Submitted March 23, 1970)

ACKNOWLEDGEMENTS

I wish to thank Dr. Nicholas George for his advice and personal encouragement during the course of this research.

I also wish to express my appreciation to Dr. Andrew Dienes for helpful suggestions and stimulating conversations.

I would like to thank Carol M. Teeter for her skill and felicity in the typing of the manuscript.

Finally, thanks go to my wife, Donna, for her steadfast love and support.

The financial assistance of the California Insitute of Technology, the National Science Foundation, and the Electronics Division of the Air Force Office of Scientific Research is gratefully acknowledged.

ABSTRACT

MAGNETIC FIELD AND PRESSURE EFFECTS IN A SATURATED GAS LASER AMPLIFIER

Theoretical and experimental studies of a gas laser amplifier are presented, assuming the amplifier is operating with a saturating optical frequency signal. The analysis is primarily concerned with the effects of the gas pressure and the presence of an axial magnetic field on the characteristics of the amplifying medium. Semiclassical radiation theory is used, along with a density matrix description of the atomic medium which relates the motion of single atoms to the macroscopic observables. A two-level description of the atom, using phenomenological source rates and decay rates, forms the basis of our analysis of the gas laser medium. Pressure effects are taken into account to a large extent through suitable choices of decay rate parameters.

Two methods for calculating the induced polarization of the atomic medium are used. The first method utilizes a perturbation expansion which is valid for signal intensities which barely reach saturation strength, and it is quite general in applicability. The second method is valid for arbitrarily strong signals, but it yields tractable solutions only for zero magnetic field or for axial magnetic fields large enough such that the Zeeman splitting is much larger than the power broadened homogeneous linewidth of the laser transition. The effects of pressure broadening of the homogeneous spectral linewidth are included in both the weak-signal and strong-signal theories;

however the effects of Zeeman sublevel-mixing collisions are taken into account only in the weak-signal theory.

The behavior of a He-Ne gas laser amplifier in the presence of an axial magnetic field has been studied experimentally by measuring gain and Faraday rotation of linearly polarized resonant laser signals for various values of input signal intensity, and by measuring nonlinearity - induced anisotropy for elliptically polarized resonant laser signals of various input intensities. Two high-gain transitions in the 3.39-μ region were used for study: a $J = 1$ to $J = 2$ ($3s_2 \rightarrow 3p_4$) transition and a $J = 1$ to $J = 1$ ($3s_2 \rightarrow 3p_2$) transition. The input signals were tuned to the centers of their respective resonant gain lines.

The experimental results agree quite well with corresponding theoretical expressions which have been developed to include the nonlinear effects of saturation strength signals. The experimental results clearly show saturation of Faraday rotation, and for the $J = 1$ to $J = 1$ transition a Faraday rotation reversal and a traveling wave gain dip are seen for small values of axial magnetic field. The nonlinearity induced anisotropy shows a marked dependence on the gas pressure in the amplifier tube for the $J = 1$ to $J = 2$ transition; this dependence agrees with the predictions of the general perturbational or weak signal theory when allowances are made for the effects of Zeeman sublevel-mixing collisions. The results provide a method for measuring the upper (neon $3s_2$) level quadrupole moment decay rate, the dipole moment decay rates for the $3s_2 \rightarrow 3p_4$ and $3s_2 \rightarrow 3p_2$ transitions, and the effects of various types of collision processes on these decay rates.

TABLE OF CONTENTS

CHAPTER ONE

1.1 Introduction

In a medium which has an inverted population with respect to two of its optically connected atomic or molecular energy levels, an electromagnetic field which has a frequency resonant with the transition frequency between these two levels will induce a larger number of stimulated emission processes than absorption processes: hence the electromagnetic signal gains in strength. A resonant traveling electromagnetic wave passing through a medium such as this will increase in intensity exponentially with distance until the rate of stimulated emissions becomes large enough to influence the populations of the energy levels. This saturation of the medium by the electromagnetic signal affects the signal in turn, so that nonlinear processes come into existence.

We are interested in gaseous media, where the atoms have a distribution of velocities; hence there is a distribution of resonance frequencies. We shall study the effects of an amplifying gaseous medium on a monochromatic resonant signal which is traveling through the medium, assuming the signal strength is large enough to saturate the medium. Nonlinear effects such as harmonic generation, competition between two frequencies in the input signal, and combination tone generation will not be discussed. Attention will be given to gain and Faraday rotation of a linearly polarized input signal which is tuned to the center of the Doppler broadened resonance of the medium, varying the applied axial magnetic field from zero to a value which is small enough so that we

are always in the weak-field Zeeman effect regime (F is assumed to be a good quantum number). We will also study the effects of a saturated medium on an elliptically polarized signal tuned to the center of resonance. As such a signal passes through the amplifying medium, its ellipticity can change as it saturates the medium, due to nonlinear effects. This effect is called "nonlinearity induced anisotropy" (1). These phenomena depend to varying degrees on the gas pressure used for the amplifying medium and on the values of the total angular momenta of the energy levels involved; a discussion of these effects will be presented as we compare results of experiments on two high gain 3.39-μ transitions in a He-Ne system with the appropriate theory.

The basis of our calculations is semiclassical radiation theory, as formulated by Kramers (2), along with a density matrix description of an ensemble of atoms, which was developed by Lamb (3) and is used to calculate the induced macroscopic polarization of the medium. The polarization is then used in Maxwell's equations to determine the behavior of the electromagnetic fields.

Armstrong, Bloembergen, Ducuing, and Pershan (4) treated the nonlinear interaction of traveling waves in dielectric media using a similar formulation and the method of selecting particular Fourier components of the response. Damping terms were not included in their analysis, and Doppler effects were not considered. Bloembergen and Shen (5) added damping terms to this formalism. The polarization character of the waves was not treated in either of these papers.

Bennett (6) evoked the concept of "hole burning" in his description of the saturation process in Doppler broadened gas lasers.

Since a laser oscillator cavity acts as an extremely narrow-band filter, only those atoms whose velocities cause their resonant frequencies to be within a natural linewidth of the cavity resonance frequency will interact with the electromagnetic signal which exists in the cavity; hence only these atoms are saturated by the signal, and a hole is burned in the Doppler gain curve at this cavity resonance. (When certain allowances are made for effects of gas pressure on the decay rates, the term "homogeneous linewidth" is used instead of natural linewidth.) The concept of hole burning will be useful for a physical understanding of several results in this work.

Gordon, White, and Rigden (7) discussed gain saturation of the 3.39-μ laser transition in a He-Ne amplifier. Their analysis was based on rate equations for the two energy levels which participate in the laser process. The electromagnetic signal was assumed to be a scalar monochromatic traveling wave.

Lamb (3) treated nonlinear effects in laser oscillators in detail, including Doppler effects in his density matrix description of the atomic medium. Most of his results were good for the case of strong Doppler broadening only; i.e., the natural linewidth was assumed to be very much smaller than the Doppler width. The induced polarization of the medium was calculated in the form of a truncated perturbation series, valid for the mildly saturating signals that exist in a laser which is oscillating near threshold. The electromagnetic signals were treated as scalar waves; no polarization effects were treated. The effects of lower level excitation by spontaneous emission from the upper level were treated only in a rate equation approximation in which

the atomic motion was ignored. Pressure effects were not considered. A number of interesting results were obtained which included mode pulling, mode competition, combination tone generation, and frequency locking phenomena.

Close (8,9) used a similar approach for an arbitrary number of monochromatic traveling waves passing through a laser amplifier. He studied effects of intermediate Doppler broadening and integrated the equations of motion for the macroscopic density matrix to study special solutions which were valid for arbitrarily strong signals. The generation of combination tones was examined in detail. An attempt was made to treat polarization effects by using vector fields and a method of averaging over possible atomic dipole orientations.

In order to properly account for the effects of polarized signals, it is necessary to consider the degeneracy of the levels. The above references did not treat level degeneracy effects on the polarization properties of the electromagnetic waves. In atoms which have no nuclear spin, such as Ne^{20}, the levels should be described in terms of their values of J, the total electronic angular momentum. For atoms which have nuclear spin, the total angular momentum F is pertinent. Since the level degeneracy is removed by the application of a magnetic field, it is natural to discuss magnetic fields when considering arbitrarily polarized signals.

A great deal of attention has been given to this field of study in the past few years. Culshaw and Kannelaud (10,11) made a detailed experimental study of the output of a He-Ne laser operating at 1.153-μ (J = 1 to J = 2 transition) in the presence of an axial

magnetic field and analyzed their results by applying Hanle effect theory to the laser. Their theoretical analysis did not suitably describe many of their observations, however.

To study the nonlinear properties of Zeeman laser oscillators, the theory developed by Lamb was extended to include vector electromagnetic signals interacting with atomic levels which are total angular momentum eigenstates. Fork and Sargent (12) considered competition and beat frequencies between two opposite circularly polarized standing waves operating at a single cavity resonance, assuming a $J = 1$ to $J = 0$ transition in an applied axial magnetic field. Culshaw and Kannelaud (13) considered beat frequency effects and the behavior of the output polarization for a $J = 1/2$ to $J = 1/2$ transition model in an axial magnetic field, including effects of cavity anisotropy. They compared results of this theory with more experimental observations on a single mode planar type He-Ne laser oscillating at 1.153-μ in an axial magnetic field (14). Later they extended their results to cover the $J = 1$ to $J = 0$ transition in both axial and transverse magnetic fields (15).

Heer and Graft (16) considered an arbitrary J_a to J_b transition, arbitrary direction of the magnetic field, and both standing and traveling waves. Although the fundamental approach was very general, actual results were obtained only for the case of a single wave of arbitrary polarization for special cases. For the case $J_a = J_b$ or $F_a = F_b$, when the signal was at line center and the magnetic field was zero or very weak, their results indicated stable solutions only for circularly polarized components. Recently attempts were made by Heer

and co-workers to apply this theory to an explanation of polarization and signal strengths of cosmic OH radiation (17-19). However, their results are rigorous only for weakly saturating signal strengths.

D'yakonov (20) analyzed the polarization and beat frequency behavior of the output of a laser in a weak axial magnetic field when a linear absorption anisotropy exists in the laser cavity. D'yakonov and Perel'(21,22) developed a general theory of a single-mode gas laser in a magnetic field based on Lamb's theory (3), expressing the density matrix of the atomic levels in terms of multipole moments of the levels and including effects of a nonzero branching ratio for spontaneous emission from the upper laser level to the lower laser level. Output power and polarization properties were discussed for special cases.

The case of a single mode laser operating on a transition between levels of arbitrary J values was also studied by de Lang and Bouwhuis (23), and by Polder and van Haeringen (24), who showed that the polarization of the output in zero magnetic field depends on ΔJ for the transition. Further experiments (24) verified these results. Doyle and White (25) also analyzed the polarization and beat frequency properties of the output of a laser oscillating on a general J_a to J_b transition in zero magnetic field. Their discussion included two-mode operation, and combination tone generation was briefly considered.

Recently Sargent, Lamb, and Fork (26) presented a comprehensive theory of a "Zeeman laser oscillator" based on the general theory of Lamb (3), valid for weakly saturating signals, including the effects of level degeneracy and a magnetic field in an arbitrary direction. Results for an arbitrary amount of Doppler broadening were obtained. Except for

references 8,9 and 25, the theoretical calculations previously had been done assuming "strong Doppler broadening", as was the case in (3). This analysis also handles multimode operation in the laser oscillator for a general F_a to F_b transition, and it includes linear phase and absorption anisotropies due to the laser cavity.

During the same period of time Dienes (27) analyzed the behavior of a saturated gas laser amplifier in the presence of an axial magnetic field. His analysis was valid for a general J_a to J_b transition and an arbitrary amount of Doppler broadening, and he treated the case of two arbitrarily polarized signals passing through the laser medium. The special case of a $J = 1$ to $J = 0$ transition was treated in detail, both for weakly saturating signals and for arbitrarily strong signals. More recently Dienes has produced results applicable to a general J_a and J_b transition for both weakly saturating signals (28) and for strong signals (29). The strong signal results yield tractable solutions only for the zero magnetic field case or for the case when the Zeeman sublevel splitting is large compared with the power broadened homogeneous linewidth of the transition. Measurements of gain saturation and nonlinearity induced anisotropy for a He-Ne 3.39-μ ($J = 1$ to $J = 2$) amplifier operating in zero magnetic field are in good agreement with the strong-signal theory (1).

Extensive experimental work done by Tomlinson and Fork (30) and by Settles and Heer (31) on gas laser oscillators has been compared with theoretical predictions based on the theory of Sargent, Lamb, and Fork (26) with generally good agreement.

Two major sources of difficulty in comparing experimental

results on laser oscillators with theories are gas pressure effects and cavity anisotropy effects. Anisotropy effects are most plausibly due to the mirrors of the laser oscillator, and detailed comments concerning anisotropy effects have been made by van Haeringen (32,33), Tomlinson and Fork (30,34), and Greenstein (35), in addition to authors previously mentioned. Theories allowing for absorption and phase anisotropies account for many of the puzzling experimental observations on the output of a gas laser oscillator. However, the complicating effects of mirror anisotropies make quantitative comparisons of theory with experiment difficult in some cases. The use of laser amplifiers operating with signals which were derived from laser oscillators, and whose input intensities, polarizations, and frequencies can be determined and controlled, can offer advantages of greater simplicity in comparing experimental results with theoretical predictions.

Pressure effects are evident in most experimental attempts to verify the existing theoretical predictions. Fork and Pollack (36) observed collision effects in a study of mode competition in a He-Ne laser oscillating on the 6328-Å transition. Studies made on the "Lamb Dip" (37) in the power output of a single-mode He-Ne laser have yielded information about pressure effects (38).

Detailed theories involving the effects of collisions on the spectral characteristics of gas laser oscillators have been published by Rautian (39,40) and by Gyorffy, Borenstein and Lamb (41). These theories do not involve the effects of magnetic fields being applied to the laser oscillator. By comparing these theories with experimental studies of the Lamb dip in the He-Ne laser, Gyorffy et.al. (41) have

obtained information about the effects of various types of collisions on the atoms which participate in the laser process.

In most cases attempts to include pressure effects in comparisons with Lamb's theory involve the following basic assumptions: (a) the phenomenological decay rates assumed for the two laser levels are composed of spontaneous decay rates plus pressure-dependent decay rates due to effects of "hard" collisions terminating the atomic interaction with the electromagnetic signal; (b) the decay rate of the dipole moment of the atom is influenced not only by these "hard" collisions, but also by "soft" collisions which perturb the energy levels slightly, resulting in a broadening of the atomic resonance and a shift in the transition frequency; (c) since at least one of the laser levels has a multiplet structure (which can be split with the application of a magnetic field), there exist collisions which mix the sublevel populations, and these lead to anisotropic relaxation of the multipole moments of the two atomic levels of interest. There is also some evidence of asymmetry in the atomic response curve due to certain pressure effects (36,38,40, 41), but these effects seem to be quite small in the case of the He-Ne laser.

Tomlinson and Fork (30) noted departures from theoretical predictions when they observed circular component coupling in single axial mode He-Ne lasers operating at 1.52-μ ($J = 1$ to $J = 0$) and at 6328-Å ($J = 1$ to $J = 2$). They later used assumption (c) above and accounted for these discrepancies by using the theory of D'yakonov and Perel' (21) for laser oscillators and postulating different decay rates for the various multipole moments of the atomic energy levels (42).

Recently Wang and Tomlinson (43,44) calculated expressions for the cross sections for collision-induced relaxation of the multipole moments of an excited atom in a state of arbitrary angular momentum J. Experiments were then performed on a He-Ne laser oscillating at 1.52-μ (J = 1 to J = 0) in order to obtain numerical values for certain collision cross sections. Decomps and Dumont (45) have also obtained values for multipole moment decay rates for certain excited levels of neon by using a laser excited Hanle effect experiment.

A recent paper by Berman and Lamb (46) discusses in detail the effects of resonant and non-resonant collisions on spectral line shapes, including the multiplet structure of the pertinent energy levels. The dipole-dipole interaction potential is used, and various decay rate parameters are computed numerically. The theory is applied to Hanle effect experiments; however no explicit applications to laser phenomena are presented. This paper is quite comprehensive and contains numerous references to previous works in the pressure broadening field.

In the work that follows we will derive expressions applicable to a laser amplifier in an axial magnetic field operating with a single monochromatic input signal of arbitrary polarization. Our theory will be based mainly on the work of Dienes (27-29) and Wang and Tomlinson (44). Dienes has obtained general expressions valid for the gas laser amplifier but has not included pressure effects or a complete account of spontaneous emission. Wang and Tomlinson have developed a theory applicable to weakly saturating signals in a laser oscillator, including pressure effects on the various decay rate parameters. We will derive a theory for a laser amplifier, applicable to weakly saturating

signals, and including pressure effects in a manner similar to that of Wang and Tomlinson. A strong signal theory will also be utilized which will be the same as Dienes' theory (29). The results will be valid for an arbitrary amount of Doppler broadening.

Our theoretical expressions will be used for comparison with experimental results obtained by using a He-Ne laser amplifier and input signals of two types: a 3.3913-μ signal operating on the neon $3s_2 \rightarrow 3p_4$ (J = 1 to J = 2) transition, and a 3.3903-μ signal operating on the neon $3s_2 \rightarrow 3p_2$ (J = 1 to J = 1) transition. These are the most favorable transitions to use for a laser amplifier study because both signals have high gains and easily reach saturation strength. A J = 1 to J = 0 transition would be the least complicated and most interesting case to study for certain nonlinear effects; however, there exist no readily available transitions of this type which have a high enough gain to be useful for study using an amplifier. An amplifier tube of several meters length would be needed for a study of the neon $2s_2 \rightarrow 2p_1$ (J = 1 to J = 0) transition at 1.52-μ, for example. On the other hand, since the two 3.39-μ signals reach saturation strength so easily and normally operate under strongly saturated conditions in a laser oscillator, a comparison of experiment with the perturbational or weak-signal theory of the Zeeman laser oscillator would be difficult for these two cases. In addition, the "strong Doppler broadening" approximation cannot be made when discussing the 3.39-μ transitions. The exact treatment of Doppler broadening used by Dienes (27-29) for laser amplifiers is appropriate here.

Since the experiments relating the gain and Faraday rotation

of a linearly polarized input signal to theoretical predictions were done predominantly with an amplifier tube at a total gas pressure of 1.1 Torr and agreed quite well with the theories which did not include modifications accounting for Zeeman sublevel-mixing collisions, the general theory developed in Chapter 3 will not be used for quantitative comparison with these experimental results. It will become clear that these phenomena do not depend on gas pressure in an obvious manner after the theoretical predictions are discussed.

However, the nonlinearity induced anisotropy for an elliptically polarized input signal passing through the amplifier in zero magnetic field does show a marked dependence on pressure, and only the general theory including Zeeman sublevel-mixing collisions can account for experimental observations. Experiments were performed for several values of gas pressure in order to clearly observe this effect.

CHAPTER TWO

THE INTERACTION OF THE FIELDS WITH THE ATOMIC SYSTEM IN THE PRESENCE OF AN AXIAL MAGNETIC FIELD

2.1 Introduction

This chapter introduces the framework for treating the interaction of a monochromatic optical frequency electromagnetic wave, or signal, with a dilute gaseous medium which is "population inverted" with respect to two energy levels. We assume the electromagnetic signal is nearly resonant with these two levels of the medium. This picture fits an experimental situation where an output signal from a single mode laser oscillator, which has a spectral width much narrower than atomic linewidth parameters, enters an amplifying medium of the same type as the laser oscillator medium. First we discuss the equations of motion for a system consisting of a single atom and an electromagnetic signal. The atomic motion will be described by the Schrödinger wave equation, while the electromagnetic field is treated classically. The atomic model is described in section 2.2, and the equations for the electromagnetic field are covered in section 2.3. The equation of motion for the macroscopic density matrix, describing the atomic medium under the influence of an electromagnetic signal, will be developed in section 2.4. Collision processes which affect the interaction of the atomic system with the electromagnetic signal will be discussed in section 2.5.

2.2 The Atomic Model

We shall explicitly discuss an atomic system because the theory will be applied to the Helium-Neon laser medium in which certain excited levels of the neon atoms become population inverted. However the theory can be applicable to molecular systems also, with suitable changes in the quantum number labeling of the energy levels. We shall also label the energy levels by their total electronic angular momentum numbers J_a and J_b. We could just as well use the quantum numbers F_a and F_b, where F denotes the total angular momentum including nuclear spin; however the Ne^{20} atom used in our He-Ne laser experiments has nuclear spin of zero. In any case the applied D.C. magnetic field will be weak enough such that the degeneracy of the atomic levels is removed according to the well known Zeeman formula:

$$\Delta E = \frac{1}{2} \frac{e\hbar B}{m} g_F M_F \tag{2.1}$$

where M_F is the angular momentum along the direction of the magnetic field.

For our purposes we shall consider only two of the eigenstates of the atom; those which are population inverted and have a transition frequency nearly resonant with the frequency of the electromagnetic field. Let us consider an atom which is excited by some means to the upper excited state $|a\rangle$ at time t_o. Then the wave function describing the perturbed excited atom at later times is a linear combination of the form

$$\psi(\underline{r},t) = a(t,t_o)u_a(\underline{r})e^{-iE_a t/\hbar} + b(t,t_o)u_b(\underline{r})e^{-iE_b t/\hbar}, \quad (2.2)$$

and the wave equations for $a(t,t_o)$ and $b(t,t_o)$ are written

$$i(da/dt) = V_{ab}(t)e^{i\omega t}b(t,t_o) - (i/2)\gamma_a\, a(t,t_o), \quad (2.3a)$$

$$i(db/dt) = V_{ba}(t)e^{-i\omega t}a(t,t_o) - (i/2)\gamma_b\, b(t,t_o), \quad (2.3b)$$

where $\hbar V_{ab}(t)$ is the matrix element for the transition $b \to a$ due to the electric-dipole interaction energy of the atom and the classical electromagnetic signal, and $\omega = \omega_a - \omega_b = 1/\hbar(E_a - E_b)$. The initial conditions are $a(t_o,t_o) = 1$, $b(t_o,t_o) = 0$. The radiative decay rates γ_a and γ_b are phenomenologically introduced here, but their form can be justified by a more rigorous treatment (47). Additions can be made to these decay rates in order to treat certain collision processes which induce transitions to the ground level (48), and this will be done later.

2.3 Equations for the Electromagnetic Field

We shall assume the electromagnetic field to be monochromatic traveling waves propagating in the direction of the D.C. magnetic field, which we shall call the $\underline{z}$ direction. The waves are considered to be transverse and nearly plane, i.e. transverse derivatives in the region of interest are assumed to be negligible. This assumption is reasonably well satisfied by a typical gas laser signal which falls off in intensity

gradually in the transverse direction over a distance of a few millimeters, and which can be made to spread in diameter no more than the diffraction limit would allow.

The electric field of the traveling waves shall be written in terms of the following vector basis:

$$\underline{E}(z,t) = \sum_{m=0,\pm} \hat{e}_m E_m(z,t) \tag{2.4}$$

and $E_m(z,t) = \underline{E}(z,t) \cdot \hat{e}_m$

where $\hat{e}_+ = -(\hat{e}_x + i\hat{e}_y) \cdot \frac{1}{\sqrt{2}}$, $e_- = (\hat{e}_x - i\hat{e}_y) \frac{1}{\sqrt{2}}$, $e_o = \hat{e}_z$.

(The dot product convention for complex vectors is $\underline{a}\cdot\underline{b} = \sum_i a_i^* b_i$, where * signifies the complex conjugate.) This base system is convenient for later calculation of matrix elements for atomic transitions.

For a D.C. magnetic field in the axial direction of the laser amplifier, (i.e. the direction of propagation of the signal) the coordinate system of the atoms (determined by the magnetic field direction) and that of the signal coincide. For other directions of the magnetic field a rotation matrix is necessary to rotate the two coordinate systems. (Reference 26 discusses the rotation in detail.) Assuming an axial magnetic field, we write the electric field for several monochromatic traveling waves:

$$\underline{E}(z,t) = \mathrm{Re} \sum_j \sum_{m=\pm} \hat{e}_m E_{jm}(z,t) e^{i(k_j z - \nu_j t + \phi_{jm}(z,t))} \tag{2.5}$$

The electric field has no z-component, and $E_{jm}(z,t)$ and $\phi_{jm}(z,t)$ are slowly varying functions of position and time. Arbitrary elliptically polarized signals result by choosing the magnitude and initial phase of each circular component appropriately.

The positive (m = +) and negative (m = -) helicity traveling waves carry angular momentum in directions parallel and antiparallel to their direction of propagation, respectively. Consider an interacting atom at a certain point on the z-axis. If we describe the motion of the resonant electron in the atom as a harmonic oscillator which is driven into oscillation by the electric field of the traveling wave, then the positive helicity polarization causes the electron to move in a circular path in the x-y plane which has a counterclockwise sense to the observer looking in the negative z direction. Thus, the atom has been given angular momentum along the z-axis. Similarly a negative helicity polarization would give the atom angular momentum in the opposite direction. (This topic is discussed in Chapter 17 of Reference 49). The positive helicity polarization is called left-circular polarization in optics (50).

The electromagnetic field is governed by Maxwell's equations, which for a nonmagnetic medium can be written (in MKS units):

$$\nabla \times \underline{E} = - \frac{\partial}{\partial t} \underline{B} \tag{2.6a}$$

$$\varepsilon_o c^2 \nabla \times \underline{B} = \frac{\partial}{\partial t} (\varepsilon_o \underline{E} + \underline{P}) + \underline{J} \tag{2.6b}$$

$$\varepsilon_o \nabla \cdot \underline{E} = - \nabla \cdot \underline{P} \tag{2.6c}$$

$$\nabla \cdot \underline{B} = 0 \tag{2.6d}$$

where $\underline{P}$ is the macroscopic polarization of the medium; and $\underline{J} = \sigma \underline{E}$ is the macroscopic current due to free electrons and ions in the laser medium, which usually consists of the positive column of a glow discharge (σ has both real and imaginary parts). This form of Ohm's Law is not valid if a D.C. magnetic field B_o is applied to the medium of strength such that $\omega_g = eB_o/m$ is comparable to the other frequencies involved in the problem. However, we shall show in the next paragraph that the optical frequency is much larger than ω_g.

These equations yield a wave equation for the electric field:

$$\nabla \times \nabla \times \underline{E} + \frac{\sigma}{\varepsilon_o c^2} \frac{\partial}{\partial t} \underline{E} + \frac{1}{c^2} \frac{\partial^2}{\partial t^2} \underline{E} = - \frac{1}{\varepsilon_o c^2} \frac{\partial^2}{\partial t^2} \underline{P} \tag{2.7}$$

Since in our case $\underline{E}(z,t)$ is transverse, we may set

$$\nabla \times \nabla \times \underline{E} = - \nabla^2 \underline{E} \, , \tag{2.8}$$

and equation (2.7) can be written as

$$-\nabla^2 \underline{E} + \frac{\sigma}{\varepsilon_o c^2} \frac{\partial}{\partial t} \underline{E} + \frac{1}{c^2} \frac{\partial^2}{\partial t^2} \underline{E} = - \frac{1}{\varepsilon_o c^2} \frac{\partial^2}{\partial t^2} \underline{P} \tag{2.9}$$

In Lamb's theory (3) the quantity $\underline{\sigma}$ is considered to be an Ohmic conductivity which gives the wave a damping, in order to account for losses at the mirrors of the laser oscillator without having to solve a boundary value problem. Although Lamb did not explicitly discuss losses due to free electrons and ions in the gas laser discharge, he neglected their contribution to $\underline{\sigma}$. Free electrons provide both loss and phase shift to an electromagnetic wave passing through them; due to their much larger masses the positive ions have much less effect on the wave. The free electrons contribute to the index of refraction of the medium through Thomson scattering (50) in the forward direction. If a weak magnetic field is applied in the direction of a linearly polarized traveling wave (axial direction), the free electrons produce a clockwise Faraday rotation. Loss due to large angle Thomson scattering of optical frequency waves is extremely small for normal gas discharges, which are weakly ionized gases (87); however loss due to collisions of electrons with neutral atoms should be considered.

We can ignore the free charge contribution to σ altogether in a gas laser medium such as the He-Ne system because the free charge density is low enough so that the electron and ion plasma frequencies are very small compared with the optical frequency of the wave. Likewise for the low pressures used in the gas lasers the collision frequencies for the electrons and ions are much lower than the optical frequency. For example, in a He-Ne laser with a 10:1 ratio of He to Ne and a total gas pressure of 1.0 Torr, a discharge current of 10 milliamps, and a tube diameter of about 3mm, the electron density is approximately 10^{11} cm^{-3} (51), and the collision frequency (ω_{coll}) for

the electrons is about 10^9 sec^{-1} (52). The electron plasma frequency,

$$\omega_{pe} = \left[\frac{ne^2}{m\varepsilon_o}\right]^{\frac{1}{2}} \tag{2.10}$$

is about 5×10^9 sec^{-1}. If an axial magnetic field of 100 gauss is applied (maximum values used in the experiments described later were about 50 gauss), the gyrofrequency of the electrons is of the order of 10^9 sec^{-1}. This means the contributions to the real and imaginary parts of $\underline{\sigma}$ due to the free electrons are of the order of $(\omega_{coll}\omega_{pe}^2/\omega^2)\varepsilon_o \simeq \frac{1}{2} \times 10^{-15}\omega\varepsilon_o$ and $(\omega_{pe}^2/\omega^2)\varepsilon_o \simeq 10^{-10}\varepsilon_o$ (53) respectively, for a wave of optical frequency. We shall see in the next chapter that even for a very low gain laser transition such as the neon $3s_2 \rightarrow 2p_4$ transition at 6328-Å wavelength, whose linear intensity gain constant is typically .05 m^{-1} ($I = I_o \exp(.05z)$), the contribution of the resonant neon atoms to the gain (or loss) and phase shift of the electromagnetic signal is more than 100 times the contribution from the free electrons. For this reason and for the reason that we do not need an effective conductivity of the medium to take care of mirror losses when discussing traveling waves passing through an amplifier, we will drop the $\underline{\sigma}$ term from equation (2.9).

We also neglect the possibility of plasma striations, or longitudinal electron and ion waves, occuring in the laser medium. Striations can effect the power and spectral character of the output signal of a laser, and their occurrence depends on both laser tube design and the external electrical circuit (54). We assume macroscopic charge neutrality in the laser medium.

The polarization of the medium due to resonant population inverted atoms will have both real and imaginary parts. The imaginary part is responsible for the gain in the medium, and the real part causes a phase shift or index of refraction. Accordingly we assume the following form for the induced polarization $\underline{P}$:

$$\underline{P}(z,t) = \mathrm{Re} \sum_j \sum_{m=\pm} \hat{e}_m (P_{jcm} - iP_{jsm}) e^{i(k_j z - \nu_j t + \phi_{jm})} \tag{2.11}$$

$$= \frac{1}{2} \sum_j \sum_{m=\pm} \left\{ \hat{e}_m (P_{jcm} - iP_{jsm}) e^{i(k_j z - \nu_j t + \phi_{jm})} \right.$$

$$\left. + \hat{e}_m^* (P_{jcm} + iP_{jsm}) e^{-i(k_j z - \nu_j t + \phi_{jm})} \right\}$$

where the summation runs over the same set as for the expression (2.5) for the electric field; and P_{jcm}, P_{jsm}, and ϕ_{jm} are slowly varying functions of z and t.

Since the phase ϕ_{jm} is assumed to be a slowly varying function of space and time, the complete nonlinear phase shift suffered by the j^{th} wave as it travels through the amplifying medium can be accounted for by the $i\phi_{jm}$ term, leaving k_j to be equal to the free space propagation constant ν/c. We can use as an alternative a real index of refraction defined by

$$k(\nu) = n(\nu) \frac{\nu}{c} \tag{2.12}$$

The index of refraction is a convenient concept for a linear medium; however, for a nonlinear medium it is more advantageous to use the accumulated phase ϕ.

The effect of the other, non-resonant transitions in the atomic medium, which we are not considering, is to contribute a very small index of refraction which is constant throughout the small frequency range of interest (about equal to the width of the resonance of the ensemble of atoms). This can be taken into account by adding a small constant term to $n(\nu)$.

If we substitute equations (2.11) and (2.5) into the wave equation (2.9), neglecting transverse derivatives and the terms

$$\frac{\partial^2\phi}{\partial z^2}E\ ,\ \frac{\partial\phi}{\partial z}\frac{\partial E}{\partial z}\ ,\ \frac{\partial^2 E}{\partial z^2}\ ,\ \frac{1}{c^2}\frac{\partial^2\phi}{\partial t^2}E\ ,\ \frac{1}{c^2}\frac{\partial E}{\partial t}\frac{\partial\phi}{\partial t}\ ,\ \frac{1}{c^2}\frac{\partial^2 E}{\partial t^2}\ ,$$

(the subscripts + and - have been dropped for simplicity) due to our assumptions of slow space and time variations for the quantities E and ϕ, we obtain two equations by equating real and imaginary parts:

$$\left[\frac{\partial\phi_{jm}}{\partial z}+\frac{1}{c}\frac{\partial\phi_{jm}}{\partial t}+\frac{\nu_j}{c}(n_{jm}-1)\right]E_{jm}=\frac{\nu_j}{2\varepsilon_o c}P_{jcm} \tag{2.13a}$$

$$\frac{\partial E_{jm}}{\partial z}+\frac{1}{c}\frac{\partial E_{jm}}{\partial t}=\frac{\nu_j}{2\varepsilon_o c}P_{jsm} \tag{2.13b}$$

The replacements $k \to \nu/c$ and $k^2-\nu^2/c^2 \to 2\frac{\nu}{c}(k-\frac{\nu}{c}) = 2\frac{\nu^2}{c^2}(n-1)$ were made in order to establish the form above for equations (2.13). These results are also present in reference (27), and similar equations can be found in reference (3). Lamb (3) calls these equations the "self-consistency" equations because the time-varying induced polarization of the medium sustains an electromagnetic field with the same frequency components, according to (2.13). When one treats terms in the expression for $\underline{P}$ which are nonlinear with respect to the electric field, new fields at combination tone or harmonic frequencies can be obtained. We shall drop the summation over j and treat the case of only one traveling wave passing through the medium in future analysis. We shall not concern ourselves with harmonics either.

2.4 Equation of Motion for the Density Matrix

2.4.1 The Atom-Field Interaction

The interaction between an atom and the electromagnetic field is commonly described in terms of the electromagnetic potentials in the quantum theory of radiation. In semiclassical radiation theory this interaction is best expressed in terms of the electric and magnetic field strengths. It has been shown by Fiutak (55) that for classical fields the nonrelativistic interaction:

$$H' = \frac{e}{2mc}(\underline{p}\cdot\underline{A} + \underline{A}\cdot\underline{p}) + \frac{e^2}{2mc^2}\underline{A}\cdot\underline{A} \qquad (2.14)$$

of a bound electron (spin neglected) with an electromagnetic field can be transformed canonically into an equivalent Hamiltonian which

explicitly exhibits the various multipole moments that are present in the interaction:

$$H'_{\text{equivalent}} = e\underline{r}\cdot\underline{E} - \underline{L}\cdot\underline{B} - \underline{\underline{Q}}:\nabla\underline{E} + \ldots. \tag{2.15}$$

We will use the long wavelength or dipole approximation and keep only the first term on the right-hand side of equation (2.15).

2.4.2 A Model For Stationary Atoms

Returning to the atomic model described by equation (2.3), we express the interaction matrix element $V_{ab}(t)$ more explicitly as

$$\hbar V_{ab}(t) = \langle a \mid e\underline{r}\cdot\underline{E}(t)\mid b\rangle = e\underline{E}(t)\cdot\langle a|\underline{r}|b\rangle \tag{2.16}$$

The space dependence of the electric field does not enter here because of the assumption that the wavelength is much longer than the size of the atom. Proceeding in the manner of Lamb and Sanders (56), we describe the behavior at time t of an ensemble of atoms which were excited independently to state a at rate r_a for all time $t_o < t$, by making use of a density matrix $\sigma^{(a)}$ with elements such as

$$\sigma^{(a)}_{aa}(t) = r_a \int_{-\infty}^{t} |a(t,t_o)|^2 \, dt_o \tag{2.17a}$$

$$\sigma^{(a)}_{ab}(t) = r_a \int_{-\infty}^{t} a(t,t_o)b^*(t,t_o)e^{-i\omega t} dt_o \tag{2.17b}$$

The diagonal element $\sigma_{aa}^{(a)}$ represents the population of state a at time t due to previous excitation of state a at rate r_a, while $\sigma_{bb}^{(a)}$ represents the corresponding population of state b. The time derivative of $\sigma_{aa}^{(a)}(t)$ is

$$(d/dt)\sigma_{aa}^{(a)}(t) = r_a + r_a \int_{-\infty}^{t} (d/dt)\left|a(t,t_o)\right|^2 dt_o \tag{2.18}$$

since $a(t_o,t_o) = 1$. The time derivatives of the other elements of the matrix $\sigma^{(a)}$ do not have the first term of the right-hand side of equation (2.18).

When we consider excitation of the atom to both states a and b, we can construct a total density matrix

$$\sigma = \sigma^{(a)} + \sigma^{(b)} \tag{2.19}$$

Using equations (2.3) we can write the differential equations for the total density matrix σ:

$$(d/dt)\sigma_{aa} = r_a - iV_{ab}\sigma_{ba} + iV_{ba}\sigma_{ab} - \gamma_a\sigma_{aa} \tag{2.20a}$$

$$(d/dt)\sigma_{ba} = i\omega\sigma_{ba} + iV_{ba}(\sigma_{bb}-\sigma_{aa}) - \tfrac{1}{2}(\gamma_a+\gamma_b)\sigma_{ba} \tag{2.20b}$$

$$(d/dt)\sigma_{ab} = -i\omega\sigma_{ab} - iV_{ab}(\sigma_{bb}-\sigma_{aa}) - \tfrac{1}{2}(\gamma_a+\gamma_b)\sigma_{ab} \tag{2.20c}$$

$$(d/dt)\sigma_{bb} = r_b - iV_{ba}\sigma_{ab} + iV_{ab}\sigma_{ba} - \gamma_b\sigma_{bb} \tag{2.20d}$$

These equations can be written in the form:

$$\dot{\sigma} = -i[H,\sigma]_- - \frac{1}{2}[\Gamma,\sigma]_+ + R \tag{2.21}$$

where H is the sum of the unperturbed Hamiltonion describing the atom, and the interaction between the atom and the electromagnetic field; Γ is the diagonal matrix

$$\begin{bmatrix} \gamma_a & 0 \\ 0 & \gamma_b \end{bmatrix}; \tag{2.22}$$

and the $-$ and $+$ subscripts denote commutator and anticommutator respectively. R is the diagonal matrix representing the excitation pumping.

2.4.3 A Model for the Gas Laser Medium, Including Collisions and An Axial Magnetic Field

In a description of a gas laser medium the effects of atomic motion must be taken into account, and collision effects must also be considered. Lamb's theory (3), (26) of the laser includes atomic motion by using a density matrix $\rho(\underline{r},\underline{v},t)$ which describes an ensemble of atoms which arrive at position $\underline{r}$ with velocity $\underline{v}$ at time t regardless of their place $\underline{r}_o$ and time t_o of excitation. It is assumed that the atoms maintain constant velocities when they are in the excited states and interacting with the electromagnetic field.

Experimental observations of the output of He-Ne lasers have

generally supported predictions based on the Lamb theory; however noticeable deviations from theoretical predictions occur due to pressure effects. Studies of pressure effects have often involved the examination of the "Lamb dip" or the power dip in the output of a single-mode laser oscillator when it is tuned through line center. This method allows one to study collision phenomena at low pressures (.5 Torr to 2.5 Torr), even though the Doppler broadening is much larger than the pressure broadening (38). Another method for studying collisions in the gas laser involves the application of an axial magnetic field. Collisions affect the coupling strength between opposite circularly polarized waves, and in certain cases this results in observable changes in the output polarization (42,44).

Realizing that some collisions will change the velocities of certain excited atoms participating in the laser process, we should first consider the constant velocity assumption which was made by Lamb (3,26) in order to greatly simplify the analysis. Interruption theories of pressure broadening, which are applicable in a low pressure gas such as that found in a gas laser, commonly assume that an interaction strong enough to appreciably change the velocity of an atom will also destroy its coherence (57). Using this assumption we shall consider an interacting atom whose velocity has changed due to a collision to have lost its coherence also, meaning that we can assume an equivalent population decay and a simultaneous isotropic pumping of the atom back into one of the "laser" levels for the purposes of our discussions. The atom after a collision of this type has lost memory of the past interaction with the electromagnetic signal, and it will be treated as a

newly excited atom.

In our theoretical formulation the interacting laser atoms will maintain constant velocities throughout the interaction, and pressure dependent additions to the atomic level and electric dipole moment decay rates will be made to account for the effects of velocity-altering collisions. Gyorffy, Borenstein, and Lamb (41) studied this type of collision effect in detail and obtained expressions for the intensity output profile of a gas laser oscillator. The major effect of velocity-altering collisions was found to be a pressure-dependent increase of the atomic "homogeneous" linewidth. This is in agreement with our qualitative arguments above. The constant velocity approximation has been used in the work done in references (42)-(44).

Collisions can produce many effects on the interacting laser atom, depending on the type of perturber and on the dynamics of the interaction. For the present we will account for collisions by making a symbolic addition to the equations of motion for the macroscopic density matrix. More detailed discussions concerning collision effects will be made in section 2.5 and in the following chapter, where a transformation to a different representation will be made in order to account for most of the pressure effects.

Effects due to populating the lower laser state by the spontaneous decay of the upper laser state will be included in the theoretical formulation presented. This means an additional phenomological decay rate parameter γ will be added to the basic model described in 2.4.2. γ will denote the inverse lifetime of the upper state relative to a spontaneous decay to the lower state. Lamb (3) treated

the effects of a non-zero value for γ (or a non-zero "branching ratio") in the rate equation approximation for stationary atoms. The results were a lower value for the linear gain constant and a higher value for the saturation intensity parameter. We shall obtain these results, and in addition we shall be able to see how a non-zero branching ratio affects the sizes of each of the terms of third-order in electric field intensity.

Since the duration of a typical binary collision is short compared with the natural lifetimes of the atomic states, and since the interaction of the atom with the electromagnetic signal is a small perturbation on the normal Hamiltonian of the atom, the collision dynamics can be considered independently of the laser interactions. Thus we write the equation of motion for the macroscopic density matrix describing an ensemble of laser atoms with velocity v along the direction of the electromagnetic signal (call this the z direction), at position z and at time t, in an applied axial magnetic field:

$$\dot{\rho}_{mm'}(z,v,t) = -(\gamma_a+i\Omega_{mm'})\rho_{mm'}(z,v,t) - \frac{i}{\hbar}\sum_{\mu}\Big[V_{m\mu}(z,t)\rho_{\mu m'}(z,v,t) - \rho_{m\mu}(z,v,t)V_{\mu m'}(z,t)\Big] + \lambda_a(z,v,t)\delta_{mm'} + (\dot{\rho}_{mm'}(z,v,t))_{collision} \tag{2.23a}$$

$$\dot{\rho}_{\mu\mu'}(z,v,t) = -(\gamma_b + i\Omega_{\mu\mu'})\rho_{\mu\mu'}(z,v,t) - \frac{i}{\hbar}\sum_m\Big[V_{\mu m}(z,t)\rho_{m\mu'}(z,v,t)$$

$$- \rho_{\mu m}(z,v,t)V_{m\mu'}(z,t)\Big] + \sum_{mm'}\Gamma^{mm'}_{\mu\mu'}\rho_{mm'}(z,v,t)$$

$$+ \lambda_b(z,v,t)\delta_{\mu\mu'} + (\dot{\rho}_{\mu\mu'}(z,v,t))_{collision} \qquad (2.23b)$$

$$\dot{\rho}_{\mu m}(z,v,t) = -(\gamma_{ab} + i\Omega_{\mu m} - i\omega)\rho_{\mu m}(z,v,t) - \frac{i}{\hbar}\Big[\sum_{m_1} V_{\mu m_1}(z,t)\rho_{m_1 m}(z,v,t)$$

$$- \sum_{\mu_1}\rho_{\mu\mu_1}(z,v,t)V_{\mu_1 m}(z,t)\Big] + (\dot{\rho}_{\mu m}(z,v,t))_{collision} \qquad (2.23c)$$

Here $\dot{\rho} = [\partial/\partial t + v(\partial/\partial z)]\rho$; the symbols m,m' denote the Zeeman sublevels of the upper state a, and μ,μ' denote the sublevels of the lower state b.

$V(z,t)$ is the interaction of the optical signal with the atom; γ_a and γ_b are the spontaneous decay rates for the upper and lower levels; $\gamma_{ab} = \frac{1}{2}(\gamma_a + \gamma_b)$ is the natural linewidth of the transition; ω is the transition frequency in the absence of a magnetic field; $\Omega_{mm'} = (m-m')\Omega_a$, $\Omega_{\mu\mu'} = (\mu-\mu')\Omega_b$, $\Omega_{\mu m} = \mu\Omega_b - m\Omega_a$, where Ω_a and Ω_b denote the Zeeman sublevel frequency splittings, $\Omega_\alpha = g_\alpha\mu_B H/\hbar$, where g is the g-factor of the level, μ_B is the Bohr magneton, and H is the applied magnetic field. The term $\Gamma^{mm'}_{\mu\mu'}$ denotes the spontaneous feeding of the lower level through spontaneous decay of the upper level:

$$\Gamma^{mm'}_{\mu\mu'} = \gamma(2j_a+1)(\langle\mu|\underline{p}|m\rangle\langle m'|\underline{p}|\mu'\rangle)/|\langle j_a\|p\|j_b\rangle|^2 \qquad (2.24)$$

where $\underline{p} = e\underline{r}$, and γ is the inverse lifetime of the upper state a relative to a spontaneous transition to the lower state b. The pumping into states a and b is assumed to be isotropic, hence the δ-functions in the equations of motion. The similarity between equations (2.23) and equations (2.20) is evident. Here we have included splittings of level degeneracies by an axial magnetic field, taken into account the velocity of the atoms, and added a term accounting for changes in the density matrix by atomic collisions. Equations (2.23) are in a form similar to the equations of motion found in references (21) and (44).

To connect the macroscopic density matrix with the assumed polarization of the medium in section 2.3, we make use of the fact that

$$\underline{P}(z,t) = \int \text{Trace}\,[\rho(z,v,t)\underline{p}]d^3v$$

$$= \int d^3v \sum_{m,\mu}\left(\rho_{\mu m}(z,v,t)\underline{p}_{m\mu} + \rho_{m\mu}(z,v,t)\underline{p}_{\mu m}\right) \qquad (2.25)$$

We assume in using equations (2.23) that the atomic medium is homogeneous and the amplitude and time dependence of the electromagnetic signal (apart from its explicit sinusoidal space and time variation) are constant over the regions of space and time covered by an interacting atom before it decays. This means the pumping rates and the quantities E_+, E_-, in equation (2.5) vary "slowly" with z and

t. Since the typical atomic decay time is about 10^{-7} sec., and the typical distance traveled by an atom before it decays is roughly (10^{-7} sec.)$\cdot v_{thermal} \simeq 10^{-4}$ meter, we can test the validity of our assumptions in particular cases. For a small-signal or linear gain of 80 db/meter, which is exceptionally large for a gas laser, the increase in signal intensity in a distance of 10^{-4} meter is about .1%, which can be neglected.

A more detailed discussion of the derivation of equations (2.23) from the isolated atom model of section 2.2 can be found in reference (27). Pressure effects and pumping of the lower laser level through spontaneous emission of the upper laser level are not included however.

2.5 Collision Processes

The effects of the other gas atoms and of the electrons and ions on an excited atom interacting with the electromagnetic field are numerous and difficult to treat in a theoretical analysis. Although Rautian has discussed effects of electron collisions (39, 40), experimentally the effects caused by collisions of excited neon atoms with electrons in a He-Ne laser have not been observed (58). Presumably this is due to the fact that typical electron densities in a He-Ne laser ($10^{11}cm^{-3}$) are much smaller than the atomic densities ($10^{16}cm^{-3}$). In a He-Ne laser the most probable collisions are with ground state neon and helium atoms. The gas pressures are small enough so that binary collision processes can be considered exclusively, i.e. the cross sections are much smaller than the square of the mean distance between atoms.

In collisions with ground state atoms an excited neon atom can suffer a phase shift, a change in velocity, or an inelastic process such as decay or magnetic (Zeeman sublevel) reorientation. A particular elastic collision can slightly shift the atomic energy levels, resulting in a phase shift

$$\phi = \frac{(\Delta E_a - \Delta E_b) t_c}{\hbar} \tag{2.26}$$

where t_c is the duration of the collision. This adds to the homogeneous linewidth or the electric dipole moment decay rate, γ_{ab}. A collision can also change the atomic velocity. Gyorffy et.al. (41) performed a complicated analysis of pressure effects on the intensity profile of a gas laser output by studying effects of velocity changes combined with phase shifts in elastic collisions, and by adding pressure-dependent parameters to account for inelastic processes. Level degeneracy and magnetic field effects were not treated. The results were compared with some experimental observations, revealing the fact that one can account for most pressure effects by assuming decay rates of the form:

$$\gamma_a = (\gamma_a)_{\text{spontaneous}} + g_a P, \tag{2.27a}$$

$$\gamma_b = (\gamma_b)_{\text{spontaneous}} + g_b P, \tag{2.27b}$$

an atomic "homogeneous" linewidth of the form:

$$\gamma_{ab} = \frac{1}{2}\left[(\gamma_a)_{spont.} + (\gamma_b)_{spont.}\right] + g_{ab}P \ ; \qquad (2.27c)$$

and a resonant frequency shift:

$$\Delta = kP \ ; \qquad (2.27d)$$

where P is the gas pressure and $g_{ab} > (g_a + g_b)/2$. Detailed expressions for the elastic collision contributions to these pressure dependent terms are given in the paper.

A theory which includes magnetic field effects must discuss level degeneracies more explicitly. Several simplifying assumptions can be made if the homogeneous linewidth is very small compared with the Doppler linewidth. Since the electromagnetic signal is monochromatic, only those atoms with velocities along the axial direction such that their resonant frequencies are within a homogeneous linewidth of the signal frequency will interact with the signal. Let us consider a neon atom in an excited state which has a total angular momentum $J > 0$, and suppose it is interacting with the electromagnetic signal. The interaction results in a coherence between the two resonant states of opposite parity (inter-coherence), which gives the atom an oscillating electric dipole moment, and a coherence between the Zeeman sublevels of each state (intracoherence) due to nonlinear atom-field interactions. A particular collision or atomic interaction process can destroy or partially destroy the intercoherence and/or the intracoherence of the atom. We shall discuss these effects for various types of collisions in which the excited neon atom takes part, pointing out the simplifi-

cations that are possible when only a small portion of the Doppler distributed atoms are capable of interacting with the signal.

Interactions of an excited neon atom with ground state neon atoms can account for several distinct processes: a mixing of the excited state sublevels, which can partially destroy the intracoherence; a spontaneous decay to the ground state with the re-absorption of the emitted photon by a resonant neon atom in the ground state (radiation trapping effect); and a direct excitation transfer. (Resonant interactions are discussed by Byron and Foley (59), and by Happer and Saloman (60)). The intercoherence of the original excited atom cannot be transferred by way of radiation trapping or excitation transfer, so that if an atom undergoes either of these processes, it has been effectively removed from the laser interaction. The intracoherence can be transferred (44) since the sublevels are of the same parity. This means that in addition to the isotropic pumping of the neon atoms to the excited states of interest, there is an effective coherent or anisotropic pumping contribution from these processes when saturating electromagnetic signals are present. However since the atom to which the excitation is transferred very probably has a different axial velocity component, the atom will not be resonant with the signal if the natural linewidth is much smaller than the Doppler linewidth, and we can account for these types of collision processes by simply changing the population decay rates.

Interactions of the excited neon atom with ground state helium atoms can also mix the sublevels. Less frequently, if the excited neon atom is in the $3s_2$ or $2s_2$ state, a collision can occur which

results in the neon being in the ground state and the helium atom being in one of the two metastable states, 2^1S or 2^3S respectively (61). This clearly adds to the decay rate of the population of these particular neon excited states.

Wang, Tomlinson, and George (44) used the approximation that the homogeneous linewidth for the neon $2s_2 \rightarrow 2p_1$ ($J = 1$ to $J = 0$) laser transition (15-100 MHz) is much less than the Doppler width (460 MHz) to assume that sublevel mixing collisions and all excitation transfer collisions affect the system in two different ways, the latter essentially removing the atom from the interaction process. Using this reasoning they performed experiments on this transition and obtained separate relaxation rates due to sublevel mixing collisions and excitation transfer collisions.

Unfortunately, for the 3.39-μ transitions in the He-Ne laser system, which we have studied experimentally, the ratio of the homogeneous to Doppler linewidths ranges from .2 to .5, depending on the gas pressure. So the simplifying assumptions mentioned are only rough approximations for these cases. We will not attempt to measure cross sections for specific types of collisions.

CHAPTER THREE

SOLUTIONS OF THE ATOMIC EQUATIONS OF MOTION FOR WEAK SIGNALS

3.1 Introduction

In this chapter we obtain formal solutions of the atomic equations of motion when the electromagnetic signal is of such intensity as to be weakly saturating. This restriction on signal strength is necessary because the polarization of the medium is expressed in the form of a truncated perturbation series. If we consider an atom which is excited to one of the laser levels and make use of the common pictorial view of the integral form of a time-dependent perturbation problem, we can say that the atom has a certain probability for interacting momentarily with the field (or "scattering"), undergoing a change of state, a given number of times before it decays. The usual perturbation theory calculations assume the probability for a certain number of scatters decreases rapidly as the number of scatters increases; thus only the first term (Born approximation-single scatter) or the first two terms are kept for purposes of calculation. We keep the first

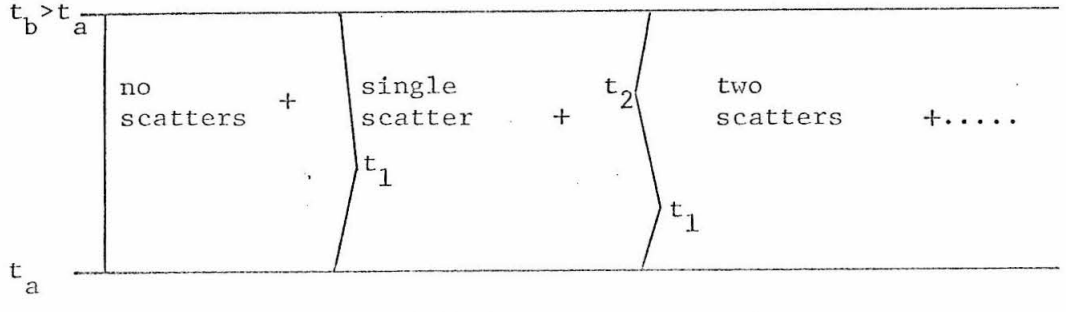

Figure 1. Pictorial View of Perturbation Series

two non-vanishing terms in our calculation of the atomic polarization; in order for the results to be accurate, the strength of the perturbation (the signal strength) must remain within certain limits.

We split the electromagnetic signal into circularly polarized components and obtain gain and phase shift equations for each component. Three cases will be discussed in detail: the $J = 1$ to $J = 0$ transition, the $J = 1$ to $J = 1$ transition, and the $J = 1$ to $J = 2$ transition. Results will be compared with previous results obtained in a different manner by Dienes (27,28), who used a theoretical technique which is more limited in its ability to account for pressure effects.

3.2 A Glossary of Pertinent Terms

3.2.1 Orientation and Alignment

A variety of distributions of atoms among the magnetic sublevels of a particular state can be obtained by subjecting a gas or vapor to a constant magnetic field and a beam of light of certain polarization (62). The two main categories are orientation and alignment. Orientation describes the situation in which the atoms are pumped in one direction only with regard to the sign of m_F, the angular momentum in the magnetic field direction. The result is a net component of angular momentum of the sample in the direction of the magnetic field. Alignment describes the case in which the atoms are pumped into the highest and lowest m_F levels simultaneously, giving an unequal population distribution but no net angular momentum component.

3.2.2 Hanle Effect

Many phenomena which depend on the observation of scattered resonance radiation from a dilute gas make possible the determination of natural linewidths of levels. A particular Hanle effect experiment is described as follows: atoms of a gas in a D.C. magnetic field are excited to an upper level by light which is traveling at right angles to the field and is polarized at right angles to the field, and the scattered radiation is observed in the direction of the field. As the magnetic field increases from zero, the degree of polarization P of the scattered radiation decreases according to the law (63):

$$P = P_o \gamma^2/(\gamma^2 + 4\Omega^2) \qquad (3.1)$$

where P_o is the degree of polarization when there is no magnetic field, and Ω is the splitting of the Zeeman sublevels. At very low gas pressures γ is the spontaneous decay rate of the upper level.

Other phenomena, such as double resonance and level crossing, give similar resonances. One property common to each of these resonances is that increasing gas pressure first causes the resonance width to narrow, due to capture of the resonance radiation by other atoms in the groundstate (radiation trapping). A further increase in the gas pressure causes the resonance width to broaden, due to binary collisions of the excited atom with other atoms (64,65,66). The collisions become important when the average interparticle separation decreases to the point where it is comparable to the radiation wavelength (66).

The Hanle resonance width at pressures such that radiation

trapping and collisions are not negligible can depend on the polarization of the exciting light beam. We know that radiation trapping and collisions should tend to equalize the sublevel populations and partially destroy any coherence that exists among the sublevels, and this is verified both by theory and experiment. It can be shown by diagonalizing the relaxation terms in the equation of motion for the density matrix that there are two characteristic upper level decay times which determine the resonance width: the decay time of the plane polarization, or the alignment decay time, and the decay time of the circular polarization, or the orientation decay time (64, 66). Each of these decay times is shorter than the decay time of the population of the level at the corresponding pressure.

3.3 The Density Matrix in an Irreducible Tensor Operator Representation

D'yakonov and Perel' (64, 66, 21), Omont (67), and Wang and Tomlinson (43), have shown that in a representation in terms of irreducible tensor operators the radiation trapping (in the case of complete capture), binary collision, and spontaneous emission feeding terms in the density matrix equation of motion are all diagonal and depend only on the tensor order. That is, they are of the form:

$$\dot{\rho}^K_q = - \gamma^K \rho^K_q \tag{3.2}$$

when we express the density operator $\rho(z,v,t)$ as

$$\rho(z,v,t) = \sum_{K,q} \rho^K_q (z,v,t)\, T^K_{-q} \quad , \tag{3.3}$$

where the quantity T^K_{-q} is an irreducible tensor operator (see references 68 and 69 for a discussion of tensor operators) whose matrix element between the states $|jm\rangle$ and $|j'm'\rangle$ is given by

$$\langle jm|\ T^K_{\pm q}|j'm'\rangle = (-1)^{j-m\mp q}\sqrt{2K+1}\begin{pmatrix} j & K & j' \\ -m & \pm q & m' \end{pmatrix}, \tag{3.4}$$

where the quantity in the spherical bracket is a Wigner 3-j symbol (68). Thus we have the transformation:

$$\langle jm|\rho(z,v,t)|j'm'\rangle = \sum_{K,q} \rho^K_q(\alpha,\beta|z,v,t)\ (-1)^{j-m+q}\sqrt{2K+1}\begin{pmatrix} j & K & j' \\ -m & -q & m' \end{pmatrix}, \tag{3.5}$$

where α,β denote the levels whose total angular momenta are j,j'. By making use of relation (C.15a) of reference 68:

$$\sum_{m_1=-j_1}^{j_1}\sum_{m_2=-j_2}^{j_2}\begin{pmatrix} j_1 & j_2 & j_3 \\ m_1 & m_2 & m_3 \end{pmatrix}\begin{pmatrix} j_1 & j_2 & j_3' \\ m_1 & m_2 & m_3' \end{pmatrix} = \frac{1}{2j_3+1}\ \delta_{j_3 j_3'}\ \delta_{m_3 m_3'} \tag{3.6}$$

we obtain the inverse transformation:

$$\rho^K_q(\alpha,\beta|z,v,t) = \sum_{m,-m'}(-1)^{-q+m-j}\sqrt{2K+1}\begin{pmatrix} j & j' & K \\ m & -m' & q \end{pmatrix}\langle jm|\rho(z,v,t)|j'm'\rangle \tag{3.7}$$

As an example, some of the transformation relations for a level with $j = 1$ are:

$$
\begin{aligned}
\rho_0^0 &= \frac{1}{\sqrt{3}} \left(\rho_{11} + \rho_{00} + \rho_{-1-1}\right) \\
\rho_0^1 &= \frac{1}{\sqrt{2}} \left(\rho_{11} - \rho_{-1-1}\right) \\
\rho_{-1}^1 &= \frac{1}{\sqrt{2}} \left(\rho_{0-1} + \rho_{10}\right) \\
\rho_0^2 &= \frac{1}{\sqrt{6}} \left(\rho_{11} - 2\rho_{00} + \rho_{-1-1}\right) \\
\rho_2^2 &= \rho_{1-1}
\end{aligned}
\tag{3.8}
$$

where ρ_q^K stands for $\rho_q^K(1,1|z,v,t)$ and $\rho_{mm'}$ stands for $\langle 1m|\rho(z,v,t)|1\ m'\rangle$. We can see from this example that the "orientation" and "alignment" of an atomic level are embodied in the quantities ρ_0^1 and ρ_0^2 respectively, whereas the off-diagonal or "coherence" terms show up in the quantities ρ_q^K, where $q \neq 0$. ρ_0^0 denotes the total population of the level.

3.4 Assumptions Used in Application to Laser Amplifiers

The derivations by D'yakonov and Perel' (64-66) and Omont (67) of equation (3.2) as a description of the effects of radiative trapping and resonant collisions were based on a model in which all atoms could participate in the resonance fluorescence process regardless of their velocities. This model is directly applicable to Hanle effect experiments. In this case, if the gas consists of atoms of only one kind, neither radiation trapping nor resonant excitation transfer collisions contribute to decay of the population (the quantity ρ_0^0) because of the inherent conservation of excited atoms in these processes. (The "new" excited atom very probably has a velocity different from that of

the "old" excited atom, however.) There is a contribution to the decay of higher order multipole moments of the excited atom due to sublevel-mixing resonant collisions in which no excitation transfer occurs, and due to sublevel mixing and incomplete transfer of intracoherence when the excitation is passed to another atom through radiation trapping or excitation transfer.

"Nonresonant" dipole-dipole collisions, as treated by Wang and Tomlinson (43, 44), mix the sublevels of an excited atom but do not lead to population decay. These collisions do not appreciably alter the velocity of the excited atom. Their effects can be put in the form of equation (3.2) also.

Collisions which alter the velocity significantly, or collisions in which the repulsive hard-core interaction becomes important (at very close encounters), can be treated as "hard" collisions in which there is no correlation between the state of the atom before and after the impact. Thus the decay due to these impacts is assumed to be isotropic (i.e. the quantities γ^K in (3.2) are equal).

In a He-Ne laser medium excited neon atoms can undergo sublevel mixing collisions and excitation transfer collisions with ground state helium atoms, and they may interact with ground state neon atoms via radiation trapping, "resonant" and "non-resonant" sublevel mixing collisions, and "resonant" excitation transfer collisions. (References 43 and 46 discuss the "resonant" and "non-resonant" approximations to dipolar interactions). In addition the excited neon atoms may suffer "hard" collisions of the type discussed in the previous paragraph.

These phenomena may be taken into account through the use of

equation (3.2), except for the radiation trapping and "resonant" excitation transfer collisions. The effects of these two processes on a laser signal differ from their effects on depolarization of resonance radiation in a Hanle effect experiment. Since only those atoms with resonant frequencies within a natural linewidth (or homogeneous linewidth) of the monochromatic signal frequency will interact with the laser signal, both radiation trapping and excitation transfer can effectively remove the excited neon from the interaction.

If the ratio of the homogeneous linewidth to the Doppler linewidth is very small, one can treat these processes as isotropic decay mechanisms; for they act as "hard" collisions in removing the excited, coherently interacting neon atom from the picture. Wang, Tomlinson, and George used this approximation in their study of collision-induced anisotropic relaxation in a He-Ne laser oscillating at the 1.52-μ ($J = 1 \rightarrow J = 0$) transition (44).

If the homogeneous linewidth is appreciable when compared with the Doppler linewidth, there is a non-negligible possibility that the newly excited atom in these two processes can still interact with the electromagnetic signal. Since intracoherence can be transferred in these processes, they produce an effective coherent pumping rate which must be taken into account in equations (2.23). We shall neglect this attribute of radiation trapping and resonant excitation transfer in our formalism, even though the transitions which we study experimentally (the 3.39-μ transitions in the He-Ne system) do have homogeneous linewidths which are appreciable when compared with their Doppler width. The high ratio of helium pressure to neon pressure

commonly used for the laser medium (about 10:1) tends to make resonant excitation transfer an interaction of minor significance when compared with other pressure dependent processes (44). Radiation trapping occurs to a large extent, however (45); a more complete theory should include the possibility of coherent pumping due to this process.

3.5 The Equations of Motion

Using the transformation relations (3.5) and (3.7), we can obtain from equations (2.23) an equation of motion for the quantity $\rho_q^K(\alpha,\beta|z,v,t)$, where α or β index either the upper level a or the lower level b. This requires the use of some relations involving the Wigner 3-j and 6-j symbols, which can be found in Appendix C of reference 68. The analysis is greatly simplified if we assume the g-factors of the two laser levels are equal. This approximation is good for most He-Ne laser transitions if we keep the magnetic field strength within certain limits. This will be discussed in more detail later.

We shall now outline the procedure. Applying (3.7) to equation (2.23b) and using some of the symmetries and selection rules of the 3-j symbols, we obtain the equation:

$$\dot{\rho}_q^K(b,b) + (\gamma_b - iq\Omega)\rho_q^K(b,b) = \text{Field-Medium Interaction Term}$$

$$+ \text{Spontaneous Emission Feeding Term} + \lambda_b\sqrt{2j_b+1}\;\delta_{K0}\delta_{q0} + \left[\dot{\rho}_q^K(b,b)\right]_{\text{coll.}}, \tag{3.9}$$

where

$$\text{Field-Medium Interaction Term} = \frac{-i}{\hbar}\sum_m \sum_{\mu,-\mu'}(-1)^{q+\mu-j_b}\sqrt{2K+1}$$

$$\cdot\begin{pmatrix} j_b & j_b & K \\ \mu & -\mu' & q \end{pmatrix}\left[(\underline{E}\cdot\underline{p})_{\mu m}\rho_{m\mu'} - \rho_{\mu m}(\underline{E}\cdot\underline{p})_{m\mu'}\right] \tag{3.10}$$

with $\underline{p} = e\underline{r}$, and

$$\text{Spontaneous Emission Feeding Term} = \sum_{m,m'} \sum_{\mu,-\mu'} (-1)^{-q+\mu-j_b}$$

$$\cdot \sqrt{2K+1} \begin{pmatrix} j_b & j_b & K \\ \mu & -\mu' & q \end{pmatrix} \gamma \left(2j_a + 1\right) p_o^2 \left(\underline{p}_{\mu m} \underline{p}_{\mu' m'}\right) \rho_{mm'} \,, \qquad (3.11)$$

with $\quad p_o^2 = | \langle j_a \| \underline{p} \| j_b \rangle |^2 \,.$

We have assumed an implicit dependence on z,v,t in order to shorten the notation.

Applying the Wigner-Eckart Theorem (68) to the matrix elements $\underline{p}_{\mu m}$, $\underline{p}_{\mu' m'}$, and using relation (C.32) of reference 68, we can write the spontaneous emission feeding term as

$$\text{S.E.F.T.} = \gamma(2j_a + 1)(-1)^{j_a + j_b + K + 1} \begin{Bmatrix} j_a & j_a & K \\ j_b & j_b & 1 \end{Bmatrix} \rho_q^K(a,a) \qquad (3.12)$$

where the quantity in curvy brackets is a Wigner 6-j symbol (68).

Now consider the Field-Medium Interaction, first transforming the matrix elements of $\underline{E} \cdot \underline{p}$ by making use of the vector base system of (2.4):

$$(\underline{E} \cdot \underline{p})_{\mu m} = \sum_M E_M \langle \mu \mid p_M \mid m \rangle = \sum_M (-1)^{1-j_a-\mu} \begin{pmatrix} j_a & 1 & j_b \\ m & M & -\mu \end{pmatrix} E_M \, p(b,a) \qquad (3.13a)$$

$$(\underline{E}\cdot\underline{p})_{m\mu'} = \sum_M E_M \langle m \mid p_M \mid \mu' \rangle = \sum_M (-1)^{1-j_b-m} \begin{pmatrix} j_b & 1 & j_a \\ \mu' & M & -m \end{pmatrix} E_M\, p(a,b). \tag{3.13b}$$

If we use (3.5) to transform $\rho_{mm'}$ into ρ_q^K and apply relation (C.33) of reference 68, we obtain:

$$\text{Field-Medium Interaction} = \frac{i}{h} \sum_{K'q'} \sum_M (-1)^{q'} E_M \sqrt{(2K+1)(2K'+1)} \begin{pmatrix} 1 & K' & K \\ -M & q' & -q \end{pmatrix}$$

$$\cdot \left[p(b,a)\rho_{q'}^{K'}(a,b) \begin{Bmatrix} 1 & K' & K \\ j_b & j_b & j_a \end{Bmatrix} + (-1)^{K-K'} p(a,b)\rho_{q'}^{K'}(b,a) \begin{Bmatrix} 1 & K' & K \\ j_b & j_b & j_a \end{Bmatrix} \right], \tag{3.14}$$

where $p(b,a) = \langle j_b \| \underline{p} \| j_a \rangle$, $p(a,b) = \langle j_a \| \underline{p} \| j_b \rangle$, and $\underline{p} = e\underline{r}$. (The conjugation relation is $[p(b,a)]^* = (-1)^{j_a - j_b} p(a,b)$; this may be deduced from (C.85) of reference 68.)

Applying the same procedure to equations (2.23a), (2.23c), and a corresponding equation of motion for $\rho_{m\mu}(z,v,t)$, we obtain the equations of motion for $\rho_q^K(a,a|z,v,t)$, $\rho_q^K(b,a|z,v,t)$, and $\rho_q^K(a,b|z,v,t)$ respectively. The form of these equations can be written in the compact notation:

$$\dot{\rho}_q^K(\alpha,\beta|z,v,t) = \lambda_\alpha(z,v,t)\sqrt{2j_\alpha+1}\;\delta_{K0}\delta_{q0}\delta_{\alpha\beta} + \Gamma^K\rho_q^K(\mu,\nu|z,v,t)\delta_{\mu a}\delta_{\nu a}$$

$$- \gamma_{\alpha\beta}^K\rho_q^K(\alpha,\beta|z,v,t) - i\left[\omega_{\alpha\beta} - q\Omega\right]\rho_q^K(\alpha,\beta|z,v,t)$$

$$+ \frac{i}{\hbar}(-1)^{j_\alpha+j_\beta}\sum_{K'q'}\sum_{M}(-1)^{q'}E_M(z,t)\sqrt{(2K+1)(2K'+1)}\begin{pmatrix}1 & K' & K\\ -M & q' & -q\end{pmatrix} \tag{3.15}$$

$$\cdot\left[p(\alpha,\mu)\rho_{q'}^{K'}(\mu,\beta|z,v,t)\begin{Bmatrix}1 & K' & K\\ j_\beta & j_\alpha & j_\mu\end{Bmatrix} + (-1)^{K+K'}\rho_{q'}^{K'}(\alpha,\nu|z,v,t)p(\nu,\beta)\begin{Bmatrix}1 & K' & K\\ j_\alpha & j_\beta & j_\nu\end{Bmatrix}\right],$$

where $$\Gamma^K = \gamma(2j_a+1)(-1)^{j_a+j_b+K+1}\begin{Bmatrix}j_a & j_a & K\\ j_b & j_b & 1\end{Bmatrix}. \tag{3.16}$$

In the notation for ρ, α and β index either the upper or lower level, and μ and ν index the levels with parity opposite to that of α and β respectively. Thus if $\alpha = a$ and $\beta = b$, then $\mu = b$ and $\nu = a$. The quantity $\omega_{\alpha\beta}$ is equal to $(E_\alpha - E_\beta)/\hbar$, where E_α and E_β are the unperturbed energies of the levels α and β.

The first term on the right-hand side of (3.15) is the assumed isotropic external pumping excitation to the laser levels, where $\lambda_\alpha(z,v,t)$ is the rate of excitation of atoms into state α at time t and position z, with velocity v. The second term denotes the pumping of the lower level by the spontaneous decay of the upper level, where γ, as stated previously, is the inverse lifetime of the upper state for a spontaneous transition to the lower state.

Taking advantage of the discussion of (3.2), we have written the third term such that

$$\gamma^K_{\alpha\alpha} \equiv \gamma^K_\alpha + \left(\gamma^K_\alpha\right)_{\text{coll.}} \tag{3.17}$$

$$\gamma^K_{ab} = \gamma^K_{ba} \equiv \frac{1}{2}\left(\gamma_a + \gamma_b\right) + \left(\gamma^K_{ab}\right)_{\text{coll.}} \tag{3.18}$$

Here γ_α represents the total spontaneous decay rate for atoms in state α. Collision induced relaxations are represented as shown. The assumptions implied in applying (3.2) to this situation are discussed in Section 3.5. The quantity $(\gamma^K_{ab})_{\text{coll.}}$ represents the collision induced relaxation of the intercoherence, and for electric dipole radiation only the $K = 1$ case is important. We shall write $\gamma^{(1)}_{ab} = \gamma_{ab}$ for simplicity.

The results of this section were also derived by Wang, Tomlinson and George (44) for use in a description of a laser oscillator operating in an axial magnetic field. However our expression for the field-medium interaction differs from theirs in that expression (3.14) contains a $(-1)^{q'}$ factor, whereas equation (9) of reference 44 contains an extra $(-1)^{q+j_\alpha+j_\beta}$ factor but no $(-1)^{q'}$ factor. The expressions in reference 44 result in a macroscopic polarization whose sign is dependent on $j_a - j_b$, which is not correct.

The assumption of equal g-factors for the laser levels is justified if the difference in the Zeeman sublevel splittings (in frequency units) for a certain value of magnetic field is much less than the smallest decay rate involved in the laser transition of inter-

est, since the "level width" is, from the uncertainty principle, $\Delta E_\alpha/\hbar \simeq \gamma_\alpha$. This can be written as

$$(g_a - g_b) << \frac{\gamma_\alpha^K}{\mu_B H/\hbar} ,$$

as was done in reference 44.

3.6 The Macroscopic Polarization

To express the macroscopic polarization in the irreducible tensor representation, we use equations (2.25) and (3.5) to obtain

$$\underline{P}(z,v,t) = \sum_{m,\mu} \sum_{K,q} \left\{ \rho_q^K(b,a|z,v,t)(-1)^{j_b-\mu+q} \sqrt{2K+1} \begin{pmatrix} j_b & j_a & K \\ \mu & -m & q \end{pmatrix} p_{m\mu} + \text{c.c.} \right\}, \tag{3.20}$$

where c.c. denotes the complex conjugate. We shall see later that the first term in the brackets is, in the rotating wave approximation, equivalent to the second term inside the curvy brackets of equation (2.11). Thus we can obtain the quantitites P_{cm} and P_{sm} directly from this term after integrating over the velocity distribution. In the future we shall set the polarization equal to the first term inside the brackets of (3.20), keeping in mind the fact that the physical quantity is obtained by taking the real part of this complex quantity.

Use of the Wigner-Eckart Theorem (68) gives:

$$P_{q_1}(z,v,t) = \sum_{K,q} \sum_{m,\mu} (-1)^{j_a-j_b} \rho_q^K(b,a|z,v,t) \sqrt{2K+1} \begin{pmatrix} j_a & j_a & K \\ \mu & -m & q \end{pmatrix} \begin{pmatrix} j_b & j_a & 1 \\ \mu & -m & q_1 \end{pmatrix} p(a,b) \tag{3.21}$$

We now use equation (3.6) to obtain:

$$P_{q_1}(z,v,t) = \frac{1}{\sqrt{3}} (-1)^{j_a - j_b} \rho^1_{q_1}(b,a|z,v,t)p(a,b), \qquad (3.22)$$

and

$$P_{q_1}(z,t) = \frac{1}{\sqrt{3}} (-1)^{j_a - j_b} p(a,b)\int \rho^1_{q_1}(b,a|z,v,t)d^3v \qquad (3.23)$$

3.7 Solutions for a Laser Amplifier

3.7.1 Derivation of the Macroscopic Polarization

In this section we integrate (3.15) in order to obtain an expression for the macroscopic polarization $\underline{P}(z,t)$ in the form of a truncated perturbation series. We note that (3.15) denotes coupled first-order differential equations for four types of density operator coefficients: $\rho^K_q(a,a|z,v,t)$, $\rho^K_q(b,b|z,v,t)$, $\rho^K_q(b,a|z,v,t)$, and $\rho^K_q(a,b|z,v,t)$. We are interested primarily in obtaining an expression for $\rho^1_q(b,a|z,v,t)$ so that we may use equation (3.22) to compute the components of $\underline{P}(z,v,t)$.

Let us write the differential equation for $\rho^K_q(b,a|z,v,t)$ from (3.15):

$$\dot{\rho}^{K}_{q}(b,a|z,v,t) = -\left[\gamma_{ab}-i(\omega+q\Omega)\right]\rho^{K}_{q}(b,a|z,v,t) + \frac{i}{\hbar}(-1)^{j_a+j_b}\sum_{K'q'}(-1)^{q'}$$

$$\sum_{M=\pm}E_{M}(z,t)\sqrt{(2K+1)(2K'+1)}\begin{pmatrix}1 & K' & K\\ -M & q' & -q\end{pmatrix}\left[p(b,a)\rho^{K'}_{q'}(a,a|z,v,t)\begin{Bmatrix}1 & K' & K\\ j_a & j_b & j_a\end{Bmatrix}\right.$$

$$\left. + (-1)^{K+K'}p(b,a)\rho^{K'}_{q'}(b,b|z,v,t)\begin{Bmatrix}1 & K' & K\\ j_b & j_a & j_b\end{Bmatrix}\right]. \qquad (3.24)$$

The integral of equation (3.24) is

$$\rho^{K}_{q}(b,a|z,v,t)$$

$$= \frac{i}{\hbar}(-1)^{j_a+j_b}\sum_{K'q'}(-1)^{q'}\sum_{M}\int_{-\infty}^{t}dt'\ e^{[\gamma_{ab}-i(\omega+q\Omega)](t'-t)}E_{M}(z-v(t-t'),t')$$

$$\sqrt{3(2K'+1)}\begin{pmatrix}1 & K' & K\\ -M & q' & -q\end{pmatrix}\left[p(b,a)\rho^{K'}_{q'}(a,a|z-v(t-t'),t')\begin{Bmatrix}1 & K' & K\\ j_a & j_b & j_a\end{Bmatrix}\right.$$

$$\left. + (-1)^{K+K'}p(b,a)\rho^{K'}_{q'}(b,b|z-v(t-t'),t')\begin{Bmatrix}1 & K' & K\\ j_b & j_a & j_b\end{Bmatrix}\right]. \qquad (3.25)$$

In a similar manner we obtain

$$\rho_q^K(a,a|z,v,t)$$

$$= \frac{\lambda_a(z,v,t)\sqrt{2j_a+1}}{\gamma_{aa}^K}\delta_{K0}\delta_{q0} + \frac{i}{\hbar}\sum_{K'q'}(-1)^{q'}\sum_M\int_{-\infty}^{t} dt'\, e^{(\gamma_{aa}^K - iq\Omega)(t'-t)}$$

$$E_M(z-v(t-t'),t')\sqrt{(2K+1)(2K'+1)}\begin{pmatrix}1 & K' & K\\ -M & q' & -q\end{pmatrix}\Bigg[p(a,b)\rho_{q'}^{K'}(b,a|z-v(t-t'),t')\begin{Bmatrix}1 & K' & K\\ j_a & j_a & j_b\end{Bmatrix}$$

$$+ (-1)^{K+K'}p(b,a)\rho_{q'}^{K'}(a,b|z-v(t-t'),t')\begin{Bmatrix}1 & K' & K\\ j_a & j_a & j_b\end{Bmatrix}\Bigg] \qquad (3.26)$$

$$\rho_q^K(b,b|z,v,t) = \frac{\lambda_b(z,v,t)\sqrt{2j_b+1}}{\gamma_{bb}^K}\delta_{K0}\delta_{q0} + (-1)^{j_a+j_b+K+1}\gamma(2j_a+1)\begin{Bmatrix}j_a & j_a & K\\ j_b & j_b & 1\end{Bmatrix}$$

$$\cdot\int_{-\infty}^{t} dt'\, e^{(\gamma_{bb}^K - iq\Omega)(t'-t)}\rho_q^K(a,a|z-v(t-t'),t') + \frac{i}{\hbar}\sum_{K'q'}(-1)^{q'}\sum_M\int_{-\infty}^{t} dt'$$

$$e^{(\gamma_{bb}^K - iq\Omega)(t'-t)}E_M(z-v(t-t'),t')\sqrt{(2K+1)(2K'+1)}\begin{pmatrix}1 & K' & K\\ -M & q' & -q\end{pmatrix}\Bigg[p(b,a)$$

$$\cdot\rho_{q'}^{K'}(a,b|z-v(t-t'),t')\begin{Bmatrix}1 & K' & K\\ j_b & j_b & j_a\end{Bmatrix} + (-1)^{K+K'}p(a,b)\rho_{q'}^{K'}(b,a|z-v(t-t'),t')\begin{Bmatrix}1 & K' & K\\ j_b & j_b & j_a\end{Bmatrix}\Bigg]$$

(3.27)

$\rho_q^K(a,b|z,v,t)$ = same as $\rho_q^K(b,a|z,v,t)$, but with b and a interchanged everywhere, and with ω replaced by $-\omega$. (3.28)

The first terms on the right-hand sides of equation (3.26) and (3.27) have already been integrated over t'.

The following prescription will now be used to obtain

expressions for $\rho_q^1(b,a|z,v,t)$ to various orders of the signal amplitude: the zero-order contributions to $\rho_q^K(a,a|z,v,t)$ and $\rho_q^K(b,b|z,v,t)$ will be substituted into equation (3.25) to obtain an expression for $\rho_q^1(b,a|z,v,t)$ which is linearly proportional to the electric field of the signal; then the expressions (3.25) and (3.28) will in turn be substituted into equations (3.26) and (3.27), and the resultant second-order expressions for $\rho_q^K(a,a|z,v,t)$ and $\rho_q^K(b,b|z,v,t)$ will be substituted into equation (3.25) to obtain a third-order expression for $\rho_q^1(b,a|z,v,t)$. The calculations will terminate with the third-order expression, although one can proceed in this manner to obtain higher order terms. In order for this procedure to give valid results, the signal amplitude must remain within certain bounds. We will see later what the intensity restriction is in terms of the atomic parameters.

First let us substitute equations (3.25) and (3.28) into equation (3.26) to obtain the following integral equation:

$$\rho_q^K(a,a|z,v,t) = \frac{\lambda_a(z,v,t)\sqrt{2j_a+1}}{\gamma_{aa}^K}\delta_{K0}\delta_{q0} + \frac{1}{\hbar^2}(-1)^{j_a+j_b}\sum_{K'q'}\sum_{K''q''}(-1)^{q'+q''}$$

$$\sum_{M,M'}\sqrt{(2K+1)(2K''+1)}\,(2K'+1)\begin{pmatrix}1 & K' & K\\ -M & q' & -q\end{pmatrix}\begin{pmatrix}1 & K'' & K'\\ -M' & q'' & -q'\end{pmatrix}\begin{Bmatrix}1 & K' & K\\ j_a & j_a & j_b\end{Bmatrix}\int_0^\infty dt_1\int_0^\infty dt_2$$

$$e^{-(\gamma_{aa}^K - iq\Omega)t_1}\, e^{-(\gamma_{ab}-i(\omega+q'\Omega))t_2}\, E_M(t-t_1,z-vt_1)E_{M'}(t-t_1-t_2,z-v(t_1+t_2))$$

$$\cdot p(a,b)\left[p(b,a)\begin{Bmatrix}1 & K'' & K'\\ j_a & j_b & j_a\end{Bmatrix}\rho_{q''}^{K''}(a,a|t-t_1-t_2,z-v(t_1+t_2)) + (-1)^{K'+K''}p(b,a)\begin{Bmatrix}1 & K'' & K'\\ j_b & j_a & j_b\end{Bmatrix}\right.$$

$$\rho_{q''}^{K''}(b,b|t-t_1-t_2,z-v(t_1+t_2))\Big]+(-1)^{K+K'}\int_o^\infty dt_1\int_o^\infty dt_2\; e^{-(\gamma_{aa}^K-iq\Omega)t_1}$$

$$e^{-(\gamma_{ba}^K+i(\omega-q'\Omega))t_2}\; E_M(t-t_1,z-vt_1)E_{M'}(t-t_1-t_2,z-v(t_1+t_2))p(b,a)$$

$$\Bigg[p(a,b)\begin{Bmatrix}1 & K'' & K'\\ j_b & j_a & j_b\end{Bmatrix}\rho_{q''}^{K''}(b,b|t-t_1-t_2,z-v(t_1+t_2))+(-1)^{K'+K''}p(a,b)\begin{Bmatrix}1 & K'' & K'\\ j_a & j_b & j_a\end{Bmatrix}$$

$$\rho_{q''}^{K'}(a,a|t-t_1-t_2,z-v(t_1+t_2))\Bigg]\Bigg\}, \qquad (3.29)$$

where we have transformed to the new variables $t_1 = t - t'$ and $t_2 = t' - t''$. The corresponding integral equation for $\rho_q^K(b,b|z,v,t)$ can be obtained from (3.29) by interchanging a and b everywhere and by adding the second term on the right-hand side of (3.27).

The zero-order contribution to $\rho_q^K(a,a|z,v,t)$ comes from the source term on the right-hand side of equation (3.26):

$$\left[\rho_q^K(a,a|z,v,t)\right]^{(o)} = \frac{\lambda_a(z,v,t)}{\gamma_{aa}^K}\,\delta_{K0}\delta_{q0}\cdot\sqrt{2j_a+1} \qquad (3.30)$$

(The following simplifications in notation will be used: $\gamma_{\alpha\alpha}^K \to \gamma_\alpha^K$ when $K \neq 0$, and $\gamma_{\alpha\alpha}^o \to \gamma_\alpha$, where $\alpha = a,b$.) Substituting (3.30) into equation (3.27), we obtain the zero-order contribution to $\rho_q^K(b,b|z,v,t)$:

$$\left[\rho_q^K(b,b|z,v,t)\right]^{(o)} = \frac{\lambda_b\sqrt{2j_b+1}}{\gamma_b}\,\delta_{K0}\delta_{q0} + \frac{\gamma(2j_a+1)\lambda_a}{\sqrt{2j_b+1}\;\gamma_b\gamma_a}\,\delta_{K0}\delta_{q0}\,, \qquad (3.31)$$

where we have used the relation (C.37) of reference (68):

$$\begin{Bmatrix} j & j' & 0 \\ J & J' & g \end{Bmatrix} = (-1)^{j+J+g}\,\frac{\delta_{jj'}\,\delta_{JJ'}}{\sqrt{(2j+1)(2J+1)}} \quad \text{for} \quad |j-J| \le g \le J+j \qquad (3.32)$$

in obtaining expression (3.31).

These zero-order solutions describe the situation in which the externally pumped atoms do not interact with the electromagnetic signal and decay spontaneously. This would correspond to the "no scatter" pictorial representation of section 3.1. These quantities are now substituted into (3.25) to obtain the polarization.

In the following calculations we shall evaluate several 3-j and 6-j symbols. Reference (70) contains an extensive tabulation of these quantities. Equation (3.32) and other special cases treated in reference (68) are also useful.

We now assume that the electric field of the signal is due to a single monochromatic traveling wave, so that we may use equation (2.4) and (2.5) to express the quantities E_M in terms of the polarization components of the traveling wave:

$$E_-(z,v,t) = \tfrac{1}{2}E_{1-}\,e^{i(kz-\nu t+\phi_-)} - \tfrac{1}{2}E_{1+}\,e^{-i(kz-\nu t+\phi_+)} \qquad (3.33a)$$

$$E_+(z,v,t) = \frac{1}{2} E_{1+} e^{i(kz-\nu t+\phi_+)} - \frac{1}{2} E_{1-} e^{-i(kz-\nu t+\phi_-)} \qquad (3.33b)$$

where E_{1+}, E_{1-}, ϕ_+, and ϕ_- are slowly varying functions of z and t. From equations (3.13a) and (3.13b) we know that the quantities E_- (E_+) are proportional to the matrix elements for transitions in which the final state has one less (more) unit of angular momentum along the axial direction than the initial state. According to time-dependent perturbation theory (with the use of the rotating-wave approximation) the $e^{-i\nu t}$ component of the perturbation induces upward transitions, or absorptions, and the $e^{+i\nu t}$ component induces downward transitions, or emissions. Thus from (3.33b) we see that the positive helicity component of the traveling wave induces absorptions in which the atom gains a unit of angular momentum along the axial direction. This is in accord with the physical argument given in Section 2.3.

Using equation (3.25) for $K = 1$, equations (3.22) and (3.33), and neglecting the antiresonant term (rotating wave approximation), we obtain the first-order (linear) polarization due to the atoms with velocity v:

$$\left[P_q(v)\right]^{(1)}_{q=\pm} = \frac{i}{6\hbar} N_o \frac{W(v)}{\gamma_{ab} - i(\omega+q\Omega-\nu+kv)} \left| < b \| p \| a > \right|^2 E_{1q}, \qquad (3.34)$$

where we have set

$$\lambda_\alpha(z,v,t) = \gamma_\alpha N^o_\alpha(z,t) W(v), \qquad (3.35)$$

and assume the variation with z and t is slow enough to be considered

negligible. The quantity N_o is the "excitation density",

$$N_o = N_a^o - N_b^o - \frac{\gamma N_a^o}{\gamma_b}\left(\frac{2j_a+1}{2j_b+1}\right). \tag{3.36}$$

The feeding of the lower state through the spontaneous decay of the upper state reduces the zero-order population inversion. If the line strength for the particular laser transition of interest is large, this should be taken into account. Often the decay rates are not known accurately enough for this effect to be seen, however, and thus it is ignored for simplicity.

We now use the zero-order solutions (3.30) and (3.31) in the expression (3.29) for $\rho_q^K(a,a|z,v,t)$ and the corresponding expression for $\rho_q^K(b,b|z,v,t)$ in order to obtain second-order solutions for these quantities. Then, by substituting these solutions into (3.25) and using the following definitions:

$$m = \begin{Bmatrix} 1 & 1 & K' \\ j_a & j_a & j_b \end{Bmatrix}\begin{Bmatrix} 1 & 0 & 1 \\ j_a & j_b & j_a \end{Bmatrix} = (-1)^{j_a+j_b}\frac{1}{\sqrt{3(2j_a+1)}}\begin{Bmatrix} 1 & 1 & K' \\ j_a & j_a & j_b \end{Bmatrix} \tag{3.37a}$$

$$n = \begin{Bmatrix} 1 & 1 & K' \\ j_a & j_a & j_b \end{Bmatrix}\begin{Bmatrix} 1 & 0 & 1 \\ j_b & j_a & j_b \end{Bmatrix} = (-1)^{j_a+j_b}\frac{1}{\sqrt{3(2j_b+1)}}\begin{Bmatrix} 1 & 1 & K' \\ j_a & j_a & j_b \end{Bmatrix} \tag{3.37b}$$

$$p = \begin{Bmatrix} 1 & 1 & K' \\ j_b & j_b & j_a \end{Bmatrix}\begin{Bmatrix} 1 & 0 & 1 \\ j_a & j_b & j_a \end{Bmatrix} = (-1)^{j_a+j_b}\frac{1}{\sqrt{3(2j_a+1)}}\begin{Bmatrix} 1 & 1 & K' \\ j_b & j_b & j_a \end{Bmatrix} \tag{3.37c}$$

$$r = \begin{Bmatrix} 1 & 1 & K' \\ j_b & j_b & j_a \end{Bmatrix} \begin{Bmatrix} 1 & 0 & 1 \\ j_b & j_a & j_b \end{Bmatrix} = (-1)^{j_a+j_b} \frac{1}{\sqrt{3(2j_b+1)}} \begin{Bmatrix} 1 & 1 & K' \\ j_b & j_b & j_a \end{Bmatrix} \tag{3.37d}$$

$$A = \frac{\lambda_a \sqrt{2j_a+1}}{\gamma_a} \tag{3.38a}$$

$$B = \frac{\lambda_b \sqrt{2j_b+1}}{\gamma_b} + \frac{\gamma(2j_a+1)\ \lambda_a}{\sqrt{2j_b+1}\ \gamma_a\gamma_b} \quad , \tag{3.38b}$$

we obtain the cumbersome looking third-order contribution to the macroscopic polarization due to the atoms with velocity v:

$$\left[P_q(z,v,t)\right]^{(3)}_{q=\pm}$$

$$= \frac{-i}{\hbar^3} (-1)^{j_a-j_b} \cdot \frac{|\langle b\|p\|a\rangle|^4}{\sqrt{3}} \sum_{K',q'} (-1)^{q'} \sum_{M,M',M''} \begin{pmatrix} 1 & 1 & K' \\ -M' & -M'' & -q' \end{pmatrix}$$

$$\cdot 3(2K'+1) \begin{pmatrix} 1 & K' & 1 \\ -M & q' & -q \end{pmatrix} \left[\begin{Bmatrix} 1 & K' & 1 \\ j_a & j_b & j_a \end{Bmatrix} \left\{ \int_o^\infty dt_1 \int_o^\infty dt_2 \int_o^\infty dt_3 \; e^{-(\gamma_{ab}-i(\omega+q\Omega))t_1} \right.\right.$$

$$\cdot e^{-(\gamma_a^{K'}-iq'\Omega)t_2} e^{-(\gamma_{ab}-i(\omega-M''\Omega))t_3} E_M(t-t_1,z-vt_1) E_{M'}(t-t_1-t_2,z-v(t_1+t_2))$$

$$\left.\left. \cdot E_{M''}(t-t_1-t_2-t_3,z-v(t_1+t_2+t_3)) \right] mA-nB \right] + (-1)^{K'+1} \int_o^\infty dt_1 \int_o^\infty dt_2 \int_o^\infty dt_3$$

$$\cdot e^{-(\gamma_{ab}-i(\omega+q\Omega))t_1} e^{-(\gamma_a^{K'}-iq'\Omega)t_2} e^{-(\gamma_{ab}+i(\omega+M''\Omega))t_3} E_M(t-t_1,z-vt_1)$$

$$E_{M'}(t-t_1-t_2,z-v(t_1+t_2))\ E_{M''}(t-t_1-t_2-t_3,z-v(t_1+t_2+t_3))\cdot\Big[nB-mA\Big]\Bigg\}$$

$$+\ (-1)^{1+K'}\begin{Bmatrix}1 & K' & 1\\ j_b & j_a & j_b\end{Bmatrix}\Bigg\{\int_o^\infty dt_1\int_o^\infty dt_2\int_o^\infty dt_3\ e^{-(\gamma_{ab}-i(\omega+q\Omega))t_1}\ e^{-(\gamma_b^{K'}-iq'\Omega)t_2}$$

$$e^{-(\gamma_{ab}-i(\omega-M''\Omega))t_3}\ E_M(t-t_1,z-vt_1)\ E_{M'}(t-t_1-t_2,z-v(t_1+t_2))$$

$$E_{M''}(t-t_1-t_2-t_3,z-v(t_1+t_2+t_3))\cdot\Big[rB-pA\Big]+(-1)^{K'+1}\int_o^\infty dt_1\int_o^\infty dt_2\int_o^\infty dt_3$$

$$e^{-(\gamma_{ab}-i(\omega+q\Omega))t_1}\ e^{-(\gamma_b^{K'}-iq'\Omega)t_2}\ e^{-(\gamma_{ab}+i(\omega+M''\Omega))t_3}\ E_M(t-t_1,z-vt_1)$$

$$E_{M'}(t-t_1-t_2,z-v(t_1+t_2))E_{M''}(t-t_1-t_2-t_3,z-v(t_1+t_2+t_3))\ \Big[pA-rB\Big]\Bigg\}$$

$$+\ (-1)^{j_a+j_b}\ \gamma(2j_a+1)\begin{Bmatrix}j_a & j_a & K'\\ j_b & j_b & 1\end{Bmatrix}\begin{Bmatrix}1 & K' & 1\\ j_b & j_a & j_b\end{Bmatrix}\Bigg\{\int_o^\infty dt_1\int_o^\infty dt_2\int_o^\infty dt_3\int_o^\infty dt_4$$

$$\cdot e^{-(\gamma_{ab}-i(\omega+q\Omega))t_1}\ e^{-(\gamma_b^{K'}-iq'\Omega)t_2}\ e^{-(\gamma_a^{K'}-iq'\Omega)t_3}\ e^{-(\gamma_{ab}-i(\omega-M''\Omega))t_4}$$

$$E_M(t-t_1,z-vt_1)E_{M'}(t-t_1-t_2-t_3,z-v(t_1+t_2+t_3))E_{M''}(t-t_1-t_2-t_3-t_4,z-v(t_1+t_2+t_3+t_4))$$

$$\cdot\Big[mA-nB\Big]\ +(-1)^{K'+1}\int_o^\infty dt_1\int_o^\infty dt_2\int_o^\infty dt_3\int_o^\infty dt_4\ e^{-(\gamma_{ab}-i(\omega+q\Omega))t_1}$$

$$e^{-(\gamma_b^{K'}-iq'\Omega)t_2}\ e^{-(\gamma_a^{K'}-iq'\Omega)t_3}\ e^{-(\gamma_{ab}+i(\omega+M''\Omega))t_4}\ E_M(t-t_1,z-vt_1)$$

$$E_{M'}(t-t_1-t_2-t_3, z-v(t_1+t_2+t_3))E_{M''}(t-t_1-t_2-t_3-t_4, z-v(t_1+t_2+t_3+t_4))$$

$$\cdot\left[nB - mA\right]\Bigg\}\Bigg] \qquad (3.39)$$

3.7.2 The General J_a to J_b Transition

We notice that there are six integral terms in expression (3.39), each being third-order in the electric field. For certain values of the summation indices, all six terms will contribute to the third-order polarization; for other values some or all of the terms will be zero, depending on whether or not certain 3-j and 6-j symbols are zero. We can determine which values for the summation indices contribute to the third-order macroscopic polarization by reviewing the selection rules for the 3-j symbols and 6-j symbols (68-70).

(a) Selection rules for 3-j symbol $\begin{pmatrix} j_1 & j_2 & J \\ m_1 & m_2 & -M \end{pmatrix}$:

(i) $m_1 + m_2 = M$

(ii) $|j_1 - j_2| \leq J \leq j_1 + j_2$ ("triangular inequalities")

(b) Selection rules for 6-j symbol $\begin{Bmatrix} j_1 & j_2 & j_3 \\ J_1 & J_2 & J_3 \end{Bmatrix}$:

In order for this symbol to be nonzero, it is necessary that the elements of each of the triads

$(j_1\ j_2\ j_3)$ $(j_1\ J_2\ J_3)$ $(J_1\ j_2\ J_3)$ $(J_1\ J_2\ j_3)$

(i) Satisfy the triangular inequalities;

(ii) have an integral sum.

Using these selection rules we can determine from the two 3-j symbols multiplying the entire square bracketed quantity in (3.39) that for $[P_+(z,v,t)]^{(3)}$ the following values for the summation indices contribute nonzero terms:

(a) $K' = 0, \quad q' = 0, \quad M = -1, \quad M' = 1, \quad M'' = -1$

(b) $K' = 0, \quad q' = 0, \quad M = -1, \quad M' = -1, \quad M'' = 1$

(c) $K' = 1, \quad q' = 0, \quad M = -1, \quad M' = 1, \quad M'' = -1$

(d) $K' = 1, \quad q' = 0, \quad M = -1, \quad M' = -1, \quad M'' = 1$

(e) $K' = 2, \quad q' = 0, \quad M = -1, \quad M' = 1, \quad M'' = -1$

(f) $K' = 2, \quad q' = 0, \quad M = -1, \quad M' = -1, \quad M'' = 1$

(g) $K' = 2, \quad q' = 2, \quad M = 1, \quad M' = -1, \quad M'' = -1$

By substituting into (3.39) the appropriate expressions for the E_M factors for each set of summation indices listed, and by neglecting antiresonant terms (rotating-wave approximation), we obtain, after a re-arrangement, the following integrated expression for the third-order macroscopic polarization due to atoms with velocity v:

$$[P_+(v)]^{(3)} = -i \frac{|\langle b||p||a\rangle|^4}{72\hbar^3} \cdot W(v) N_o \left\{ \frac{3}{2} E_{1+}^3 \left[\left(\frac{2\alpha_o^1}{\gamma_a^o} + \frac{3\alpha_1^1}{\gamma_a^1} + \frac{\alpha_2^1}{\gamma_a^2} \right) + \left(\frac{2\alpha_o^o}{\gamma_b^o} + \frac{3\alpha_1^o}{\gamma_b^1} + \frac{\alpha_2^o}{\gamma_b^2} \right) - \gamma \left(\frac{2\alpha_o^2}{\gamma_a^o \gamma_b^o} + \frac{3\alpha_1^2}{\gamma_a^1 \gamma_b^1} + \frac{\alpha_2^2}{\gamma_a^2 \gamma_b^2} \right) \right] \left[\left(\frac{1}{\gamma_{ab} - i(\omega+\Omega-\nu+kv)} \right)^2 \right.$$

$$+\frac{1}{\gamma_{ab}-i(\omega+\Omega-\nu+kv)}\,\frac{1}{\gamma_{ab}+i(\omega+\Omega-\nu+kv)}\Bigg]+\frac{3}{2}\,E_{1+}\,E_{1-}^{2}\Bigg[\left(\frac{2\alpha_0^1}{\gamma_a^0}-\frac{3\alpha_1^1}{\gamma_a^1}+\frac{\alpha_2^1}{\gamma_a^2}\right)$$

$$+\left(\frac{2\alpha_0^0}{\gamma_b^0}-\frac{3\alpha_1^0}{\gamma_b^1}+\frac{\alpha_2^0}{\gamma_b^2}\right)-\gamma\left(\frac{2\alpha_0^2}{\gamma_a^0\gamma_b^0}-\frac{3\alpha_1^2}{\gamma_a^1\gamma_b^1}+\frac{\alpha_2^2}{\gamma_a^2\gamma_b^2}\right)\Bigg]\Bigg[\left(\frac{1}{\gamma_{ab}-i(\omega+\Omega-\nu+kv)}\right)$$

$$\left(\frac{1}{\gamma_{ab}+i(\omega-\Omega-\nu+kv)}+\frac{1}{\gamma_{ab}-i(\omega-\Omega-\nu+kv)}\right)\Bigg]+9E_{1+}E_{1-}^{2}\Bigg[\frac{\alpha_2^1}{\gamma_a^2-i(2\Omega)}$$

$$+\frac{\alpha_2^0}{\gamma_b^2-i(2\Omega)}-\frac{\gamma\alpha_2^2}{\gamma_a^2-i(2\Omega)\quad\gamma_b^2-i(2\Omega)}\Bigg]\Bigg[\left(\frac{1}{\gamma_{ab}-i(\omega+\Omega-\nu+kv)}\right)^2+\frac{1}{\gamma_{ab}-i(\omega+\Omega-\nu+kv)}$$

$$\cdot\,\frac{1}{\gamma_{ab}+i(\omega-\Omega-\nu+kv)}\Bigg]\Bigg\} \tag{3.40}$$

$[P_{-}(v)]^{(3)}$ is given by the corresponding expression with $-$ and $+$ interchanged in the electric field subscripts. The quantities $\lambda_\alpha(z,v,t)$ have been factored into space-time and velocity dependent terms according to (3.35), and N_o is given by (3.36). The coefficients α_K^0, α_K^1, α_K^2 are

$$\alpha_K^1=\begin{Bmatrix}1 & 1 & K\\ j_a & j_a & j_b\end{Bmatrix}2\,, \qquad \alpha_K^0=\begin{Bmatrix}1 & 1 & K\\ j_b & j_b & j_a\end{Bmatrix}2\,,$$

$$\alpha_K^2=(-1)^{j_a+j_b+1}\,(2j_a+1)\begin{Bmatrix}j_a & j_a & K\\ j_b & j_b & 1\end{Bmatrix}\begin{Bmatrix}K & 1 & 1\\ j_b & j_a & j_a\end{Bmatrix}\begin{Bmatrix}K & 1 & 1\\ j_a & j_b & j_b\end{Bmatrix}. \tag{3.41}$$

The values of these quantitites for the transitions J=1 to J=0, J=1 to J=1, and J=1 to J=2 are given in Table 1.

	α_0^0	α_1^0	α_2^0	α_0^1	α_1^1	α_2^1	α_0^2	α_1^2	α_2^2
J=1 → J=0	$\frac{1}{3}$	0	0	$\frac{1}{9}$	$\frac{1}{9}$	$\frac{1}{9}$	$\frac{1}{3}$	0	0
J=1 → J=1	$\frac{1}{9}$	$\frac{1}{36}$	$\frac{1}{36}$	$\frac{1}{9}$	$\frac{1}{36}$	$\frac{1}{36}$	$\frac{1}{9}$	$\frac{1}{72}$	$\frac{1}{72}$
J=1 → J=2	$\frac{1}{15}$	$\frac{1}{20}$	$\frac{7}{300}$	$\frac{1}{9}$	$\frac{1}{36}$	$\frac{1}{900}$	$\frac{1}{15}$	$\frac{1}{40}$	$\frac{7}{3000}$

Table 1

Values of the coefficients α_K^0, α_K^1, α_K^2 for three transitions of interest.

3.7.3 The Maxwellian Velocity Distribution

In a gas laser the velocity distribution of excited atoms active in the laser process is usually Maxwellian. This is the case in the He-Ne laser, for example. Thus

$$W(v) = \frac{1}{\sqrt{\pi}u} e^{-v^2/u^2} \tag{3.42}$$

where $u^2 = 2kT/m$. The half-intensity width of the Doppler line is related to ku:

$$\Delta\nu_D = \left(\frac{\sqrt{\ln 2}}{\pi}\right) ku \tag{3.43}$$

It is important to note that all frequency and decay rate symbols used thus far denote circular frequencies; this also includes ku. When numerical values are given for these quantities, e.g. 1000 MHz, we are using ordinary frequency units; thus the quantities used in the analysis should be divided by 2π before giving them numerical values. In some publications this is implicitly understood, and the 2π factor is not written.

Using (3.42) we can integrate (3.34) and (3.40) over the velocity distribution. The details of the integrations for the velocity-dependent functions which are found in these expressions will not be given in this work. The details for functions of this type can be found in reference 27. The results are expressed in terms of the error function of complex argument, defined by

$$w(z) = \exp(-z^2)\operatorname{erfc}(-iz) = (2/\sqrt{\pi})\exp(-z^2)\int_z^\infty \exp(-t^2)dt \qquad (3.44)$$

An integral representation which is the basis for our integrations is

$$w(z) = \frac{i}{\pi}\int_{-\infty}^{\infty} \frac{e^{-t^2}\,dt}{z-t} \qquad (\mathrm{Im}\ z > o) \qquad (3.45)$$

and a useful property of $w(z)$ is

$$w(-x + iy) = w^*(x + iy) \qquad (3.46)$$

The definition, mathematical properties, and tables of this function can be found in reference 71. Plots of the real and imaginary parts of

w(z) for various values of its complex argument are given in Figure 2.

The results of the integration over velocities are:

$$\frac{\nu}{\varepsilon_o c}\left[P_+\right]^{(1)+(3)} = i\alpha E_{1+}\left\{w(x_o+y+ia) - b(y)\left(\frac{E_{1+}^2}{2E_o^2}\right) - c(y)\left(\frac{E_{1-}^2}{2E_o^2}\right)\right\} \tag{3.47}$$

where

$$b(y) = \frac{3}{2} A_o B_o\left[\left(\frac{2\alpha_o^1}{A_o} + \frac{3\alpha_1^1}{A_1} + \frac{\alpha_2^1}{A_2}\right) + \left(\frac{2\alpha_o^0}{B_o} + \frac{3\alpha_1^0}{B_1} + \frac{\alpha_2^0}{B_2}\right)\right.$$

$$\left. - G\left(\frac{2\alpha_o^2}{A_o B_o} + \frac{3\alpha_1^2}{A_1 B_1} + \frac{\alpha_2^2}{A_2 B_2}\right)\right] f_1(y) \quad , \tag{3.48a}$$

$$c(y) = \frac{3}{2} A_o B_o\left[\left(\frac{2\alpha_o^1}{A_o} - \frac{3\alpha_1^1}{A_1} + \frac{\alpha_2^1}{A_2}\right) + \left(\frac{2\alpha_o^0}{B_o} - \frac{3\alpha_1^0}{B_1} + \frac{\alpha_2^0}{B_2}\right)\right.$$

$$\left. - G\left(\frac{2\alpha_o^2}{A_o B_o} - \frac{3\alpha_1^2}{A_1 B_1} + \frac{\alpha_2^2}{A_2 B_2}\right)\right] f_2(y) + 9A_o B_o\left[\frac{\alpha_2^1}{A_2 - iy}\right.$$

$$\left. + \frac{\alpha_2^0}{B_2 - iy} - \frac{G\alpha_2^2}{(A_2 - iy)(B_2 - iy)}\right] f_3(y) \tag{3.48b}$$

and

$$f_1(y) = \left[\frac{2}{\sqrt{\pi}} - 2(a - i(x_o+y))w(x_o+y+ia) + \frac{1}{a}\,\mathrm{Re}\; w(x_o+y+ia)\right], \tag{3.49a}$$

$$f_2(y) = \left[\frac{i}{2y}\left(w(x_o-y+ia) - w(x_o+y+ia)\right) + \frac{1}{2(a-iy)}\left(w(x_o+y+ia)+w^*(x_o-y+ia)\right)\right], \tag{3.49b}$$

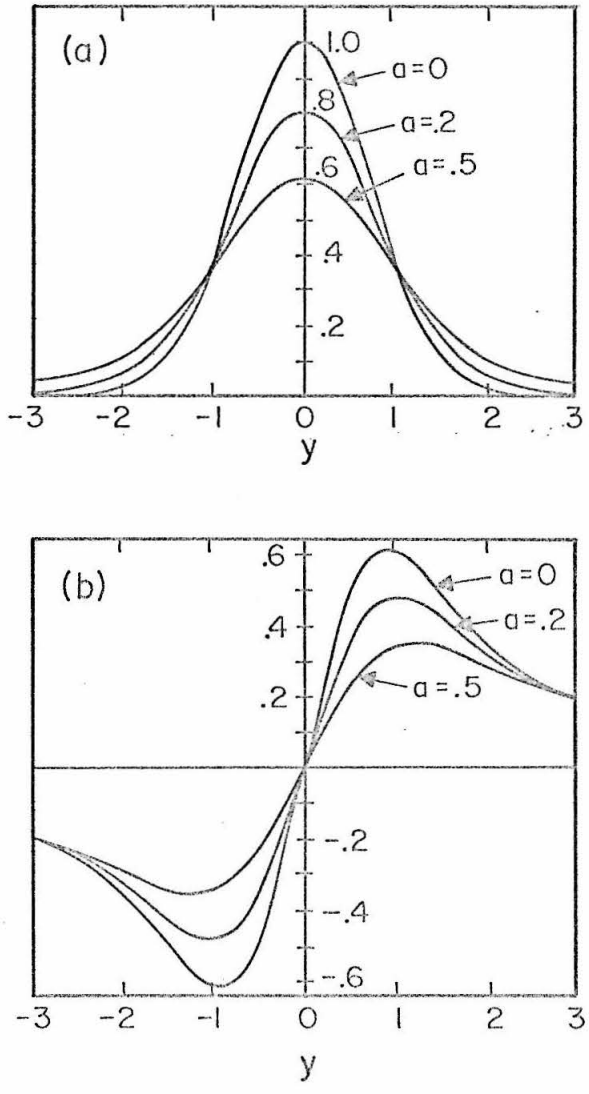

Figure 2

The Linear Polarization Function $w(y + ia)$

(a) Real Part (b) Imaginary Part

$$f_3(y) = \left[\frac{2}{\sqrt{\pi}} - 2(a-i(x_o+y))w(x_o+y+ia) + \frac{1}{2(a-iy)}\left(w(x_o+y+ia)+w(x_o-y+ia)\right)\right]. \tag{3.49c}$$

The following limiting case is necessary:

$$\lim_{y\to o} \frac{i}{2y}\left(w(x_o+y+ia) - w(x_o-y+ia)\right) = \frac{2}{\sqrt{\pi}} - 2(a-ix_o)w(x_o+ia) \tag{3.49d}$$

The definitions of the new symbols are:
$\alpha = \nu N_o \sqrt{\pi}\ |\langle b\|p\|a\rangle|^2/6\varepsilon_o hcku$, the small signal gain parameter;
$E_o^2 = 3\hbar^2\gamma_a^0\gamma_b^0/|\langle b\|p\|a\rangle|^2$, the saturation signal intensity; $a = \gamma_{ab}/ku$, $A_K = \gamma_a^K/2ku$, $B_K = \gamma_b^K/2ku$, $G = \gamma/2ku$, the normalized decay rates; $x_o = (\omega-\nu)/ku$, the normalized deviation of the frequency from line center; $y = \Omega/ku$, the normalized Zeeman splitting. The corresponding expression for $[P_-]^{(1)+(3)}$ can be obtained by interchanging + and - in all the subscripts and by replacing y by -y.

3.7.4 Discussion of the Nonlinear Effects

The leading term in (3.47) is the linear contribution, while the remaining terms show the lowest-order nonlinear effects. We shall not compute any higher order nonlinear expressions. The functions f_1, f_2, f_3 are similar to the functions F_1, F_2, F_3 of reference 26 and H_1, H_6, H_7 of reference 27, for the case of a single frequency wave. They differ in two respects: (1) by multiplicative constants, and (2) through the sign of their imaginary parts.

We shall be concerned with the case when the signal frequency is tuned to the line center, i.e. $x_o = 0$. In this case the real parts

of f_1, f_2, f_3 are symmetric about $y = 0$, and their imaginary parts are antisymmetric about $y = 0$.

The function f_1 describes the self saturation of the polarization component. We can represent this pictorially by drawing the Doppler gain curves of the two circularly polarized transitions, as shown in Figure 3. The gain curve for each polarization indicates the population inversion density of the atoms which are resonant with that polarization component of the signal. When the rate of stimulated emission and absorption becomes comparable with the rates of the processes which establish the unperturbed population inversion, the populations of the two levels tend to equalize. Thus a "hole" is burned in the region where the atoms have the proper velocities for interaction with the signal. This picture presupposes a Doppler width (inhomogeneous linewidth) larger than the interaction width of the single atoms (homogeneous linewidth). Figure 3 shows "holes" being burned in the gain curves by the signal. (The gain curve for the negative polarization component is shown as a dotted line for pictorial simplicity.) The variation of f_1 with y has a width roughly equal to the Doppler width.

The function f_2 describes cross saturation - due to the fact that the two types of transitions have some common levels, each polarization component burns a hole not only in its own Doppler gain profile, but also in that of its counterpart, at the corresponding point in its velocity space. Thus the additional holes shown in Figure 3 are due to this type of interaction. The size of f_2 depends more critically on y; after y has become larger than the homogeneous linewidth a,

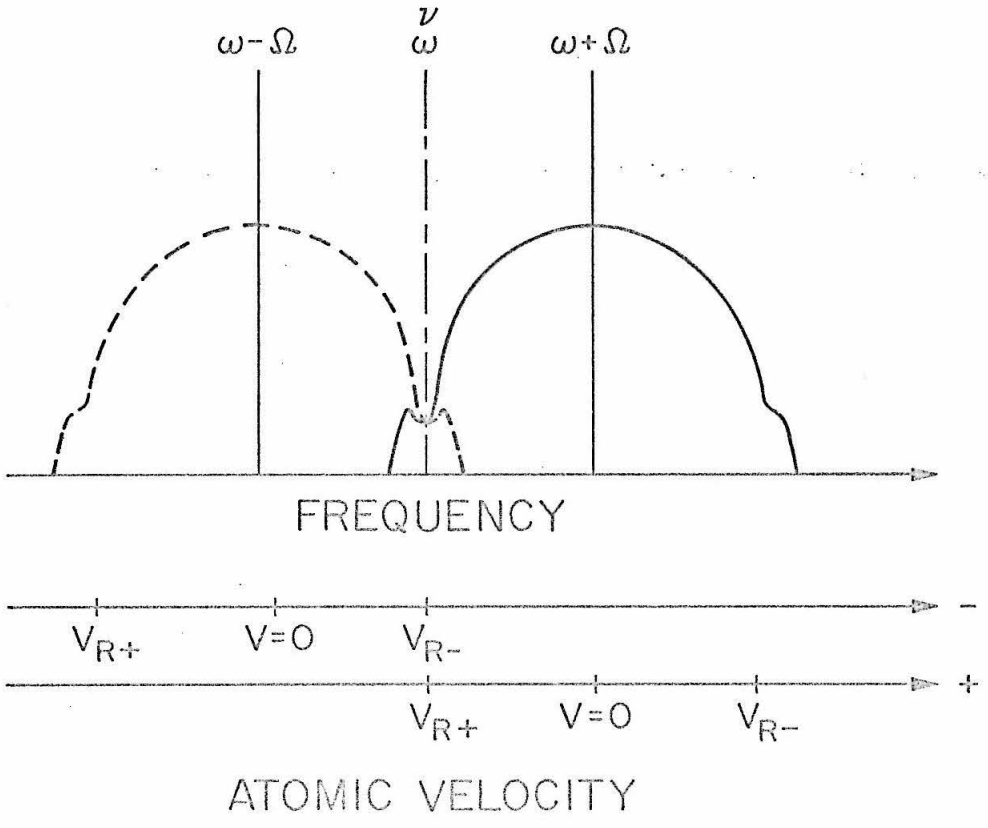

Figure 3

Hole Burning in the Doppler Broadened Gain Curves. $V_{R\pm}$ is the resonant velocity for interaction with the $\pm$ polarization component of a signal of frequency ν.

this type of interaction rapidly decreases in strength. In Figure 3 the Zeeman splitting is larger than the homogeneous linewidth; thus the effects on the signal of the holes burned through interaction are negligible.

The last term in (3.48b) describes a different sort of interaction. This term comes from the set of summation indices for which $K = 2$, $q = 2$. This means it originates from the existence of an intracoherence, or a coherence among the Zeeman sublevels, whereas the other nonlinear terms do not depend on the existence of intracoherence. The multiplicative factor in square brackets predominantly determines the dependence of this type of coupling on the Zeeman splitting. We see that the sublevel coherence drops off if the sublevel splitting becomes larger than the level widths, given by γ_a^2 and γ_b^2.

Since the maximum values of $b(y)$ and $c(y)$ are of the order of unity, we see that the perturbation approach is valid only when the signal intensity is much less than E_o^2, the saturation signal intensity.

3.8 Gain and Faraday Rotation

The expression (3.47) for the polarization corresponds to the term $\frac{1}{2}(P_{cm}-iP_{sm})^* = \frac{1}{2}(P_{cm}+iP_{sm})$ inside the curvy brackets of (2.11). By equating real and imaginary parts and applying the result to the self-consistency equations for a laser amplifier in steady state operation, where there is no time-dependence,

$$\frac{d\phi_{\pm}}{dz} E_{\pm} = \frac{\nu}{2\varepsilon_o c} P_{c\pm} , \tag{3.50a}$$

$$\frac{dE_{\pm}}{dz} = \frac{\nu}{2\varepsilon_o c} P_{s\pm} , \tag{3.50b}$$

we obtain the following expressions for a signal tuned to line center:

$$\frac{d\phi_{\pm}}{dz} = -\alpha \mathrm{Im}\left\{w(\pm y+ia) - b(\pm y)\left(\frac{E_{1\pm}^2}{2E_o^2}\right) - c(\pm y)\left(\frac{E_{1\mp}^2}{2E_o^2}\right)\right\} \tag{3.51}$$

$$\frac{dE_{1\pm}}{dz} = \alpha E_{1\pm} \mathrm{Re}\left\{w(\pm y+ia) - b(\pm y)\left(\frac{E_{1\pm}^2}{2E_o^2}\right) - c(\pm y)\left(\frac{E_{1\mp}^2}{2E_o^2}\right)\right\} \tag{3.52}$$

For a linearly polarized signal $E_+ = E_- = E/\sqrt{2}$, and we can write the equation for the amplification, or gain, as

$$\frac{dE}{dz} = \alpha E \ \mathrm{Re}\left\{w(y+ia) - \frac{E^2}{4E_o^2}[b(y) + c(y)]\right\}, \tag{3.53}$$

since the real parts of the functions w, b, c are symmetric with respect to y. The Faraday rotation angle is given by

$$\Phi = (\phi_- - \phi_+)/2 \tag{3.54}$$

and its differential equation is

$$\frac{d\Phi}{dz} = \alpha \mathrm{Im}\left\{w(y+ia) - \frac{E^2}{4E_o^2}[b(y) + c(y)]\right\} \tag{3.55}$$

Since $\mathrm{Im}w(y+ia)$ is a linear function of y for small values of y, the Faraday rotation in the linear approximation is directly proportional to the applied magnetic field for values of the field such that the Zeeman splitting is much smaller than the Doppler width. For larger values of magnetic field the Faraday rotation ceases to be linearly proportional to the field. Note that this is true only for weak signals. If the signal strength approaches saturation intensity the rotation is a function of signal strength, its value at each value of magnetic field being less than the unsaturated rotation value. Since the signal strength depends on z, we must integrate (3.53) before we can evaluate Φ as a function of z.

In a typical gas laser, such as the He-Ne laser, the homogeneous linewidth is much smaller than the Doppler width. Thus it can be concluded, after looking at the dependence of the functions $w(y)$, $b(y)$, and $c(y)$ on y, that the third-order contributions to the gain (equation (3.53)) and Faraday rotation (equation (3.55)) would be most noticeable for small values of magnetic field; since, as the field increases, $c(y)$ reaches its maximum far sooner than the "linear" function $w(y)$. Particularly if the quantity α_2^1 in the f_3 term (see expression (3.48b)) were large, the nonlinear contribution would be quite noticeable at small values of magnetic field. This is due to the fact that for most gas laser transitions the upper level decay rates (A_K) are smaller than the lower level decay rates (B_K); thus the term

with "width" equal to A_2 would reach its peak value at a value of y for which $w(y)$ would be quite small. In this case the curves for gain and Faraday rotation versus applied magnetic field would take forms similar to those pictured in Figure 4.

From Table 1 we see that the value of α_2^1 depends on the J values of the levels involved in the transition. Dienes (27, 28) analyzed the gain and Faraday rotation of a linearly polarized signal, using the weak-signal perturbation method, for the isotropic decay limit ($\gamma_\alpha^K = \gamma_\alpha$ for all K), assuming $\gamma_{ab} = \frac{1}{2}(\gamma_a + \gamma_b)$. He made a detailed study of the $J = 1$ to $J = 0$ case, which is the most favorable transition for observance of the nonlinear "dips" shown in Figure 4, and he predicted that these effects should be easily observable if a reasonably high gain $J = 1$ to $J = 0$ transition could be found. The existence of a traveling wave dip for strongly Doppler broadened transitions had previously been shown by Heer and Graft (16). It has been discussed more recently by Sargent, Lamb, and Fork (26) in their theory of Zeeman laser oscillators. The isotropic decay limit was used for these analyses also.

We shall discuss in detail the dependence of these nonlinear characteristics upon the J values of the energy levels for the three cases listed in Table 1. High gain $J = 1$ to $J = 2$ and $J = 1$ to $J = 1$ transitions exist in the He-Ne laser medium - thus it is pertinent to discuss these transitions if one desires to study these nonlinear effects experimentally. We shall also discuss the effects of gas pressure on the nonlinear "dips" in the gain and Faraday rotation curves.

Equation (3.53) can be written as

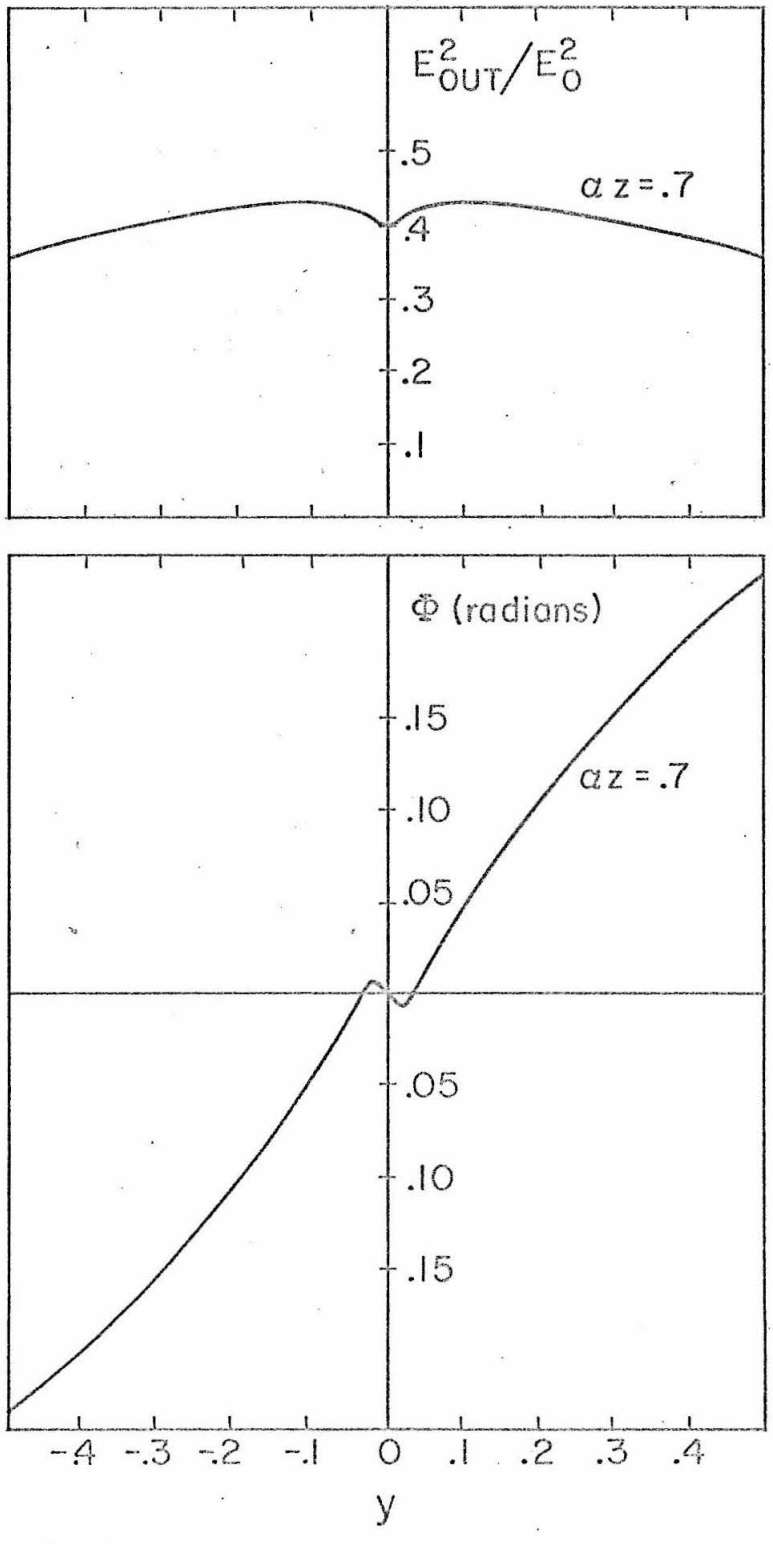

Figure 4
Gain and Faraday Rotation for a Linearly Polarized Signal.
J = 1 to J = 0 transition; I_{in} = .15, a = .2, A = .03, B=.17

$$\frac{dE^2}{dz} = 2\alpha E^2 \mathrm{Re}\left\{w(y) - \left(\frac{E^2}{E_o^2}\right) F(y)\right\} \tag{3.56}$$

where $F(y) = \frac{1}{4}[b(y) + c(y)]$. (We are explicitly showing only the dependence on y for convenience.) This has the form of Bernoulli's equation $(df/dz + c_1 f = c_2 f^2)$ and can be integrated by making the substitution $g = 1/f$, the result being a linear first-order differential equation for g. The result of this procedure is

$$I(z) = \frac{I_o \exp[2\alpha \mathrm{Re}\ w(y) z]}{1 + [I_o \mathrm{Re}\ F(y)/\mathrm{Re}\ w(y)][\exp(2\alpha \mathrm{Re}\ w(y) z) - 1]} \tag{3.57}$$

where $I = E^2/E_o^2$ and $I_o = I(z = 0)$. The numerator exhibits the familiar "linear" gain, while the denominator shows the effects of saturation. Now we can integrate (3.55), using (3.57), to obtain the Faraday rotation as a function of z. After some algebraic manipulation we obtain

$$\Phi(z) = \alpha\left\{\mathrm{Im}\ w(y) z - [\mathrm{Im}\ F(y)/\mathrm{Re}\ F(y)][\mathrm{Re}\ w(y) z + \frac{1}{2\alpha} \ln \right.$$

$$\left. |I_o \mathrm{Re}\ F(y)/\mathrm{Re}\ w(y) + (1 - I_o \mathrm{Re}\ F(y)/\mathrm{Re}\ w(y))\ \exp\ (-2\alpha \mathrm{Re}\ w(y) z)|]\right\} \tag{3.58}$$

Thus if we know the values of $w(y)$ and $F(y)$ for certain values of y, the Faraday rotation can be computed from this expression, keeping in mind the fact that this is valid only for weakly saturating fields.

Figure 4 is the result of a computation based on these results. The expressions (3.57) and (3.58) differ from those derived by Dienes (27) in the same manner. His expressions are incorrect due to an improper statement of the initial condition at $z = 0$.

3.9 Circular Component Coupling

The gain equations (3.52) for the circular components are coupled if $c(y)$ is nonzero. "Strong coupling" occurs when $[\text{Re } c(y)]^2 > [\text{Re } b(y)]^2$. For this case if the intensities are unequal at $z = 0$ the gain of the weaker signal is reduced to a larger extent than that of the stronger one by the nonlinear terms, the results being that the amplification of the stronger signal is greater than that of the weaker signal. Thus an elliptically polarized signal would tend to become circularly polarized when passing through a medium with strong coupling. "Weak coupling" occurs when $[\text{Re } c(y)]^2 < [\text{Re } b(y)]^2$. In this case the weaker signal amplification is greater than that of the stronger signal. An elliptically polarized signal would tend toward linear polarization in this type of medium. "Neutral coupling" is the designation for the case $[\text{Re } c(y)]^2 = [\text{Re } b(y)]^2$. In this case the saturated gains of the two components are equal regardless of their relative sizes.

Since the magnitudes of $b(y)$ and $c(y)$ depend on the α-coefficients given by (3.41), one would suspect that the degree of coupling depends on the values of J for the energy levels involved in the transition. This is indeed the case, and we shall discuss this dependence in the following section.

In addition the coupling strength depends on the rate of sublevel mixing collisions - these collisions affect the sizes of the decay rates A_K and B_K for $K > 0$. Tomlinson and Fork (30) noticed in their experiments with He-Ne laser oscillators that the observed coupling was stronger than that predicted by the isotropic decay theory for both $J = 1$ to $J = 2$ and $J = 1$ to $J = 0$ transitions. They postulated that sublevel mixing collisions were the cause of these discrepancies. It is evident that this type of collision process tends to equalize the populations of the sublevels; thus the coupling would be driven closer to neutral. Fork and Tomlinson's 6328-Å ($J = 1$ to $J = 2$) observations agreed with this argument; however the 1.52-μ ($J = 1$ to $J = 0$) transition should have been neutral to begin with, according to the isotropic decay theory; yet the coupling was strong. It is less clear that sublevel mixing collisions could cause this effect. The tentative explanation given for this observation was that for the $J = 1$ to $J = 0$ transition the sublevel mixing collisions are more effective in causing $|\Delta m| = 2$ transitions (decay of orientation) than $|\Delta m| = 1$ transitions (decay of alignment) (29). If we consider a $J = 1$ to $J = 0$ transition in zero field, the degenerate sublevels can be represented in different ways. If we quantize along the axial direction (direction of $\underline{k}$-vector of the signal), it is convenient to break up an elliptically polarized signal into circular components, each operating on one of the $|\Delta m| = 1$ transitions. If we quantize along a transverse direction, it is convenient to use as a basis two perpendicular linear polarizations, one being parallel to the quantization axis and operating on the $\Delta m = 0$ transition, and the other operating on both of the $|\Delta m| = 1$ transitions.

Now $|\Delta m| = 1$ collisions would assist each of the circular components and each of the linear components, but $|\Delta m| = 2$ collisions would assist a particular circular component while having no effect on the linear components. This physical argument is rather tenuous, but the idea received support when it was found that a theory which allowed for anisotropic decay could account for the $J = 1$ to $J = 0$ observations by allowing the orientation decay rate to be greater than the alignment decay rate (42).

Another mechanism which is probably responsible for the tendency toward strong coupling in these He-Ne laser transitions is trapping of resonance radiation by ground state neon atoms. If a neon atom in the upper laser level decays to the ground state, there is a large probability that the emitted radiation will be trapped and excite another neon atom to the upper laser level. If the initially excited atom were in a coherent mixture of substates, there is a chance that this intra-coherence would be passed on to the second atom. Since the coherence of the atom is a result of its nonlinear interactions with both polarization components of the signal, only those excited atoms within a natural linewidth of the signal frequency will originally develop an intra-coherence. Assuming no transfer of intra-coherence to other atoms, the velocity dependence of the elements of the macroscopic density matrix which reflect this coherence is a product of a Lorentzian distribution, centered at the signal frequency with width γ_{ab}, and the overall Doppler distribution. The inclusion of the radiation trapping process would add a Doppler-width velocity distribution term to the intra-coherency elements. This would add to the function $c(y)$ in (3.47),

resulting in a stronger amount of coupling. When the Doppler width is much larger than the natural linewidth, one can assume for purposes of simplicity that the ground state atom which traps the resonance radiation has a velocity such that it is outside the region of interaction. Thus the radiation trapping process is ignored. However for the 1.52-μ transition used by Tomlinson and Fork (30), the ratio of the homogeneous linewidth to the Doppler linewidth is about .2 at the pressure indicated. The question whether or not the intra-coherence transfer due to radiation trapping can be ignored for this case requires further investigation.

3.10 The Isotropic Decay Limit

3.10.1 Introduction

Isotropic decay implies equal decay rates for the various multipole moments of an energy level, i.e. $\gamma_\alpha^K = \gamma_\alpha$ for all K. Thus far the theoretical studies of the gas laser oscillator and amplifier have assumed isotropic decay, with the exceptions of references (42) and (44), which deal with a He-Ne laser oscillating on the 1.52-μ (J = 1 to J = 0) transition. We shall describe the weak-signal nonlinear effects in this limit in order to perceive the regions of applicability of this theory when it is compared with experimental data for various ranges of gas pressure. Chronologically, the experimental information we obtained from a study of the 3.39-μ transitions in the He-Ne system was first compared with the isotropic decay theory, and not until then did the need for a more general theory for a laser amplifier become evident. This parallels the chronological development of an anisotropic decay theory in order to explain results obtained from the 1.52-μ laser

oscillator, as related in references (30) and (42)-(44). The results of our investigations showed that certain nonlinear phenomena could be matched quite well using the isotropic decay theory if the gas pressure remained within certain bounds, while the anisotropic theory provided good fits to the experimental data over a wider range of pressures. The pressure range for which the isotropic decay theory is adequate depends on the particular phenomenon under investigation. These results will be discussed in the succeeding chapters.

In the isotropic decay limit we can use (3.40) to write $[P_+(v)]^{(3)}$ for the J = 1 to J = 0 transition in the form:

$$[P_+(v)]^{(3)} = -i \frac{|\langle b\|p\|a\rangle|^2}{24\hbar} W(v) N_o \left\{ \frac{E_{1+}^2}{E_o^2} \left(\gamma_a + \gamma_b - \frac{2}{3}\gamma\right) \left[\left(\frac{1}{\gamma_{ab} - i(\omega+\Omega-\nu+kv)} \right)^2 \right.\right.$$

$$\left. + \frac{1}{\gamma_{ab} - i(\omega+\Omega-\nu+kv)} \cdot \frac{1}{\gamma_{ab} + i(\omega+\Omega-\nu+kv)} \right] + \frac{E_{1+}E_{1-}}{E_o^2} \left(\gamma_a - \frac{2}{3}\gamma\right) \left[\frac{1}{\gamma_{ab} - i(\omega-\Omega-\nu+kv)} \right.$$

$$\left. \cdot \left(\frac{1}{\gamma_{ab} + i(\omega-\Omega-\nu+kv)} + \frac{1}{\gamma_{ab} - i(\omega-\Omega-\nu+kv)} \right) \right] + \frac{E_{1+}E_{1-}}{E_o^2} \left(\gamma_a \gamma_b\right) \frac{1}{\gamma_a - i(2\Omega)}$$

$$\left. \cdot \left[\left(\frac{1}{\gamma_{ab} - i(\omega+\Omega-\nu+kv)} \right)^2 + \frac{1}{\gamma_{ab} - i(\omega+\Omega-\nu+kv)} \frac{1}{\gamma_{ab} + i(\omega-\Omega-\nu+kv)} \right] \right\} \qquad (3.59)$$

When the integration over velocities is performed, the result is

$$\frac{\nu}{\varepsilon_o c} [P_+]^{(1+3)} = i\alpha E_{1+} \left\{ w(x_o + y + ia) - b(y) \left(\frac{E_{1+}^2}{2E_o^2} \right) - c(y) \left(\frac{E_{1-}^2}{2E_o^2} \right) \right\} \qquad (3.60)$$

where

$$b(y) = (A + B - \frac{2}{3} G)\ f_1(y) \qquad (3.61a)$$

$$c(y) = (A - \frac{2}{3} G)\ f_2(y) + \frac{AB}{A-iy}\ f_3(y) \qquad (3.61b)$$

If we neglect G and apply the condition $a = A + B$, then $b(y)$ and $c(y)$ respectively become equal to Dienes' functions $H_1(y)$ and $H_6(y) + H_7(y)$ for the case of a single frequency input signal (28).

We can apply these relations for the $J = 1$ to $J = 0$ transition to more complicated transitions by treating the sublevel structure as a composition of $J = 1$ to $J = 0$ substructures. To help picture this construction, Figure 5 shows the three transitions with which we are primarily concerned. The $J = 1$ to $J = 1$ transition can be split into two independent basic sublevel structures, a $J = 1$ to $J = 0$ substructure and a $J = 0$ to $J = 1$ substructure. The $J = 1$ to $J = 2$ transition can be split into four basic sublevel structures: three $J = 0$ to $J = 1$ substructures, two of which have a common level as shown, and one $J = 1$ to $J = 0$ substructure. In each case the relative component strengths for the left and right circular polarizations are given in the figure, in units of $|\langle b\|p\|a\rangle|^2/3$. (A component of a line results from a radiative transition between two states of an atom; a line results from the totality of transitions between two levels. Component strength is the absolute square of the matrix element for that transition (72).)

Since we assume incoherent pumping to each of the levels of a transition, the first-order contribution to the polarization is a

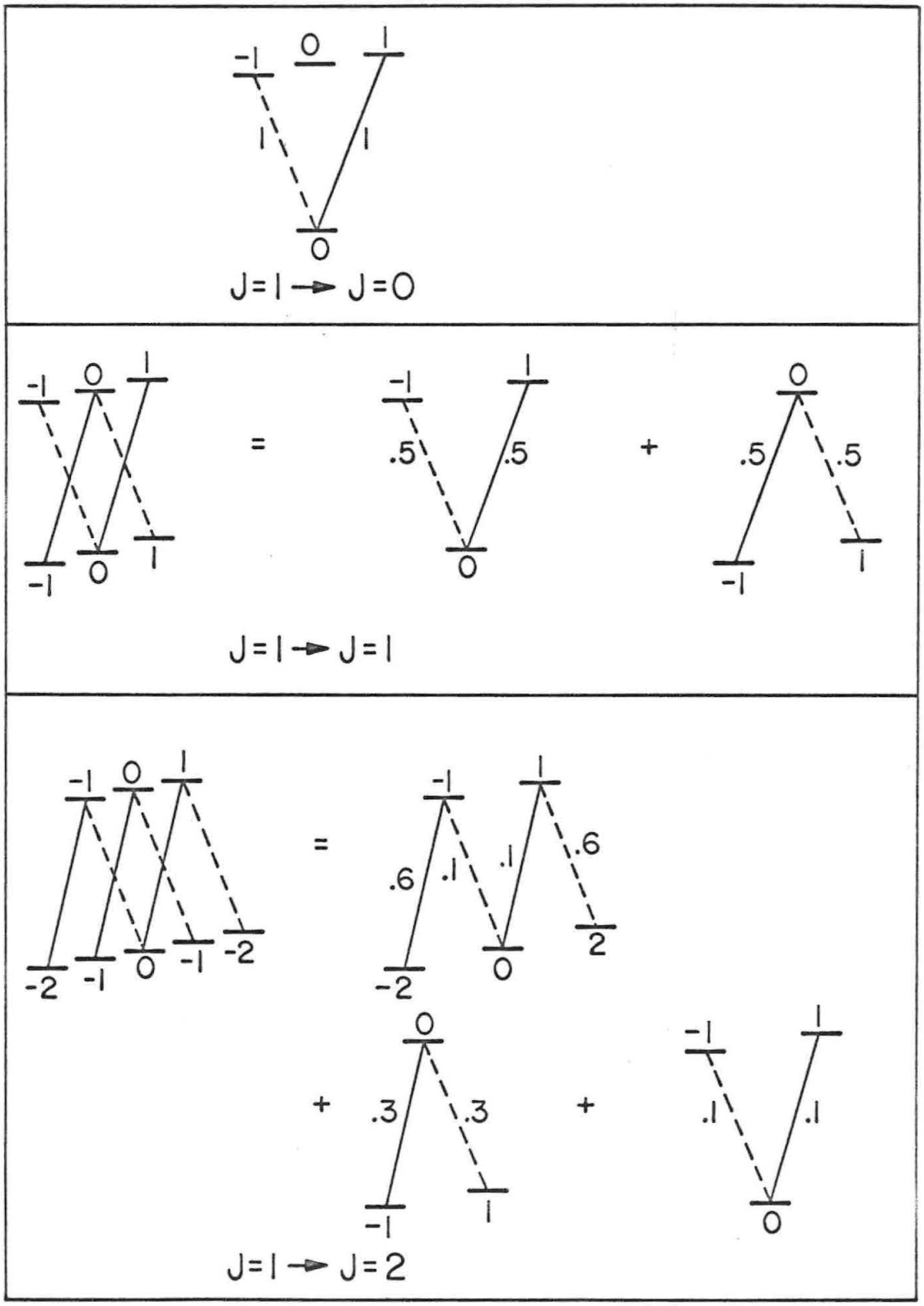

Figure 5
Sublevel Structures for Three Transitions.

result of the atom interacting once with the signal during its interaction period; and the third order contribution to the polarization is a result of three interactions with the signal during the atom's interaction period. The contributions to f_1 (H_1) result from multiple transitions between the same two sublevels, whereas the contributions to f_2 and f_3 $(H_6$ and $H_7)$ result from transitions involving three sublevels. With this in mind, using (3.60) as our basic expression for a $J = 1$ to $J = 0$ building block, we can write down by inspection the corresponding expressions for the $J = 1$ to $J = 1$ and $J = 1$ to $J = 2$ transitions. Allowing for different g-values in this case by calling the upper level splitting y_a and the lower level splitting $y_b = y_a - \delta$, we obtain for a line-centered signal operating on the $J = 1$ to $J = 1$ transition:

$$\frac{\nu}{\varepsilon_o c} P_+^{(1)} = i\alpha E_+ \left\{ .5w(y_a+ia) + .5w(y_b+ia) \right\} \tag{3.62a}$$

$$\frac{\nu}{\varepsilon_o c} P_+^{(3)} = -i\alpha E_+ \left\{ \frac{E_+^2}{2E_o^2} \left[.25b(y_a) + .25b(y_b) \right] + \frac{E_-^2}{2E_o^2} \left[.25c(y_a) + .25c'(y_b) \right] \right\} \tag{3.62b}$$

or on the $J = 1$ to $J = 2$ transition:

$$\frac{\nu}{\varepsilon_o c} P_+^{(1)} = i\alpha E_+ \left\{ .1w(y_a+ia) + .3w(y_b+ia) + .6w(y_b-\delta+ia) \right\} \tag{3.63a}$$

$$\frac{\nu}{\varepsilon_o c} P_+^{(3)} = -i\alpha E_+ \left\{ \frac{E_+^2}{2E_o^2} \left[.01b(y_a) + .09b(y_b) + .36b(y_b-\delta) \right] \right.$$

$$\left. + \frac{E_-^2}{2E_o^2} \left[.01c(y_a) + .09c'(y_b) + .06c'(y_b)\Big|_{x_o=\delta} + .06c'(y_b)\Big|_{x_o=-\delta} \right] \right\}, \quad (3.63b)$$

where the symbol $|_{x_o=\delta}$ means to evaluate the function at $x_o=\delta$ instead of $x_o=0$. Here $c'(y)$ is obtained by interchanging A and B in $c(y)$. ($b(y)$ is invariant with respect to this interchange.) This interchange is necessary because these functions result from the "inverted" $J = 0$ to $J = 1$ substructures.

These results can also be obtained from (3.4), using the values for the α's listing in Table 1, if we assume $y_a = y_b$ in the expressions (3.62) and (3.63). The difference in g-factors for the two levels of a general transition can be taken into account much more easily in the isotropic decay theory.

3.10.2 Linearly Polarized Signal-Gain and Rotation

We are now in a position to determine the size of the function $F(y)$ (defined following equation (3.56)), which determines the entire third-order contribution to the polarization for a linearly polarized signal, for these three transitions. Figures 6 through 11 depict the real and imaginary parts of the nonlinear polarization function $F(y)$ in comparison with the linear function $w(y)$, for each of the three transitions. It is evident that the relative size of $F(y)$ decreases as we go from the $J = 1$ to $J = 0$ transition to the $J = 1$ to $J = 1$

transition and finally to the $J = 1$ to $J = 2$ transition.

The function $c(y_a)$ contains a term with a linewidth equal to A, as shown in (3.61b). It was stated previously that this function peaks most sharply at low values of magnetic field, since A is the smallest of the decay rates involved in the transition. If the coefficient of $c(y_a)$ is large, one would expect "dips" to appear in the gain and Faraday rotation curves for magnetic field near zero. For the $J = 1$ to $J = 0$ transition, the coefficient of $c(y_a)$ is unity; for the $J = 1$ to $J = 1$ transition, the coefficient of $c(y_a)$ is .25; and for the $J = 1$ to $J = 2$ transition, the coefficient is .01. These marked differences are clearly portrayed in the small field regions of Figures 6 through 11.

Thus for a $J = 1$ to $J = 1$ transition we would expect a small, narrow dip in the rotation curve at low magnetic field values (where $y \lesssim A$). If the signal strength increases beyond the region of validity for the weakly saturating signal theory, the dip should increase, although not as much as predicted by (3.57) and (3.58), and a reversal of the rotation might actually occur. A detectable dip in the gain at zero magnetic field should also occur.

For a $J = 1$ to $J = 2$ transition the effect of the $c(y_a)$ term is so small that we do not expect to observe a dip in the Faraday rotation, and for analogous reasons we would not expect to see the very small dip in the gain curve. However the other nonlinear terms contribute to the saturation for larger values of the magnetic field.

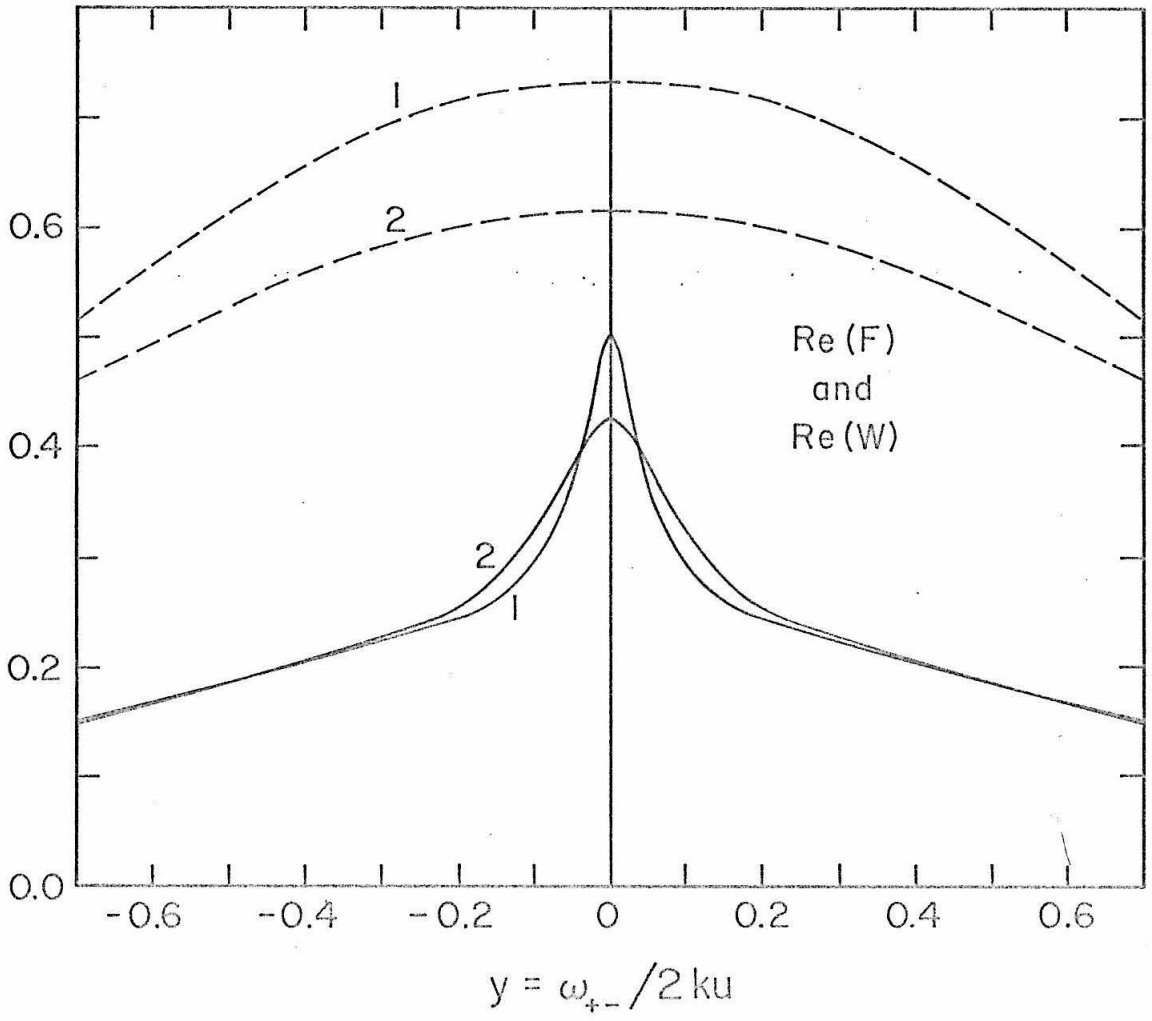

Figure 6

The Linear and Nonlinear Polarization Functions for J = 1 to J = 0: (1) a = .3, A = .05, B = .25 (2) a = .5, A = .1, B = .4

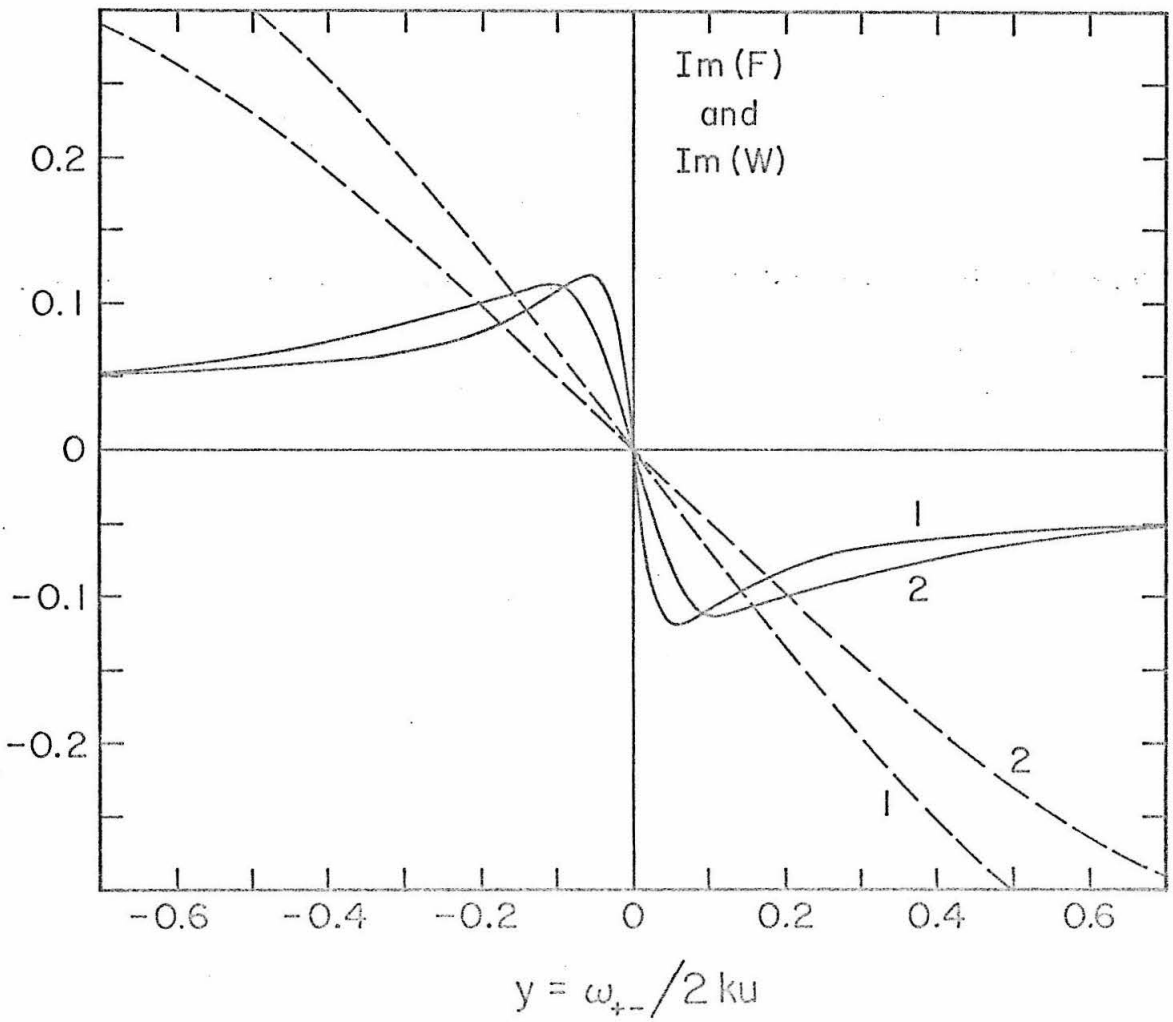

Figure 7

The Linear and Nonlinear Polarization Functions for J = 1 to J = 0: (1) a = .3, A = .05, B = .25 (2) a = .5, A = .1, B = .4

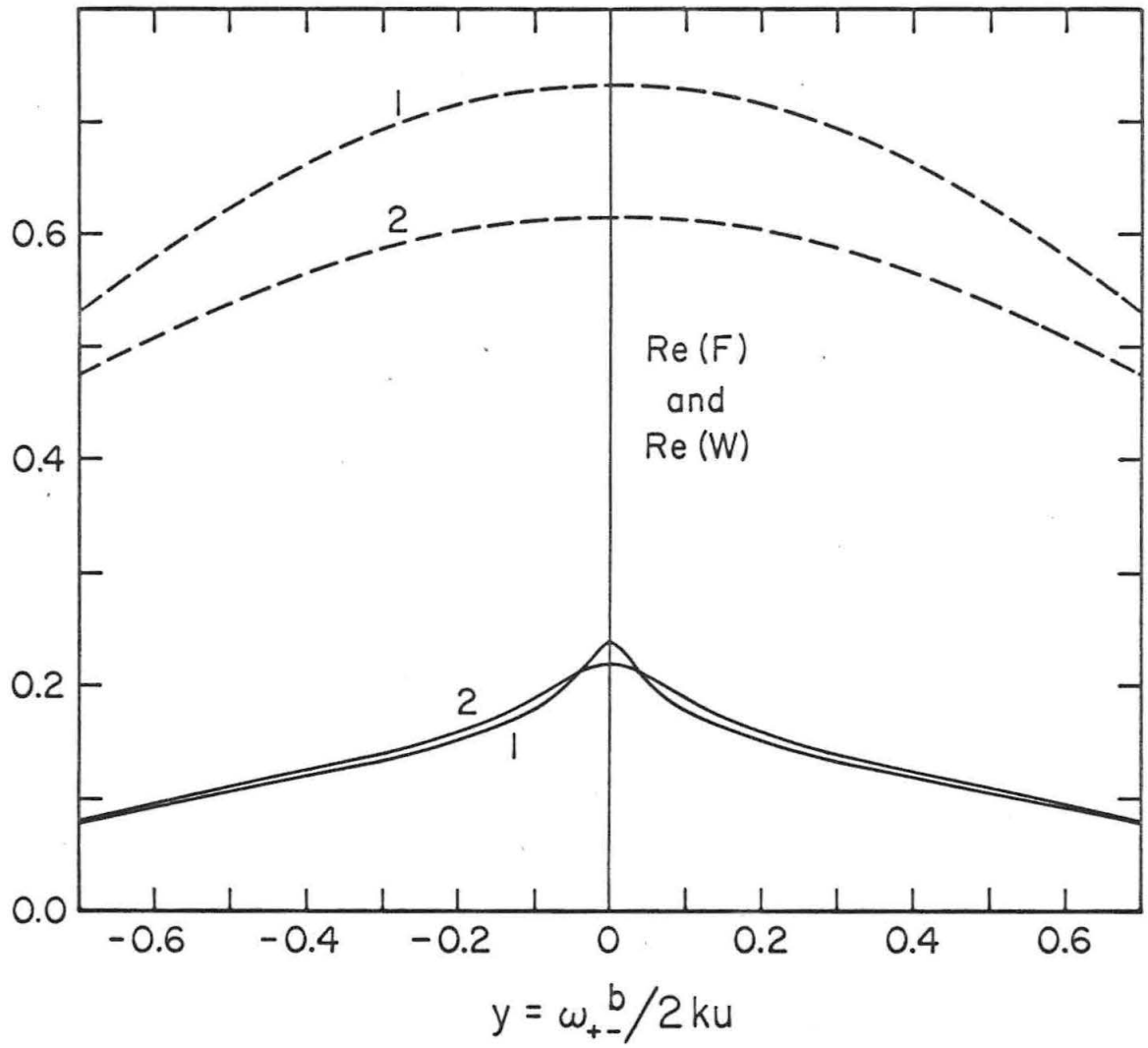

Figure 8

The Linear and Nonlinear Polarization Functions for J = 1 to J = 1 :

$y^a = .927y^b$; (1) a = .3, A = .05, B = .25, (2) a = .5, A = .1, B = .4

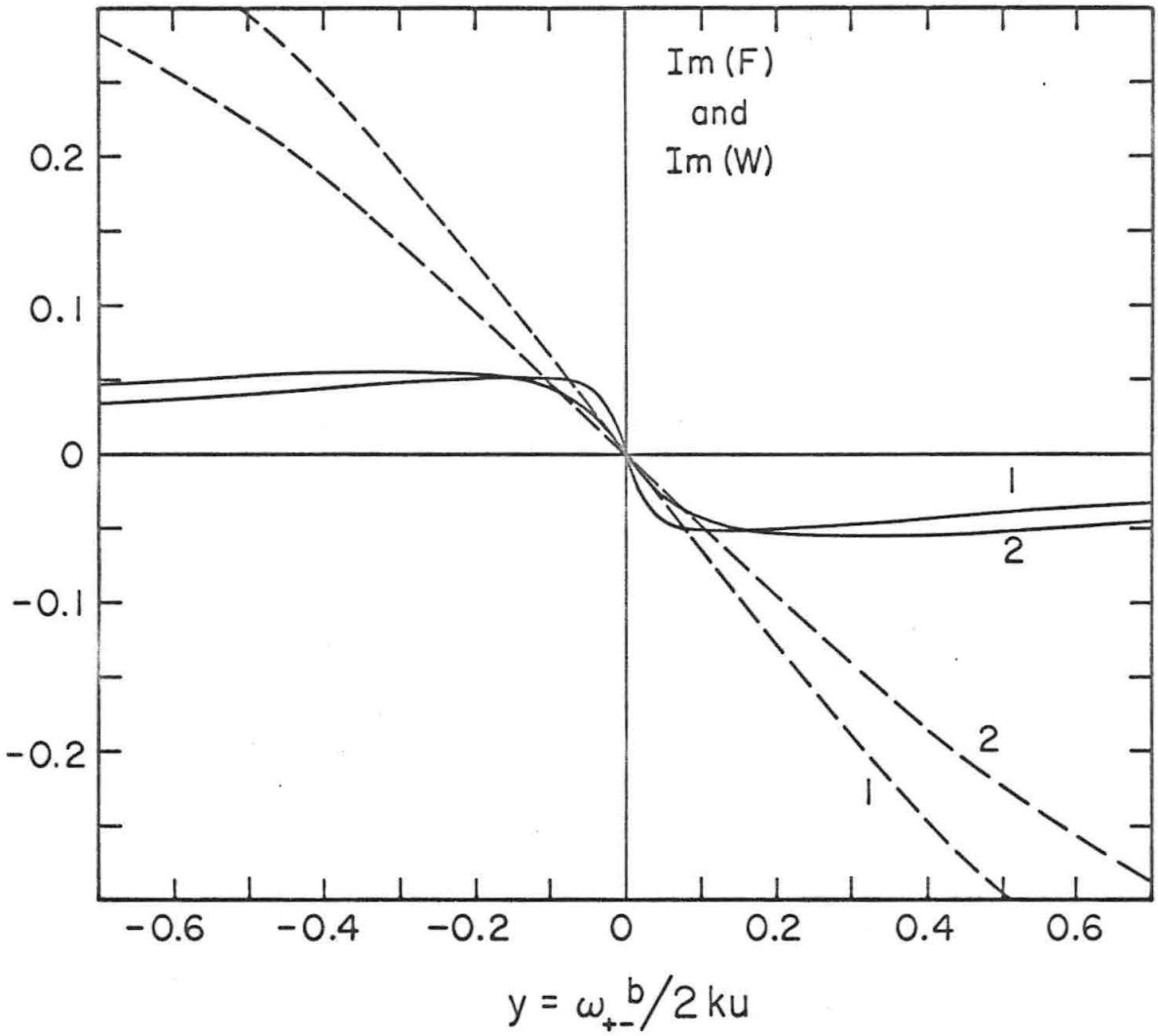

Figure 9

The Linear and Nonlinear Polarization Functions for J = 1 to J = 1 : $y^a = .927y^b$; (1) a = .3, A = .05, B = .25, (2) a = .5, A = .1, B = .4

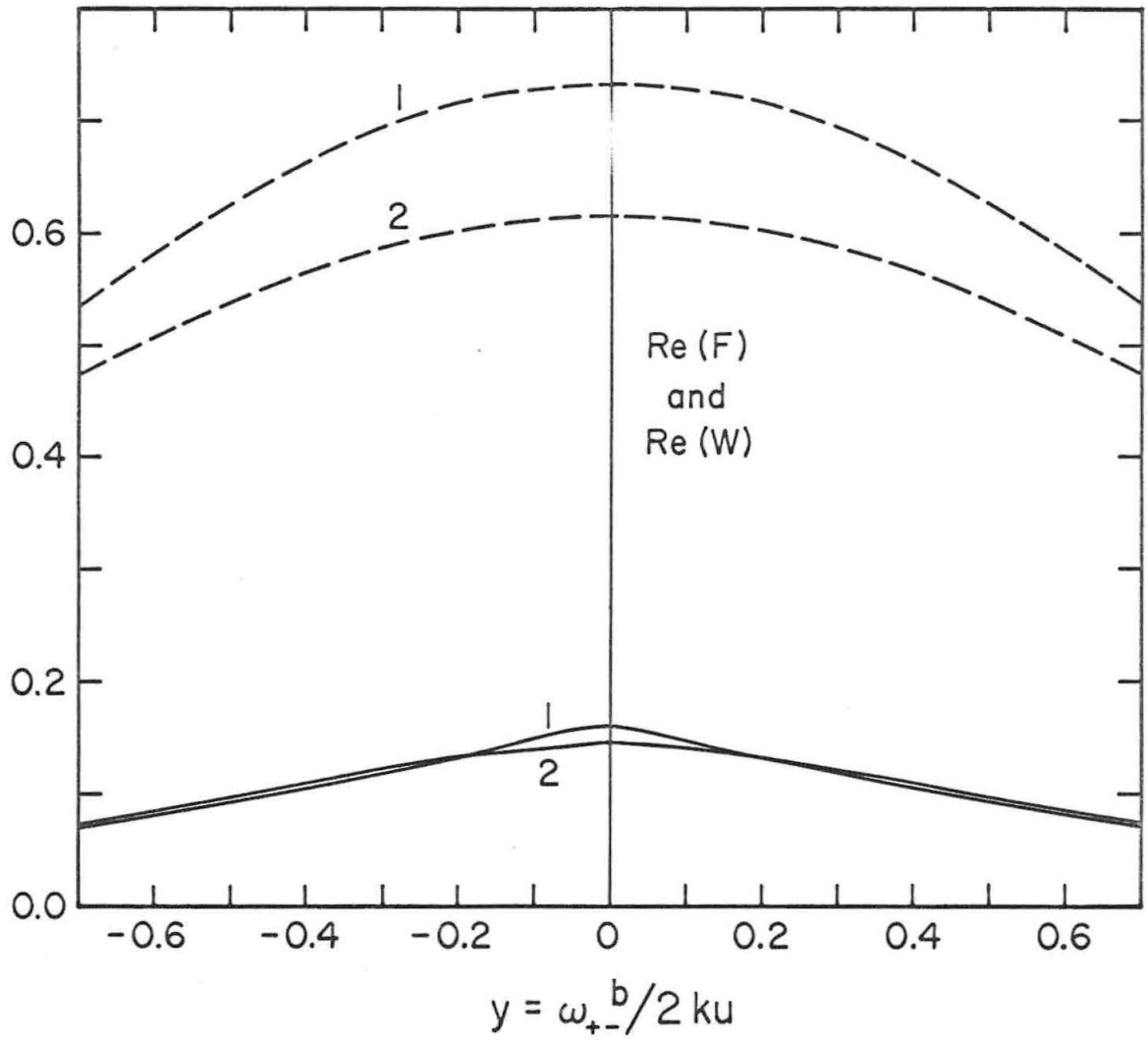

Figure 10

The Linear and Nonlinear Polarization Functions for J = 1 to J = 2 : $y^a = 1.094y^b$; (1) a = .3, A = .05, B = .25, (2) a = .5, A = .1, B = .4

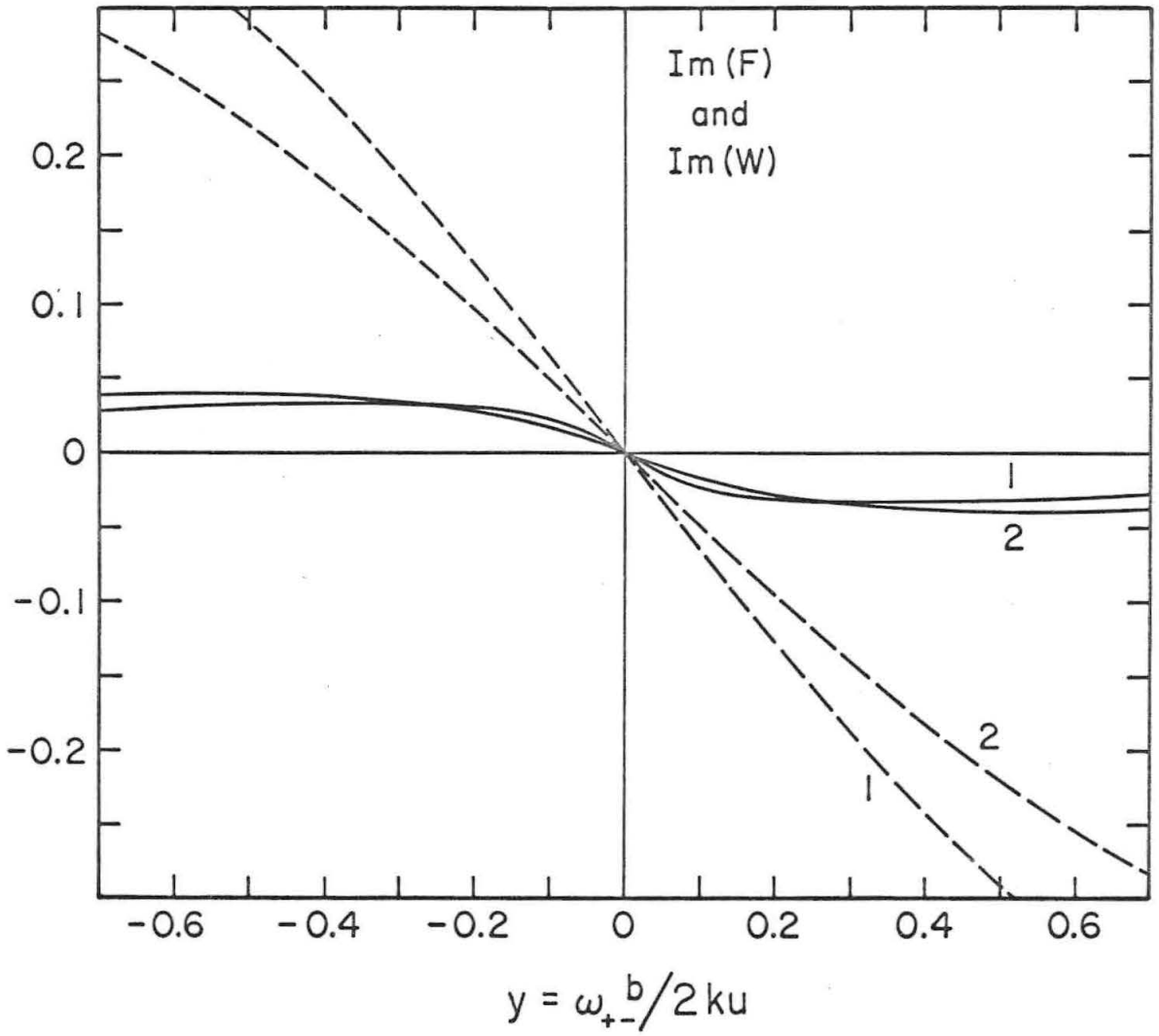

Figure 11

The Linear and Nonlinear Polarization Functions for J = 1 to J = 2 : $y^a = 1.094y^b$; (1) a = .3, A = .05, B = .25, (2) a = .5, A = .1, B = .4

3.10.3 Elliptically Polarized Signal - Nonlinearity-Induced Anisotropy

Circular component coupling has been discussed by Dienes (27)-(29), by Sargent, Lamb and Fork (26), and by Tomlinson and Fork (30). The isotropic decay theories used by these authors predict that at zero magnetic field the coupling strength depends only on the J values of the transition: for $\Delta J = \pm 1$ transitions the coupling is weak, and for $\Delta J = 0$ transitions the coupling is strong, excepting the cases $J = 1$ to $J = 0$ and $J = 1$ to $J = 1$, for which the coupling is neutral.

Let us write the expression for the positive component of the induced polarization for the general J_a to J_b transition, assuming the signal is at line center:

$$\frac{\nu}{\varepsilon_o c} P_+^{(1)+(3)} = i\alpha E_+ \left\{ \sum_M 3 \begin{pmatrix} J_a & 1 & J_b \\ M & -1 & -(M-1) \end{pmatrix}^2 w(y_b+M\delta+ia) \right.$$

$$- \frac{E_+^2}{2E_o^2} \sum_M 9 \begin{pmatrix} J_a & 1 & J_b \\ M & -1 & -(M-1) \end{pmatrix}^4 b(y_b+M\delta) - \frac{E_-^2}{2E_o^2} \sum_M \left[9 \begin{pmatrix} J_a & 1 & J_b \\ M & -1 & -(M+1) \end{pmatrix}^2 \begin{pmatrix} J_a & 1 & J_b \\ M & 1 & -(M+1) \end{pmatrix}^2 \right.$$

$$\left. \left. c'(y_b+M\delta) + 9 \begin{pmatrix} J_a & 1 & J_b \\ M & -1 & -(M-1) \end{pmatrix}^2 \begin{pmatrix} J_a & 1 & J_b \\ M-2 & 1 & -(M-1) \end{pmatrix}^2 c(y_b+M\delta) \right] \right\} \qquad (3.64)$$

If we examine the values of the 3-j symbols for the various sublevel transitions between levels, we find that for a $\Delta J = \pm 1$ transition the outer sublevel transitions (i.e. $M_a = \pm J_a \rightarrow M_b = \pm J_b$) are

strong and the inner transitions (e.g. $M_a = J_a \rightarrow M_b = J_b - 2$) are weaker. The $J = 1$ to $J = 2$ transition pictured in Figure 5 is a good example of this. As we can see from (3.63), this results in weak coupling for $J = 1$ to $J = 2$, and with the help of (3.64) we can reason that this will be the case for all $\Delta J = \pm 1$ transitions. For the $J = 2$ to $J = 2$ and higher $\Delta J = 0$ transitions, the sublevel transitions are of more equal strengths, and the outer transitions are not the strongest. For these cases the coefficients of c' and c add up to a larger value than the coefficient of b, resulting in strong coupling.

Since the nonlinear terms in the polarization are responsible for the coupling, the change in the ellipticity of the signal as it passes through the amplifier is called nonlinearity-induced anisotropy. Heer and coworkers invoked this phenomenon in an attempt to describe the polarization and relative intensity properties of the cosmic OH radiation lines (17)-(19).

3.11 Pressure Effects

Lamb's theory for nondegenerate energy levels (3) can include the effects of "hard" collisions which cause the atom to decay or lose memory of its previous interaction with the signal. These collisions cause γ_a, γ_b, and $\gamma_{ab} = \frac{1}{2}(\gamma_a + \gamma_b)$ to become pressure dependent, but no further changes are necessary.

One of the earliest modifications of Lamb's theory to account for other effects of atomic interactions was a relaxation of the condition $\gamma_{ab} = \frac{1}{2}(\gamma_a + \gamma_b)$. One example is the work of Fork and Pollack in fitting experimental results on mode competition to Lamb's theory

(36). This allows for effects of "soft" collisions which slightly perturb the energy levels of the atom that is interacting with the signal. The result is a time varying shift in the atomic resonant frequency, which broadens the natural linewidth of the atomic resonance. Gyorffy, Borenstein, and Lamb (41) discuss in detail this type of pressure effect on the spectral profile of the output intensity versus cavity tuning curve for a single mode laser oscillator.

The "hard" collisions evidently increase the saturation signal intensity, E_o^2, by increasing the level decay rates. The "soft" collisions make the value of $a = \gamma_{ab}/ku$ larger; and this makes the gain of a signal of given input intensity saturate to a greater extent as it passes through the amplifying medium. The reason for this lies in the fact that Re $w(0+ia)$ decreases faster with increasing a than the sum of the nonlinear polarizations functions Re $b(y=0)$ and Re $c(y=0)$, assuming the other decay rates are kept constant. Since these two types of collisions seem to have opposite effects on the gain saturation of a signal, it is not clear what the overall effect will be unless an experimental study is made.

Increasing γ_{ab}, γ_a and γ_b will broaden the "dips" in the gain and rotation versus magnetic field curves for a linearly polarized signal. The effects on the size, or depth, of these dips are strongly dependent on the relative sizes of γ_a and γ_b, and this will not be affected a great deal by varying the gas pressure. Changing the values of γ_{ab}, γ_a and γ_b will have no effect on the nonlinearity-induced anisotropy of an elliptically polarized signal.

The collision-induced anisotropic decay of degenerate levels

has a marked effect on the zero field circular component coupling for the $J = 1$ to $J = 2$ transition. In the expressions for $b(y)$ and $c(y)$ given in (3.48), the sign of the α_1 term is positive in the coefficient of $f_1(y)$ but negative in the coefficient of $f_2(y)$. If A_K and B_K for $K \neq 0$ are allowed to become larger than A_o and B_o respectively, in order to account for sublevel mixing collisions, the size of the function $b(y=0)$ decreases, while the size of the first term of $c(y=0)$ increases. The second term in the expression for $c(y=0)$ decreases also; however the overall effect is an increase in the ratio of $c(y=0)/b(y=0)$, with a resultant increase in the strength of the coupling. This effect implies a pressure dependence of the nonlinearity induced anisotropy of an elliptically polarized signal.

The zero field coupling for the $J = 1$ to $J = 0$ and $J = 1$ to $J = 1$ transitions is neutral in the isotropic decay limit. If the decay rates for orientation and alignment are equal but larger than the decay of the population, the coupling remains neutral. If, however, the orientation decay rate is larger than the alignment decay rate, the coupling becomes strong; if the opposite is true, the coupling becomes weak. These results are obtained from expressions (3.40) or (3.48), setting Ω and $\omega-\nu$ equal to zero, and using Table 1. Hence the overall effect of anisotropic decay on zero-field coupling strength is not likely to be as large for these two transitions as it is for the $J = 1$ to $J = 2$ transition.

The width of the nonlinear dips in the curves for Faraday rotation and gain versus magnetic field is equal to A_2, the quadrupole moment (alignment) decay rate of the upper level, since the

dominant nonlinear term for small values of field is the first term in the coefficient of $f_3(y)$, given by (3.48b). Thus the dip width is influenced not only by "hard" collisions but also by sublevel mixing collisions, and it should show a marked dependence on gas pressure, although at higher pressures the dip would not be as noticeable.

3.12 Extension of Theory to Two Signals

The analysis presented in section 3.7 can be extended to the case of two monochromatic signals of arbitrary polarization passing through the amplifying medium. The equations corresponding to (3.33a,b) would each include two more terms, and these would be substituted into the appropriate integral expressions in order to obtain the macroscopic polarization. Functions in addition to $f_{1,2,3}$ would be obtained in the third-order expression for the polarization. These functions would be the same as the H-functions in Dienes' work (28) with respect to their dependence on the sublevel splitting and the signal frequencies. The coefficients of the functions, which involve the decay rates, would be different. Combination tones would be generated from the third-order polarization expression.

The theory presented here is more comprehensive than the theory developed by Dienes in that it includes the effects of spontaneous feeding of the lower level by the upper level in addition to the effects of anisotropic decay. However its use is restricted to transitions in which the g-factors of the levels are nearly the same.

CHAPTER FOUR

SOLUTIONS OF THE ATOMIC EQUATIONS OF MOTION FOR STRONG SIGNALS

4.1 Introduction

The low-pressure equations of motion for the density matrix, namely equations (2.23) without the collision terms, can be integrated exactly for simple transitions which consist of noninteracting 3-level subsystems, such as the $J = 1$ to $J = 1$ transition pictured in Figure 5. For each 3-level subsystem one has three equations with three unknowns, and these equations can be solved in principle, the solutions being valid for all values of signal strength. Dienes (27,29) has carried out this procedure and has found that tractable solutions can be obtained only for special cases. For our purposes these special cases are: (1) zero magnetic field, and (2) large values of magnetic field, such that the Zeeman splitting is much larger than the power broadened natural linewidth for the transition.

Dienes (29) has found that strong signal solutions can also be obtained for more complicated transitions in these special cases, by relying on the process of induction. These results are useful for a study of gain saturation and its dependence on signal polarization, and nonlinearity-induced anisotropy (1), if the gas pressure is low enough such that the neglect of collision contributions is justifiable.

In this chapter some of these theoretical results for strong signals will be developed in order to apply them to the experimental results obtained for the 3.39-μ transitions in He-Ne. Expressions

will be presented which describe gain saturation, nonlinearity-induced anisotropy, and Faraday rotation.

4.2 Solutions for Simple Transitions

The equations (2.23), excluding the collision terms, can be written in the following manner for a simple $J = 1$ to $J = 0$ transition:

$$\dot{\rho}_{--} = -\gamma_a\rho_{--} + \frac{i}{\hbar}(V_{b-}\rho_{-b} - V_{-b}\rho_{b-}) + \lambda_a \tag{4.1a}$$

$$\dot{\rho}_{++} = -\gamma_a\rho_{++} + \frac{i}{\hbar}(V_{b+}\rho_{+b} - V_{+b}\rho_{b+}) + \lambda_a \tag{4.1b}$$

$$\dot{\rho}_{bb} = -\gamma_b\rho_{bb} - \frac{i}{\hbar}(V_{b-}\rho_{-b} - V_{-b}\rho_{b-}) - \frac{i}{\hbar}(V_{b+}\rho_{+b} - V_{+b}\rho_{b+}) + \lambda_b \tag{4.1c}$$

$$\dot{\rho}_{+-} = -(\gamma_a + 2i\Omega)\rho_{+-} + \frac{i}{\hbar}V_{b-}\rho_{+b} - \frac{i}{\hbar}V_{+b}\rho_{b-} \tag{4.1d}$$

$$\dot{\rho}_{-b} = -(\gamma_{ab} + i(\omega-\Omega))\rho_{-b} + \frac{i}{\hbar}V_{-b}(\rho_{--} - \rho_{bb}) + \frac{i}{\hbar}V_{+b}\rho_{-+} \tag{4.1e}$$

$$\dot{\rho}_{+b} = -(\gamma_{ab} + i(\omega+\Omega))\rho_{+b} + \frac{i}{\hbar}V_{+b}(\rho_{++} - \rho_{bb}) + \frac{i}{\hbar}V_{-b}\rho_{+-} \tag{4.1f}$$

where $\gamma_{ab} = \frac{1}{2}(\gamma_a + \gamma_b)$, and where each element of the density matrix is a function of z,v,t. These equations can be integrated to form a set of integral equations. Defining the quantities

$$N_{-b} = \rho_{--} - \rho_{bb} \tag{4.2a}$$

$$N_{+b} = \rho_{++} - \rho_{bb} \tag{4.2b}$$

we can substitute the integrated expressions for ρ_{-b} and ρ_{+b} into the integrated expressions for N_{-b}, N_{+b}, and ρ_{+-}. After performing the integrations and manipulating, we obtain the following (assuming a monochromatic signal at frequency $\nu = \omega$ as the perturbation):

$$N_{+b} = N_o - C_{+b}^2(E_+^2/E_o^2)\gamma_{ab}^2[\gamma_{ab}^2+(\omega+\Omega-\nu+kv)^2]^{-1}N_{+b} - C_{-b}^2(E_-^2/E_o^2)\tfrac{1}{2}\gamma_{ab}\gamma_a$$

$$[\gamma_{ab}^2+ (\omega-\Omega-\nu+kv)^2]^{-1}N_{-b} - C_{+b}C_{-b}(E_-E_+/E_o^2)\Big\{\tfrac{1}{2}\gamma_{ab}[\rho'_{+-}(\gamma_{ab}+i(\omega+\Omega-\nu+kv))^{-1}$$

$$+ \rho'^{*}_{+-}(\gamma_{ab}-i(\omega+\Omega-\nu+kv))^{-1}]+ \tfrac{1}{4}\gamma_a[\rho'_{+-}(\gamma_{ab}-i(\omega-\Omega-\nu+kv))^{-1}$$

$$+ \rho'_{+-}{}^{*}(\gamma_{ab} + i\ (\omega-\Omega-\nu+kv))^{-1}]\Big\} \tag{4.3}$$

N_{-b} = same as N_{+b} with the + and - subscripts interchanged, and with Ω replaced by $-\Omega$.

$$\rho'_{+-} = -\tfrac{1}{4}(\gamma_a\gamma_b)[\gamma_a + i(2\Omega)]^{-1}\Big\{C_{+b}C_{-b}(E_+E_-/E_o^2)[N_{+b}(\gamma_{ab} + i(\omega+\Omega-\nu+kv))^{-1}$$

$$+ N_{-b}(\gamma_{ab} - i(\omega-\Omega-\nu+kv))^{-1}] + C_{-b}^2(E_-^2/E_o^2)(\gamma_{ab} + i(\omega+\Omega-\nu+kv))^{-1}$$

$$+ C_{+b}^2(E_+^2/E_o^2)(\gamma_{ab} - i(\omega-\Omega-\nu+kv))^{-1}\rho'_{+-}\Big\} \tag{4.5}$$

Using the integrated forms for (4.1e) and (4.1f), we can write the macroscopic polarization components in terms of these three

quantities:

$$\frac{\nu}{\varepsilon_o c} P_+(v) = i(\alpha_o/N_o)W(v)\left\{\gamma_{ab}(C_{+b}^2 E_+ N_{+b} + C_{+b}C_{-b}E_-\rho'^{*}_{+-})\right.$$

$$\left.[\gamma_{ab} - i(\omega+\Omega-\nu+kv)]^{-1}\right\} \qquad (4.6)$$

$\frac{\nu}{\varepsilon_o c} P_-(v)$ = same as (4.6) with subscripts + and - interchanged, Ω replaced by $-\Omega$, and ρ'^{*}_{+-} replaced by ρ'_{+-}, where $\rho'_{+-} = \rho_{+-}\exp[i(\phi_+-\phi_-)]$, and C_{+b}, C_{-b} are the normalized component strengths for the sublevel transitions. The same equations describe a $J = 0$ to $J = 1$ structure if the subscripts $\pm b$ are replaced by $a\pm$, and if γ_a and γ_b are interchanged. When there is more than one of these 3-level structures, their contributions add.

These expressions are equivalent to equations (1) to (3) in reference 29 when $\nu_+ = \nu_- = \nu$ in that paper. Differences in notation exist, however; the expressions written in this section are in accord with the notation used in Chapter 2, and our expressions for $P_\pm(v)$ are equal in the rotating wave approximation to $\frac{1}{2}(P_{cm} - iP_{sm})^*$ in expression (2.11). This is the complex conjugate of the quantities defined in equations (3a,b) of reference 29. In addition Dienes' vector base system for the components of $\underline{E}$ and $\underline{P}$ is obtained by interchanging the + and - subscripts in our system. Our system is in accord with the physical convention that a traveling wave with positive helicity polarization carries positive angular momentum in its direction of propagation.

When $\Omega = 0$, the results, after integration over velocities, are:

$$\frac{\nu}{\varepsilon_o c} P_{\pm} = i\alpha E_{\pm} \begin{Bmatrix} C^2_{+b} \\ C^2_{-b} \end{Bmatrix} (2b)^{-1}[(a+b)w(0+ib) + (a-b)w^*(0+ib)] \qquad (4.7)$$

where

$$b = (\gamma_{ab}/ku)[1 + C^2_{+b}(E^2_+/E^2_o) + C^2_{-b}(E^2_-/E^2_o)]^{\frac{1}{2}} \qquad (4.8)$$

and $w(z)$ is the error function for complex argument, defined in reference 71 and discussed in Chapter 3. We see that the homogeneous linewidth of the transition is power broadened.

Applying these results to the $J = 1$ to $J = 1$ transition, we obtain:

$$\frac{dE_+}{dz} = 2\alpha E_+ \left\{.5[1 + .5(E^2_+/E^2_o) + .5(E^2_-/E^2_o)]^{-\frac{1}{2}} \text{ Re } w(0+ib)\right\} \qquad (4.9)$$

dE_-/dz = same as (4.9) with + and − subscripts interchanged, and $b = a[1 + .5(E^2_+/E^2_o) + .5(E^2_-/E^2_o)]$. Setting

$E^2_+/E^2_o = I_+$, $E^2_-/E^2_o = I_-$, $I = I_+ + I_-$, and $r = (E_- - E_+)/(E_- + E_+)$, we

can write the equations for gain and change of ellipticity of a line-centered signal passing through the amplifier. These are

$$dI/dz = 2\alpha I\left\{(1 + .5I)^{-\frac{1}{2}} \text{ Re } w(0 + ib)\right\} , \quad b = a[1 + .5I]^{\frac{1}{2}} \tag{4.10}$$

$$dr/dz = \frac{2E_+(dE_-/dz) - 2E_-(dE_+/dz)}{E_+^2 + E_-^2 + 2E_-E_+} = 0 \tag{4.11}$$

Thus for a $J = 1$ to $J = 1$ transition the gain saturation does not depend on the ellipticity of the signal, and the ellipticity does not change. This agrees with the isotropic decay theory for weakly saturating signals discussed in Chapter 3, where the zero field coupling was found to be neutral for a $J = 1$ to $J = 1$ transition.

When $\Omega >> \gamma_{ab}(1 + E_\pm^2/E_o^2)^{\frac{1}{2}}$ and $\gamma_b >> \gamma_a$, such that $\gamma_{ab} \sim \frac{1}{2}\gamma_b$, the contribution of the ρ'_{+-} term to the macroscopic polarization (4.6) is negligible; and the integration over velocities can be carried out. The resulting expressions for the gain and Faraday rotation of a linearly polarized signal $(I_+ = I_- = I/2)$ interacting with a $J = 1$ to $J = 1$ transition are

$$I^{-1}(dI/dz) = 2\alpha\left\{.5(1 + 0.25I)^{-\frac{1}{2}} \text{ Re } w(y_a + ib) + .5(1 + 0.25I)^{-\frac{1}{2}} \text{ Re } w(y_b + ib)\right\}, \tag{4.12}$$

$$d\Phi/dz = \alpha\left\{.5 \text{ Im } w(y_a + ib) + .5 \text{ Im } w(y_b + ib)\right\}, \tag{4.13}$$

where $b = a[1 + .25I]^{\frac{1}{2}}$.

These expressions for the $J = 1$ to $J = 1$ transition will be compared with experimental results in the appropriate regions of validity.

4.3 Solutions for the $J = 1$ to $J = 2$ Transition

The more complicated transitions prove to be exceedingly difficult to handle. The special case of degenerate levels (zero magnetic field) and an arbitrarily polarized signal tuned to line center has been treated by integrating the density matrix equations of motion to obtain exact solutions for increasingly complicated transitions. The general result is then found by induction (29). Dienes has developed a clever physical interpretation of the resulting expressions, which are written in the form of continued fractions (see reference 29). Only the final results for the $J = 1$ to $J = 2$ transition gain equations will be written here. These are

$$I^{-1}dI/dz = 2\alpha\left\{\frac{c_1}{(1+c_1I)^{\frac{1}{2}}}\,\mathrm{Re}\;w(0+ib_1) + \frac{c_2}{(1+c_2I)^{\frac{1}{2}}}\,\mathrm{Re}\;w(0+ib_2) + \frac{c_3}{(1+c_3I)^{\frac{1}{2}}}\,\mathrm{Re}\;w(0+ib_3)\right\}, \tag{4.14}$$

$$dr/dz = -\alpha r\left[\frac{1-r^2}{1+r^2}\right]\frac{.12}{c_2-c_1}\left\{\frac{1}{(1+c_1I)^{\frac{1}{2}}}\,\mathrm{Re}\;w(0+ib_1) - \frac{1}{(1+c_2I)^{\frac{1}{2}}}\,\mathrm{Re}\;w(0+ib_2)\right\}, \tag{4.15}$$

where

$$b_i = (\gamma_{ab}/ku)(1 + c_i I)^{\frac{1}{2}} , \qquad (4.16)$$

$$c_{1,2} = .35 \mp .5\left\{.49 - .24\left[1 + \frac{1-r^2}{1+r^2}\right]\right\}^{\frac{1}{2}} , \quad c_3 = .3$$

The values of $c_{1,2}$ for $r = 0$ (linear polarization) and $r = 1$ (circular polarization) are:

$$r = 0: \quad c_1 = .3, \quad c_2 = .4$$

$$r = 1: \quad c_1 = .1, \quad c_2 = .6$$

Using these values for $r = 1$ in (4.14) results in an expression similar to that for the $J = 1$ to $J = 1$ case (4.10). The representation of the (degenerate) energy sublevels given in Figure 5 gives the proper noninteracting sublevel transitions for a circular polarization, along with their relative component strengths; and these match the values for the c_i coefficients given here. In this case the circularly polarized signal saturates each of its allowed sublevel transitions independently; since there is only one polarization component, there is no interaction.

The form for (4.14) when $r = 0$ can be understood by considering the normalized strengths for the sublevel transitions $-1 \to -1$, $0 \to 0$, $1 \to 1$ in the $J = 1$ to $J = 2$ scheme. These component strengths are .3, .4, .3 respectively. In this case if we pick the quantization axis in the direction of the polarization of the signal, then the

allowed transitions would be these three, and each would saturate according to (4.14) for $r = 0$.

A similar picture can be given for a linearly polarized signal interacting with a $J = 1$ to $J = 1$ transition. In this case the component strengths for the $-1 \rightarrow -1$, $0 \rightarrow 0$, and $1 \rightarrow 1$ sublevel transitions are .5, 0, and .5. So for linear polarization we would expect the same form for the gain equation as for circular polarization. Actually equation (4.10) is valid for polarization of arbitrary ellipticity, whereas the form of (4.14) depends on r.

The preceeding results for the $J = 1$ to $J = 2$ transition can be found in reference 1. Note that equation (4.15) predicts a negative value for dr/dz, which agrees with the weak coupling results of Chapter 3.

A look at the $J = 1$ to $J = 2$ transition in Figure 5 shows that the component strengths for the sublevel transitions $\pm 1 \rightarrow 0$ are quite small. Based on this fact, we can approximately describe the transition as a sum of three independent $J = 0$ to $J = 1$ substructures by ignoring the $\pm 1 \rightarrow 0$ sublevel transitions. Use can then be made of the formulation outlined in section 4.2 for simple transitions. By making the approximation $\gamma_b >> \gamma_a$ (i.e. $\gamma_{ab} \sim \frac{1}{2}\gamma_b$), the ρ'^{*}_{+-} contribution to the expression (4.6) for the polarization can be ignored. Summing the results for three 3-level substructures, we obtain:

$$I^{-1}\, dI/dz \;+\; 2i\, d\Phi/dz$$

$$= \frac{2\alpha}{\pi} \sum_{i=1,2,3} \int_{-\infty}^{\infty} \frac{c_i[a-i(y+\xi)][a^2+(y-\xi)^2]\, \exp(-\xi)^2\, d\xi}{[a^2(1+0.5c_iI)+(y+\xi)^2][a^2(1+0.5d_iI)+(y-\xi)^2]+0.25c_id_ia^4I^2}$$

where $\quad c_{1,2,3} = 0.6,\ 0.1,\ \text{and}\ 0.3\ ,$

$$d_{1,2,3} = 0.1,\ 0.6,\ \text{and}\ 0.3 \qquad (4.18)$$

In this approximation the left and right circular components interact via the upper sublevels only. Expression (4.18) was first developed by Dienes during a joint discussion; we have made use of a numerical integration of (4.18) in order to compare strong-signal Faraday rotation results for the 3.39-μ $J = 1$ to $J = 2$ laser transition with the strong signal theory.

In the region where there is no interaction between the opposite circular components ($\Omega >> \gamma_{ab}\,(1 + I_{\pm})$, an extension of the equations of type (4.12) and (4.13) to more complicated transitions can be made by the process of induction (28). In this case each sublevel transition saturates independently of the others. We can write for the general J_a to J_b transition

$$\frac{\nu}{\varepsilon_o c} P_{\pm} = \alpha \sum_{M} \frac{C^2_{M,M\pm1}}{[1 + C^2_{M,M\pm1}(E^2_{\pm}/E^2_o)]^{\frac{1}{2}}}\; w(y_b + M\delta + ib_{M\pm}) \ , \qquad (4.19)$$

where

$$b_{M\pm} = (\gamma_{ab}/ku)[1 + C^2_{M,M\pm1}(E^2_{\pm}/E^2_o)]^{\frac{1}{2}}$$

are the power broadened linewidth parameters, and

$$C^2_{M,M'} = 3\begin{pmatrix} J_a & 1 & J_b \\ M & -1 & -M' \end{pmatrix}^2$$

are the normalized line strengths for the sublevel transitions. Then for a linearly polarized signal, we can write the gain and Faraday rotation equations as follows:

$$\frac{1}{I}\frac{dI}{dz} = 2\alpha\left[\sum_M C^2_{M,M-1}(1 + 0.5IC^2_{M,M-1})^{-\frac{1}{2}} \text{ Re } w(y + ib_M)\right], \tag{4.20}$$

$$\frac{d\Phi}{dz} = \alpha\sum_M C^2_{M,M-1} \text{ Im } w(y + ib_M) , \tag{4.21}$$

where

$$b_M = a(1 + 0.5\ I\ C^2_{M,M-1})^{\frac{1}{2}}.$$

For a $J = 1$ to $J = 2$ transition these equations are

$$\frac{1}{I}\frac{dI}{dz} = 2\alpha\ \text{Re}\Big[0.6(1 + .3I)^{-\frac{1}{2}}\, w(y_b - \delta + ib_1) + 0.3(1 + .15I)^{-\frac{1}{2}}$$

$$\cdot\ w(y_b + ib_2) + 0.1(1 + .05I)^{-\frac{1}{2}}\, w(y_a + ib_3)\Big], \tag{4.22}$$

$$\frac{d\Phi}{dz} = \alpha \, \mathrm{Im} \left[0.6 \, w(y_b - \delta + ib_1) + 0.3 \, w(y_b + ib_2) \right.$$

$$\left. + 0.1 \, w(y_a + ib_3) \right] , \qquad (4.23)$$

where

$$b_1 = a[1 + .3I]^{\frac{1}{2}}, \quad b_2 = a[1 + .15I]^{\frac{1}{2}}, \quad b_3 = a[1 + .05I]^{\frac{1}{2}}.$$

These expressions for the $J = 1$ to $J = 2$ transition will be utilized in Chapters 6 and 7, where experimental results are discussed.

CHAPTER FIVE

AN EXPERIMENTAL TEST: THE 3.39 MICRON TRANSITIONS IN THE HE-NE SYSTEM

5.1 Introduction

In this chapter we first discuss some of the salient characteristics of the He-Ne medium when it is used for laser purposes. Methods for enhancement of power output at 6328-Å wavelength will be dealt with. We shall then focus attention on two high gain transitions at 3.39-μ in the infrared; these prove to be suitable for the study of saturation effects in a gas laser amplifier. Since these two transitions have a common upper level and easily saturate the population inversion, they compete with each other inside a laser cavity. We shall discuss the use of methane as a selective absorber of the stronger of the two lines, thereby providing a means of eliminating the oscillation of the stronger line in the laser cavity.

Finally we describe the experimental facility, including the basic setup and appartus necessary to perform studies of Faraday rotation, gain, and nonlinearity-induced anisotropy. Results of the use of a single-mode 3.39-μ laser to probe a methane vibration-rotation absorption line will complete the chapter.

5.2 The Common Transitions in the He-Ne Laser

Figure 12 shows the energy levels of neon which are involved in the common visible and near infrared laser transitions. Also shown are the helium metastable states which play an important role in ex-

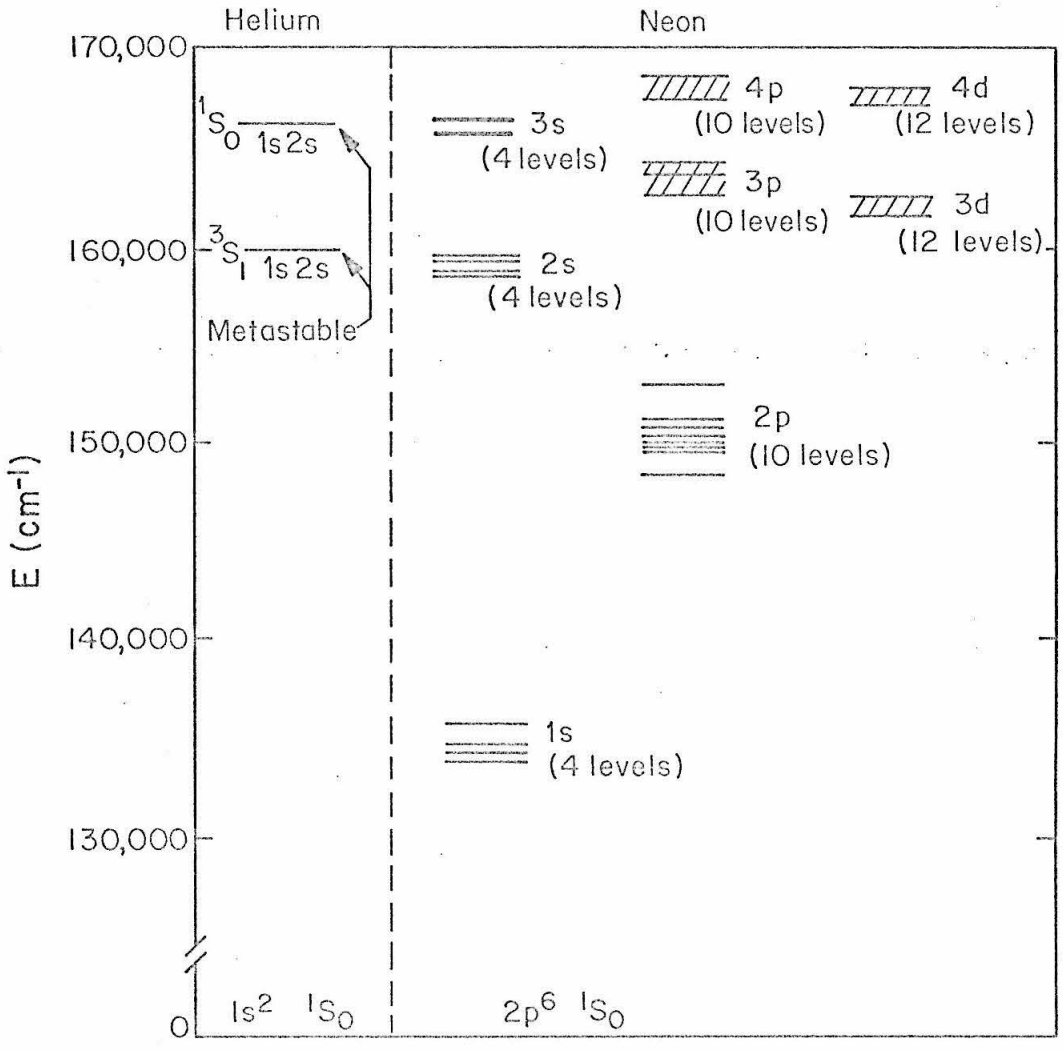

Figure 12

Atomic Energy Levels Pertinent to the He-Ne Laser

citation of the upper laser levels. Tables of the helium and neon energy levels, along with their designations and electron configurations, are found in reference 73. Paschen notation will be used in our discussions of the neon levels, and values for wavelengths in air will be used in discussing the transitions.

In a typical He-Ne laser tube the pressure ratio of He-Ne is about 10:1. The electrons of the gas discharge collide inelastically with helium ground state atoms and populate the helium metastable levels. Then excitation transfer collisions between the metastable helium atoms and ground state neon atoms populate some of the 2s and 3s levels of neon. The levels $3s_2$ and $2s_{2,3,4,5}$ are particularly populated as a result, and population inversion is created between these levels and the 3p and 2p levels.

The strongest emission line of the first He-Ne laser was the 1.1523-μ radiation from the $2s_2 \rightarrow 2p_4$ transition; laser oscillation was obtained on other 2s → 2p transitions at the same time (74). Visible red output can also be obtained; the most common line is at 6328-Å wavelength, from the $3s_2 \rightarrow 2p_4$ transition. The transition with by far the highest gain has been found to be the $3s_2 \rightarrow 3p_4$ transition at 3.3913-μ. This transition and the similar high gain $3s_2 \rightarrow 3p_2$ transition at 3.3903-μ are easily saturated, however. These properties make the 3.39-μ lines useful for studies of saturation effects in a laser amplifier.

If we disregard saturation effects for the present, we can write the gain equation for signal intensity in the form

$$dI/dz = 2\bar{\alpha}I \ , \tag{5.1}$$

which results in the common exponential gain behavior

$$I(z) = I_o \exp(2\bar{\alpha}z) = I_o \exp(2\alpha \mathrm{Re}\ w(0+ia)z) \ . \tag{5.2}$$

We defined the linear gain parameter α in Chapter 3, following (3.49); we write it again for convenience:

$$\alpha = \nu N_o \sqrt{\pi}\ |\langle b\|p\|a\rangle|^2/6\varepsilon_o hcku \tag{5.3}$$

The only parameters in this expression that depend on the particular transition are: N_o - the population inversion, $|\langle b\|p\|a\rangle|^2$ - the line strength, ν - the frequency, and ku - the Doppler width. Since the Doppler width is proportional to the frequency of the radiation, the latter two quantities cancel each other, and we are left with two quantities which depend on the transition: the population inversion and the line strength.

The experimentally determined gain parameters for the three transitions mentioned previously are

$$2\bar{\alpha}\ (3.3913\text{-}\mu) \sim 6\ m^{-1}$$
$$2\bar{\alpha}\ (1.1523\text{-}\mu) \sim .12\ m^{-1}$$
$$2\bar{\alpha}\ (\ .6238\text{-}\mu) \sim .06\ m^{-1}$$

when the discharge current is 10 ma., which is near the optimum current value for the 6328-Å oscillation when our lab processed tubes are used. (The gain value for the 1.1523-μ transition was obtained from reference 75; the other values were determined in the lab using a laser tube with gas pressure of 1 Torr and a ratio He:Ne = 10:1.) To obtain corresponding values for α, we must know the value for $a = \gamma_{ab}/ku$ for each transition. From our measurements, the value for the 3.3913-μ transition is a = 0.3 at the gas pressure given above. Comparing our measurements of the decay rates (described in the following chapters) with those of Decomps and Dumont (45), we conclude that the decay rate of the $3p_4$ level is about twice as large as that of the $2p_4$ level. Thus the value of $a = \gamma_{ab}/ku$ for the 6328-Å line should be about .03. The corresponding value of a for the 1.1523-μ transition should be about 0.1, according to the decay rate results in (45). We can now compute values for Re w(0 + ia) and obtain the following values for α:

$$\alpha(3.3913\text{-}\mu) \sim 4.0$$

$$\alpha(1.1523\text{-}\mu) \sim .07$$

$$\alpha(\ .6328\text{-}\mu) \sim .03$$

Faust and McFarlane (75) discussed the relative gains of these three transitions and calculated their line strengths, based on the j-1 coupling scheme of Racah (76) and the Coulomb approximation method of Bates and Damgaard (77). Their results gave a $3s_2 \rightarrow 3p_4$ (3.3913-μ) line strength about 5.5 times that of the $2s_2 \rightarrow 2p_4$ (1.1523-μ) line strength and slightly more than 100 times that of the $3s_2 \rightarrow 2p_4$ (.6328-μ) line. The reasons lay in the facts that the spatial overlap for tran-

sitions between states with the same principal quantum number is much larger, resulting in larger values for the overlap integrals; and that the larger spatial extent of the higher excited levels leads to larger values for these overlap integrals.

On the basis of these line strength calculations we conclude from looking at equation (5.3) that the measured values for α at 3.3913-μ and at 6328-$\mathring{A}$ are much different mainly because the line strengths for the two transitions are much different. Since the ratio of the measured values is $4.0/.03 \simeq 130$, the calculated line strengths do not quite account for the entire difference. Possibly the line strength calculations are slightly inaccurate, or possibly the remainder is due to differences in population inversion, N_o. The latter reason is possible since the $3p_4$ level decay rate is larger than that of the $2p_4$ level, meaning the steady-state population of the $3p_4$ level could be significantly less than that of the $2p_4$ level.

Faust and McFarlane did not allow for a non-negligible value of γ_{ab}/ku when making comparisons of gain measurements with line strengths; i.e., they set $\bar{\alpha} = \alpha$, using our notation. Thus their conclusions are not completely correct.

These results are in accord with the observations that the saturation signal intensity,

$$E_o^2 = 3\hbar^2 \gamma_a^0 \gamma_b^0 / |\langle b \| p \| a \rangle|^2, \tag{5.4}$$

as defined following (3.49), is about 50 mw/cm^2 for the 3.3913-μ line

and a few watts/cm^2 for the 6328-Å line (78). (We should note here that the discussion of gain constants for the 3.3913-μ and 6328-Å transitions in the introduction to reference 7 is misleading. The authors stated that one reason for the larger gain parameter at the longer wavelength transition was due to the smaller Doppler width; this is incorrect.)

5.3 Competition Effects in the He-Ne Laser

5.3.1 Effect of 3.39-μ Oscillation on Visible Output

Probably the most popular laser in the past decade has been the 6328-Å He-Ne laser. Since the 3.39-μ and visible transitions, such as the 6328-Å transition, have a common upper level, a He-Ne laser which is designed to oscillate at the 6328-Å wavelength will suffer due to the presence of 3.39-μ oscillation, since this tends to deplete the upper level population. Oscillation occurs at 3.39-μ even though the mirrors (which are dielectric coated for very high reflectance at 6328-Å) may reflect only 20% of the 3.39-μ radiation; the gain of this particular transition is high enough to overcome these large cavity losses.

Various methods of eliminating this 3.39-μ oscillation have been devised. One method of impeding 3.39-μ oscillation and simultaneously enhancing the 6328-Å output involves the use of magnetic fields. Experiments on this subject were first reported by Bell and Bloom (79), and as a result of these observations many commerical 6328-Å lasers now have small alnico magnets placed near the discharge tube to enhance the output.

A He-Ne laser tube with Brewster angle windows allows one

linear polarization component to pass through the window with no reflection losses, while the orthogonal component suffers fairly large reflection losses; hence the laser radiation is linearly polarized. This type of configuration is especially important for the visible output, since the low gain transition demands a low loss cavity in order to oscillate. Experience with laser tubes processed in the laboratory has shown that those tubes with Brewster angle windows which are slightly misaligned will allow the 3.39-μ line to oscillate more strongly, at the expense of the 6328-Å oscillation, due to the fact that the low gain transition is affected to a much greater degree by slight cavity losses.

When axial magnetic fields exist in the region of a laser discharge tube with Brewster angle windows, the 3.39-μ oscillation is selectively impeded due to two characteristics: the Doppler width at 3.39-μ is 5.5 times smaller than at 6328-Å, leading to a much more pronounced splitting of the gain curves for the circular polarization components; and the much higher gain of the 3.39-μ line means corresponding larger Faraday rotation of a linearly polarized signal. It has been shown theoretically (20, 35) that if a linearly polarized mode is oscillating at line center in a cavity with x-y anisotropies (due to the Brewster angle windows in our case), it will remain linearly polarized for values of applied axial magnetic field up to a certain critical value. (For larger fields this mode will split into circularly polarized components at slightly different frequencies.) However the polarization direction rotates as the field increases; the angle between the polarization direction at the critical field value and the original low-loss

polarization direction will be between 45° and 90°, depending on the amount of anisotropy in the cavity (35). This rotation occurs because the opposite effects of Faraday rotation and rotation at the anisotropy surfaces must balance each other in order for the condition of resonance to be met. As a consequence of this rotation, the cavity losses rise due to reflections at the Brewster angle windows. The polarization rotation of a 3.39-μ mode is much greater than that of a 6328-Å mode at a given value of axial field because Faraday rotation is proportional to α and is a monotonically increasing function of y (Ω/ku) for these transitions (see equation (3.55) and the following discussion). Hence the losses for the 3.39-μ mode are correspondingly larger than those of the 6328-Å mode. Bell and Bloom found that these loss effects on the 6328-Å radiation are more than offset by the beneficial effects of eliminating the 3.39-μ competition (79). If the magnetic field is larger than the critical value for the 3.39-μ mode but much lower than the critical value for the 6328-Å mode, the circular polarizations of the 3.39-μ radiation will suffer large losses at the Brewster angle windows, and the result will again be enhancement of the visible radiation. These ideas should remain valid for modes which are displaced slightly from line center because Faraday rotation is insensitive to this type of deviation.

For short laser cavities, such that the spacing of the cavity resonances is about the same as the 3.39-μ Doppler width, transverse magnetic fields can also be effective in reducing the effect of 3.39-μ competition on the visible output. If we call the direction of the magnetic field the y-direction, then the Brewster angle windows should

be set to pass x-polarized radiation with no reflection losses. The gain curves for the 3.39-μ x-polarization will split as the magnetic field increases, and the total gain for a cavity resonance near line center will decrease. Since the Doppler width for the 6328-Å transition is much larger, the Zeeman splitting will have an insignificant effect on its gain. Laboratory experiments with a 55 cm. laser cavity have shown that the use of small alnico magnets arranged to give inhomogeneous transverse and axial fields will reduce the amount of 3.39-μ power output to a greater extent if the Brewster angle windows are set to pass x-polarization with no losses, as described above, rather than being set to pass y-polarization with no losses.

Another method of eliminating 3.39-μ oscillation in a 6328-Å laser involves the use of methane gas in the cavity. The peak of the P_7 branch of the ν_3 vibration-rotation absorption band of methane is within .01 $cm.^{-1}$ of the neon $3s_2 \rightarrow 3p_4$ transition (81, 82). This coincidence allows one to use a methane absorption cell of short length (1 cm.) in the laser cavity to completely eliminate 3.39-μ oscillation. If the absorption cell is made with Brewster angle windows, it will pass the 6328-Å radiation with no significant losses; hence the overall effect is an enhancement of the visible output. A more detailed discussion of this methane absorption line will be given in section 5.5.

5.3.2 The Effect of Methane Gas on the 3.39-μ Laser

Optimum power output at 3.39-μ calls for a pair of mirrors with reflectance product equal to about .5 - higher than the reflect-

ances that the mirrors which are dielectric coated for use at 6328-Å happen to give, yet much lower than the required reflectances for 6328-Å oscillation. When methane gas is introduced into this type of cavity, the $3s_2 \rightarrow 3p_4$ oscillation is quenched, as expected; however Moore (80) first noticed that, as a consequence, another line oscillates: the $3s_2 \rightarrow 3p_2$ line at 3.3903-μ, about 1 $cm.^{-1}$ higher than the dominant 3.3913-μ line. The linear gain parameter, α, for this transition was estimated to be 1/3 that of the $3s_2 \rightarrow 3p_4$ transition (80). This is quite high compared with other transitions, but not high enough to oscillate in the usual visible laser cavity with mirrors coated for high reflectance at the red wavelengths.

When the stronger $3s_2 \rightarrow 3p_4$ line is allowed to oscillate, it saturates the transition quite easily, reducing the $3s_2$ level population and raising the $3p_4$ and $3p_2$ level populations (the latter effect is due to collisions - the extent of this collision induced transfer is not known). This prevents oscillation on the $3s_2 \rightarrow 3p_2$ transition. The use of higher reflectance mirrors would require less gain at the 3.3903-μ line in order for it to oscillate, but this also would cause the 3.3913-μ oscillation to saturate the transition to a greater extent, and the result is the same - no 3.3903-μ oscillation. Only the introduction of the selective absorber methane changes the picture.

We have studied this 3.39-μ competition effect by placing a 1 cm. methane absorption cell in a He-Ne laser cavity with mirror reflectances at 3.39-μ of 99% and 50%, and discharge tube measurements of 50 cm. length and 2.6 mm. diameter. The total pressure in the tube was 1.5 Torr, with a He:Ne ratio of 14:1. The laser output was passed through a Spex spectrometer with a resolution of .2 cm^{-1} in order to

observe the relative intensities of the two 3.39-μ lines for various pressures of methane in the absorption cell. The intensities of the two lines were almost equal when the pressure was about 7 Torr, and above 10 Torr the 3.3913-μ line was eliminated, leaving only the 3.3903-μ line. The results were substantially the same for pressures ranging from just above 10 Torr to about .5 atmosphere. At atmospheric pressure the 3.3903-μ power output was slightly lower, due most likely to pressure broadening of the methane absorption peak.

5.4 The Experimental Facility

The experimental apparatus for the study of saturation effects in a 3.39-μ laser amplifier was assembled on a heavy steel table whose surface dimensions are 260 cm. by 120 cm. This table rests on a concrete slab in a sub-basement laboratory. Most of the apparatus was bolted to the table for long-term stability. Power supplies for the apparatus resided in a rack beside the table.

Figure 13 depicts schematically the basic setup for the measurements of gain, Faraday rotation, and nonlinearity-induced anisotropy. The abbreviations in the Figure are

A - analyzer

BS - beam splitter

C - chopper

D_1, D_2 - InAs detectors

I - iris

L_1, L_2, L_3 - lenses

MG - magnet

P_1, P_2 - attenuating polarizers

PZT - piezo-electric tuner

QWP - quarter wave plate

R - one-ohm resistor

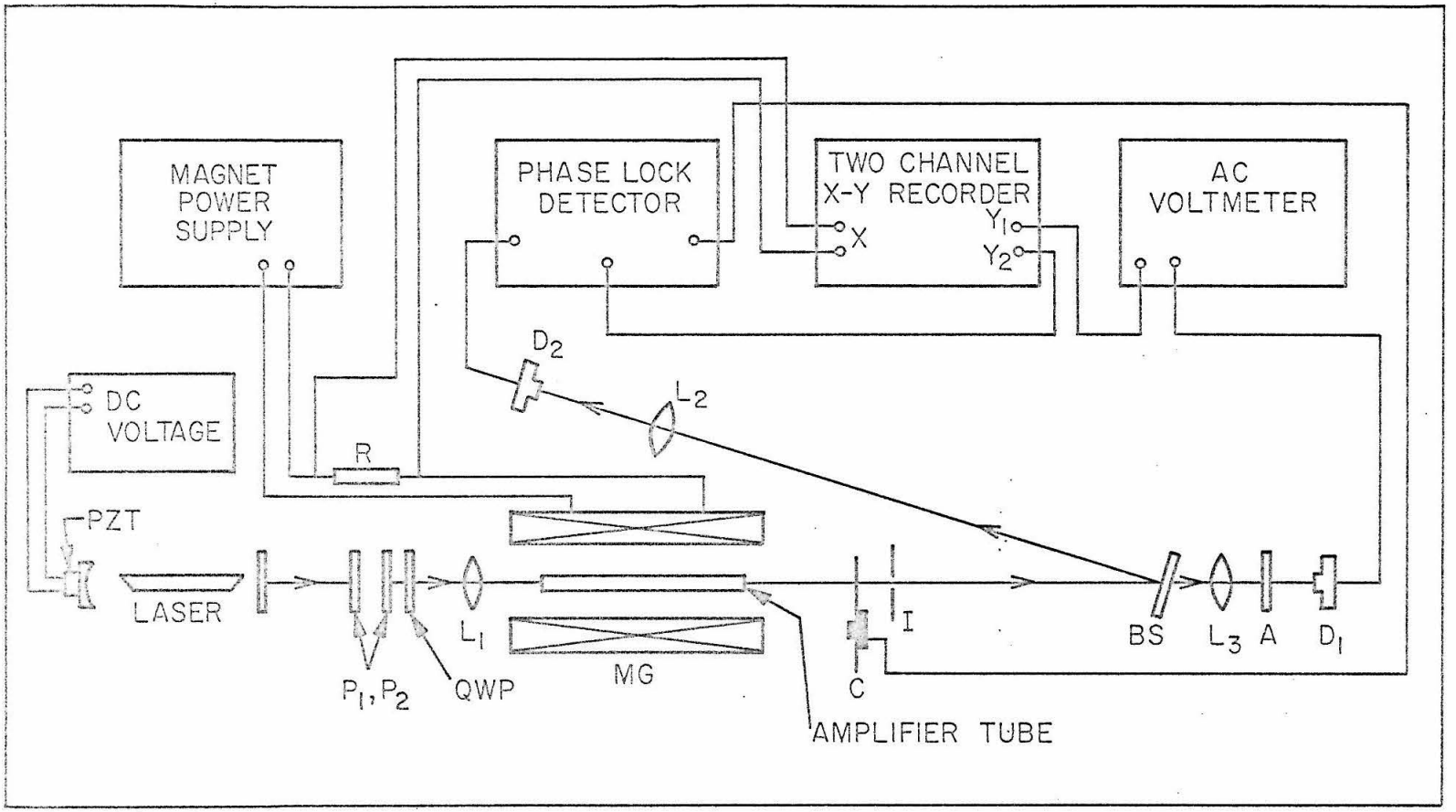

Figure 13

The Experimental Setup

A	Analyzer	I	Iris	PZT	Piezo-electric Tuner
BS	Beam Splitter	L_1, L_2, L_3	Lenses	QWP	Quarter-Wave Plate
C	Chopper	MG	Magnet	R	Resistor
D_1, D_2	InAs Detectors	P_1, P_2	Attenuating Polarizers		

The length of the He-Ne laser oscillator cavity was 55 cm., which produced a longitudinal cavity resonance spacing of about 275 MHz. This was sufficient spacing to obtain single TEM_{ooq} mode output at either of the 3.39-μ wavelengths. The spherical mirror which was connected to the PZT had a reflectance of nearly 100%, while the reflectance of the flat output mirror was 50%. This reflectance was low enough such that only the $3s_2 \rightarrow 3p_4$ line at 3.3913-μ could oscillate under normal conditions. By placing a 1 cm. length methane absorption cell in the cavity, with methane pressure above 10 Torr, we could quench the $3s_2 \rightarrow 3p_4$ oscillation and obtain oscillation on the $3s_2 \rightarrow 3p_2$ line at 3.3903-μ. The He-Ne discharge tube used in the laser cavity was 45 cm. long with a bore diameter of 2.6 mm., and it had Brewster angle windows.

The laser oscillator output was passed through a variable attenuator consisting of two calcite polarizers and given the desired polarization ellipticity with the quarter wave plate. (The measurements of gain and rotation versus magnetic field for a linearly polarized signal were conducted without the quarter wave plate.) The beam was collimated with a quartz lens and then passed through a He-Ne amplifier tube with a discharge length of 50 cm. and a bore diameter of 3.8 mm. The beam diameter was slightly greater than 2 mm. throughout the length of the tube. The amplifier tube was first filled to a pressure of 1.0 Torr with a 9:1 mixture of He^3 and Ne^{20} and sealed off. For later measurements it was connected to a vacuum station so that the pressures of the He^3 and Ne^{20} could be varied. The tube was centered in a magnetic field solenoid which covered the entire section of the discharge

that took part in the laser process. The normals to the plane windows of the amplifier tube were tilted about 2° from the axial direction in order to reduce reflection instabilities.

The amplifier output beam was chopped at a frequency of 220 Hz; and then it passed through an iris, which blocked almost all of the axially directed spontaneous emission from the amplifier. In later experiments the chopper was placed in front of the amplifier tube, the result being that only the chopped laser signal could be detected by the AC detection system. This method is more effective in eliminating spontaneous emission "noise"; however, for our experiments both methods proved to be adequate.

The beam was then split by a silicon flat whose normal was placed at a small angle with respect to the beam direction. The transmitted portion was analyzed with a calcite analyzer and detected with an indium arsenide photodiode. The reflection channel was focused directly onto another InAs photodiode. The photodiode signal outputs were fed into separate detector meters, each having a DC output proportional to its meter deflection. (The PAR phase-lock detector is superior in sensitivity to the signal, since it can reduce the noise bandwidth to a few hertz or less. It was used alone when making gain saturation measurements.)

For most of the measurements the DC outputs of the AC detection channels were each connected to a Y channel of an XY two-channel recorder. When the magnetic field was a variable, the x-axis channel was connected as shown in Figure 13, so that the x-axis deflection was proportional to the axial magnetic field. When the mea-

surements of zero-field nonlinearity-induced anisotropy were made, the x-axis was swept at a low rate of 50 sec./in. by an internal sawtooth signal. More detailed accounts of the detection methods pertinent to each experiment will be given in the following chapters.

In order to tune the signal from the laser oscillator to line center, the signal was attenuated and passed through the amplifier tube in the presence of an axial magnetic field of approximately 60 gauss. Then the PZT voltage was varied (this changes the mirror separation, or cavity length, over a distance of a few microns) to tune the oscillator signal to the point at which the ellipticity of the amplifier output decreased to zero. Since the amplifier input signal was linearly polarized, it would remain linearly polarized under these conditions only if it were at line center. The high gains of the 3.39-μ signals make this method of tuning to line center quite effective. The maximum drift encountered during the observation periods was about ±2 MHz. These results were obtained when the mirror connected to the PZT unit was shielded from air currents, due mainly to the chopper. The shielding was effected by placing a glass slide or the absorption cell directly in front of the mirror holder, or by placing a cylindrical plexiglass sheath between the mirror holder and the discharge tube.

Magnetic field measurements were made using a Bell Model 120 Gaussmeter with an axial probe. Effects of the steel table on the magnetic field produced at the position of the amplifier tube were found to be negligible. The axial component of the earth's field could be balanced out by the solenoid, leaving a residual transverse magnetic field of .38 gauss. The effects of this residual transverse field and

the effects of the slight inhomogeneities in the axial field produced by the solenoid will be discussed in chapter 8.

5.5 A Study of the Methane Absorption Line at 3.3913-μ

By placing an absorption cell of 15 cm. length in the path of the reflected beam of Figure 13, we were able to scan the absorption profile of the P_7 branch of the ν_3 absorption band of methane at 3.3913-μ. A short (32 cm. length) laser tube was placed in a cavity of 40 cm. length for use as a single-mode laser oscillator, tuneable over a 300 MHz region. The discharge current of the laser oscillator tube was set at a low value (about 4 to 5 ma) in order to reduce the gain of the oscillating $3s_2 \rightarrow 3p_4$ line and the consequent mode pulling effect. The PZT voltage was varied over a finely controlled range by a Helipot, and the voltage was monitored with a Darcy 440 Voltmeter, so that voltage precision of one part in 500 could be attained - the limit was set by the output fluctuations of the Hewlett-Packard Model 712A voltage supply. The voltage precision meant a 1 MHz frequency tuning precision capability for the laser oscillator.

The line center was first determined by the method discussed in the previous section. Using the 3.3913-μ line, we were able to determine line center to within ±1 MHz in this manner. Following this determination the amplifier tube was turned off, and a calibration plot of the channel sensitivities was taken. Then the methane was introduced into the absorption cell, and the laser tuning voltage was varied in order to scan the methane absorption peak. After each run at a particular pressure of methane, a line center determination was made in order to

take slow drifts into account.

Due to the high gain of the 3.39-μ laser ($\bar{\alpha} \simeq 1.0\ m^{-1}$ for the low values of discharge current used), there was appreciable mode pulling toward line center. Calculations based on Bennett's analysis (6) show that the mode pulling for this case is about 6% of the separation from line center for a frequency separation between cavity resonance and line center of less than .5 times the Doppler width. The methane peak occurs barely within this interval, and we have corrected our results to account for this effect. This mode pulling phenomenon reduces our accuracy, though; our calculated distance of the methane peak from the neon $3s_2 \rightarrow 3p_4$ line center could be off by a few MHz. For this reason we have rounded off the result to the nearest 5 MHz.

Our results for three pressures of methane are shown in Figure 14. The absorption peak is displaced 125 MHz higher than the $3s_2 \rightarrow 3p_4$ line center, which is at 2947.902 $cm.^{-1}$ (73). The line half-width increases at higher pressures due to pressure broadening. The low pressure half-width is 130 MHz, which corresponds very well with the Doppler half-width at half-maximum intensity of 130 MHz for methane at 290°K. The values for the peak absorption at the three pressures correspond to an absorption coefficient of about 0.12 $cm.^{-1}$ $Torr^{-1}$. This value is consistent with our experimental studies involving the use of the 1 cm. length intracavity absorption cell, discussed in section 5.3.

The 3.39-μ laser has been used to scan this methane absorption line in a different manner by Gerritsen and Heller (82), and by Goldring et.al. (83). They tuned the output of a multi-mode 3.39-μ laser over a

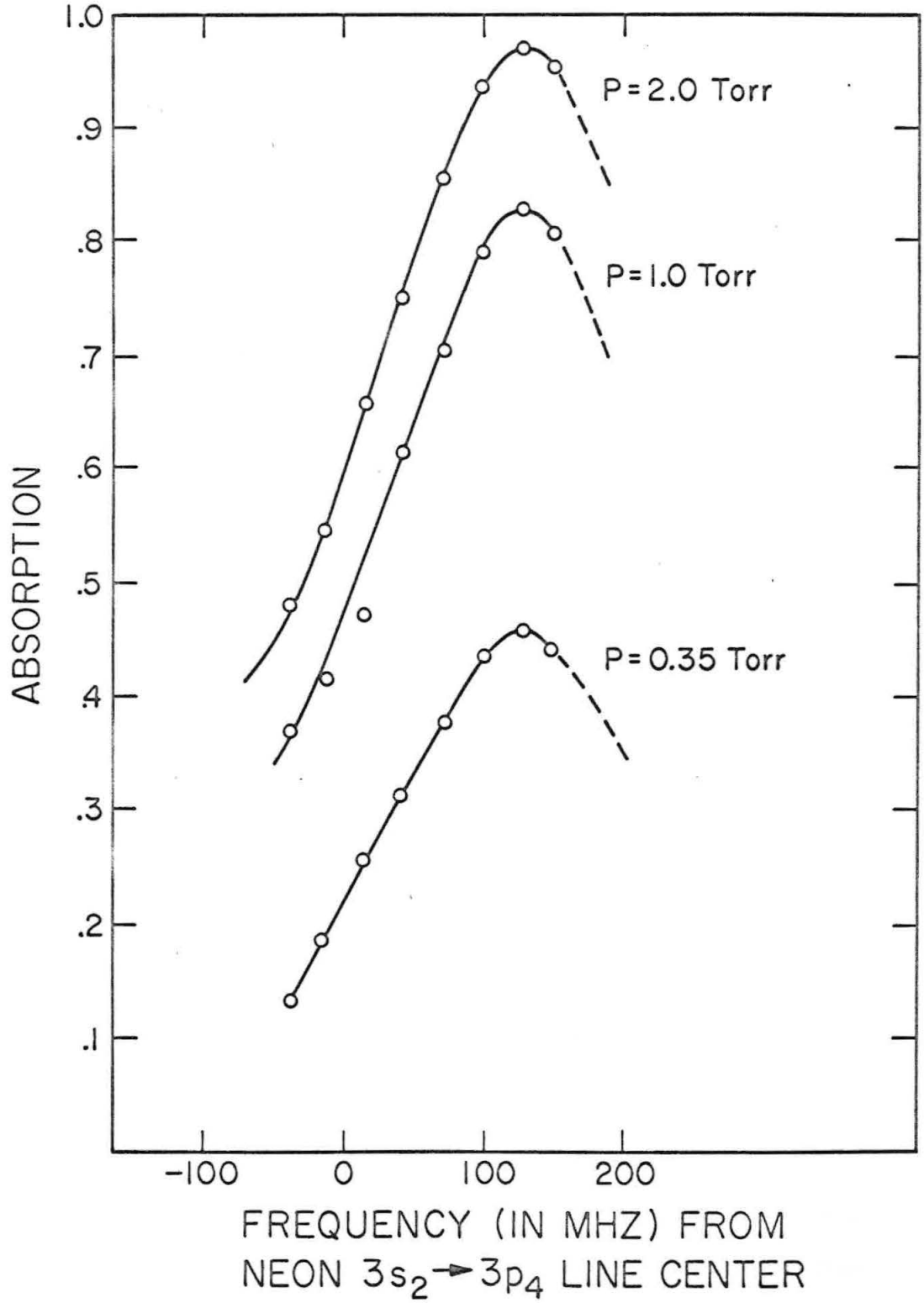

Figure 14
The Methane Absorption Peak Near the $3s_2 \rightarrow 3p_4$ Neon Transition

much larger range by applying an axial magnetic field and eliminating one polarization component. They assumed that the spectral output of the laser could be approximated by a continuous Doppler lineshape whose center frequency was tuned by the magnetic field. Aside from the questionable accuracy of this approximation, this puts a limitation on the "slitwidth" of the laser spectrometer of about 100 MHz (82), which is about four orders of magnitude larger than the resolution obtained through the use of a single-mode output scan. This method also suffers from mode pulling effects, which would weight the center of the assumed "Doppler lineshape" more than the wings. The mode pulling effects probably do not play as significant a part as they do in the single-mode method, however. The main advantage of the method of Gerritsen and Heller is the capability of a larger tuning range.

A clever means of studying the "phase-memory" linewidth of this methane line involves the saturation of its absorption by the intracavity 3.39-μ laser signal (84). This is similar to the study of the homogeneous linewidth of a laser transition by observing the "Lamb dip". Both methods succeed in being able to study pressure broadening of the natural linewidth even though the pressure broadening is much smaller than the Doppler broadening.

Gerritsen and Heller (82) concluded that the peak of the methane line was about 120 MHz blue of the neon $3s_2 \rightarrow 3p_4$ line center, which agrees fairly well with our results. Their estimated value for the absorption coefficient, based on measurements taken at a methane pressure of 0.7 Torr, was 0.18 cm^{-1} $Torr^{-1}$. This is quite a bit higher than our value of 0.12 cm^{-1} $Torr^{-1}$.

Now let us consider the amount of pressure broadening which we observed. References 82 and 84 report a pressure broadening half-width coefficient of about 8 MHz/Torr for pure self-broadening. Using this value, we would expect to observe a slight broadening of the Doppler lineshape at the wings of the line when the methane pressure is 1 to 2 Torr. The lineshapes would be broadened in a manner similar to those shown in Figure 2. The lineshape for low pressures corresponds to $a = 0$, and the lineshape for 2.0 Torr pressure would correspond to a value of $a \simeq .125$. (This is based on a Doppler halfwidth of 130 MHz.) Our experimental lineshape for a methane pressure of 2.0 Torr corresponds to a value of $a \simeq .25$, however. This discrepancy is probably due to an incomplete compensation for the effect of mode pulling in our analysis.

CHAPTER SIX

APPLICATION OF LOW PRESSURE THEORIES TO THE 3.39 MICRON TRANSITIONS OF He-Ne

6.1 Introduction

Our first experimental studies of saturation effects were performed with an amplifier tube which was filled to a pressure of 1.0 Torr, with a 10:1 ratio of He:Ne. The tube was sealed off, so there was no way of varying the gas pressure and observing effects on the amplifier characteristics. The experimental data were compared with the existing low pressure theories: the weak signal isotropic decay theory of Chapter 3 and the strong signal theory of Chapter 4. It was felt at the time that the gas pressure for this tube was low enough so that these theories would be applicable.

The results of these experiments are presented in this chapter. The gain and Faraday rotation data for a linearly polarized input signal correspond quite well with theoretical curves, assuming certain values for the decay rates and linewidths. The nonlinear "dips" for low values of magnetic field are observable for the $(J = 1 \text{ to } J = 1)$ 3.3903-μ line but not for the $(J = 1 \text{ to } J = 2)$ 3.3913-μ line. The nonlinearity-induced anisotropy data for an elliptically polarized input signal operating on the $J = 1$ to $J = 2$ transition deviate from the theoretical predictions, however. The deviation is slight, so that one could logically blame this on some sort of systematic error. However we shall see in the following chapter that this type of deviation should be ex-

pected when pressure effects are considered.

6.2 Linearly Polarized Input Signal: Gain and Faraday Rotation

The basic setup for the gain and Faraday rotation measurements is described in Section 5.4 and pictured in Figure 13. The quarter wave plate shown in Figure 13 was not used for these experiments, so that the input signal to the amplifier was linearly polarized.

First the magnetic field was set at zero while the gain was measured for input signals of various intensities. Care was taken to keep the signal at line center by monitoring the signal in the manner described in Section 5.4. It was also important to wait until the amplifier tube was warmed up before taking gain measurements. The experimental results for each of the 3.39-μ signals are shown in Figures 15 and 16, along with theoretical curves which are based on the strong signal equations (4.10) and (4.14), for $r = 0$. These data demonstrate the previously mentioned fact that the small signal gain for the $3s_2 \rightarrow 3p_4$ ($J = 1$ to $J = 2$) transition is significantly larger than that for the $3s_2 \rightarrow 3p_2$ ($J = 1$ to $J = 1$) transition. The degree of gain saturation at high signal strengths depends on the value of the normalized homogeneous linewidth, a. For a given value of the parameter a, the saturated gain remains relatively constant even though the small signal gain varies over a certain range; this is demonstrated in Figure 16 by the two gain curves for $a = 0.3$. The data for both transitions fit the gain saturation curves when $a = 0.3$. Further measurements of gain saturation yielded values for a which were consistently between 0.3 and 0.35. We used these results to assume for purposes of later

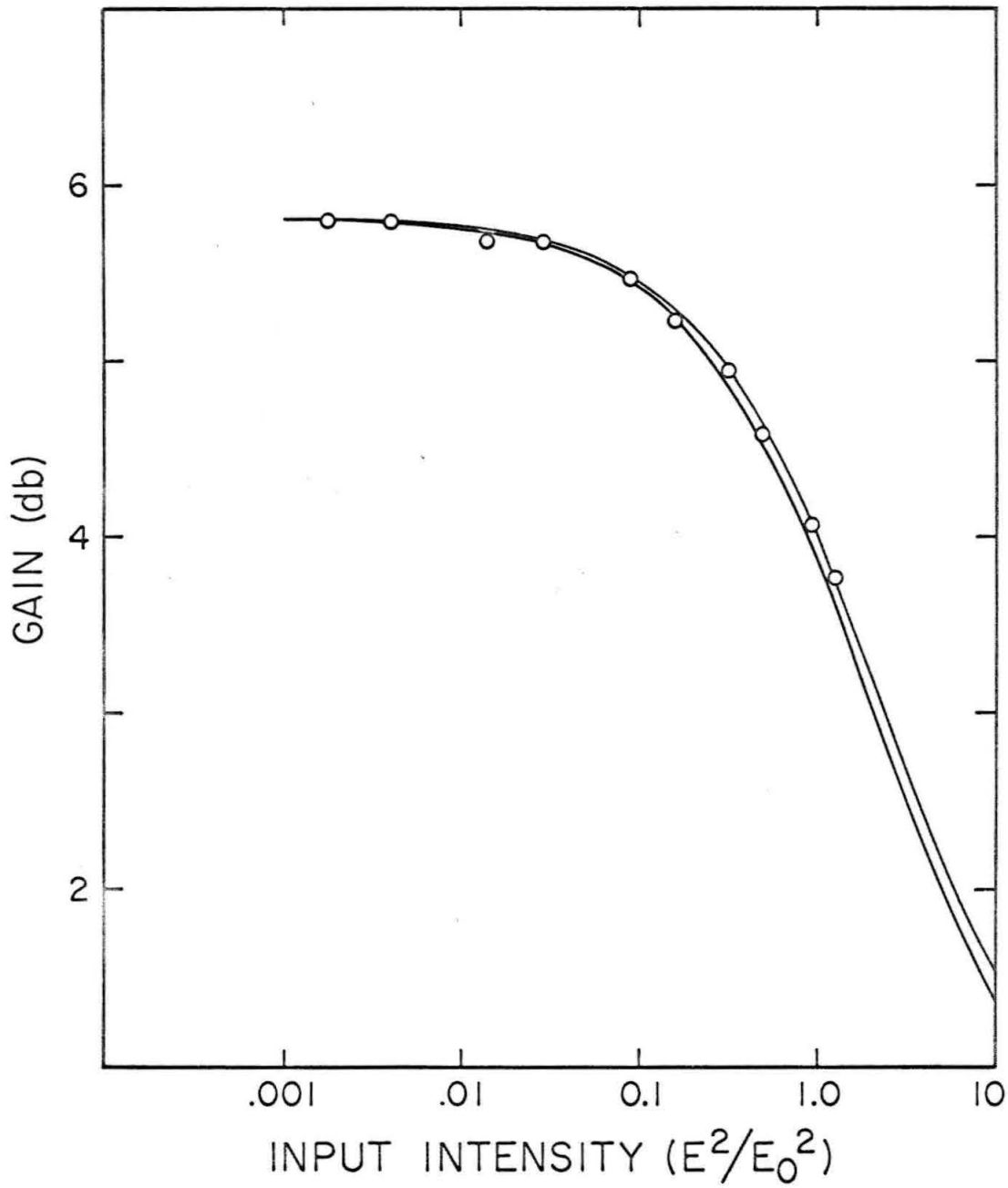

Figure 15

Gain Saturation for J = 1 to J = 1, with Strong-Signal Theoretical Curves: G_o = 5.75 db, a = 0.3 (upper); G_o = 5.75 db, a = 0.4 (lower)

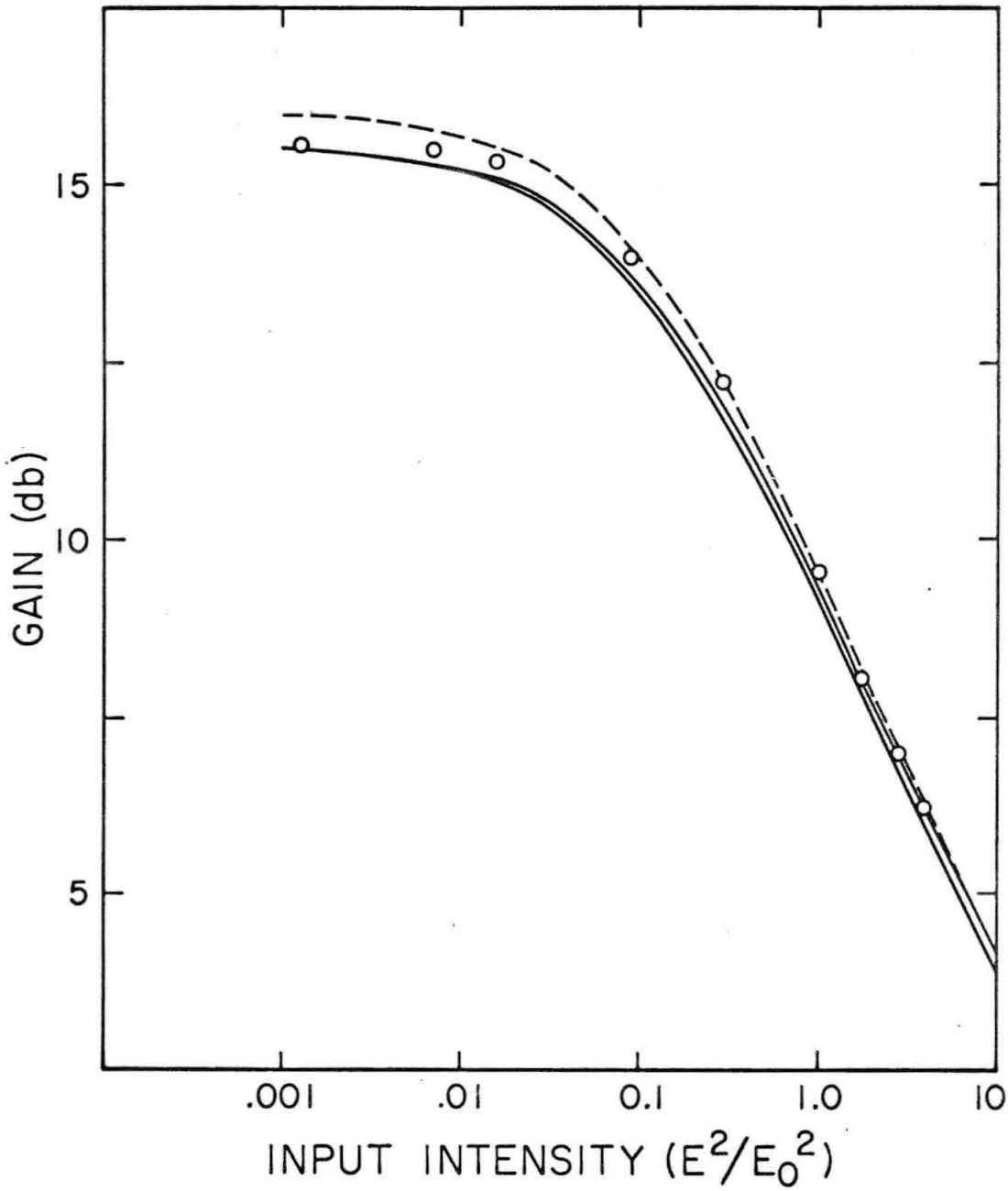

Figure 16

Gain Saturation for J = 1 to J = 2, with Strong-Signal Theoretical Curves: G_o = 16.0 db, a = 0.3 (dashed); G_o = 15.5 db, a = 0.3 (upper solid); G_o = 15.5 db, a = 0.4 (lower solid).

calculations that the decay rates of the $3p_2$ and $3p_4$ levels are equal, and that the homogeneous linewidths were 0.3 times the Doppler width parameter, ku.

Measurements of Faraday rotation and gain versus axial magnetic field were then taken, making use of the two-channel XY recorder shown in Figure 13. The x-axis deflection was arranged to be proportional to the axial field. Then the analyzer A in the transmission channel (channel 1) was set at 45° with respect to the plane of polarization of the signal when the magnetic field was zero. If we call the output signal intensity at zero magnetic field I_o, and the output signal intensity at a non-zero value of magnetic field I(y), then the two recorder plots simultaneously yielded the quantities $I(y)\cos^2\theta/I_o\cos^2(\pi/4)$ and $I(y)/I_o$. Thus the gain variation with magnetic field was obtained directly, and the Faraday rotation angle, $\Phi = \theta-(\pi/4)$, was obtained through simple calculations. Four plots were taken for each value of input signal intensity, and the process was repeated for various values of input signal intensity.

The results of these measurements are shown in Figures 17 through 20. In these figures each experimental point represents an average from four successive measurements taken under the same conditions. The error brackets represent plus and minus one standard deviation based on these measurements. With the values of $\alpha = 1.76\ m^{-1}$ and $a = 0.3$, determined from the gain saturation data, and with $\Omega_a/2\pi$=1.82 MHz/gauss, $\Omega_b/2\pi$=1.97MHz/gauss, good fits to the experimental points of Figures 17 through 19 were obtained for $A = 0.05$, $B = 0.25$, and $\frac{1}{2}ku = 165$ MHz. The discharge current was 12 ma. during the course of these measurements.

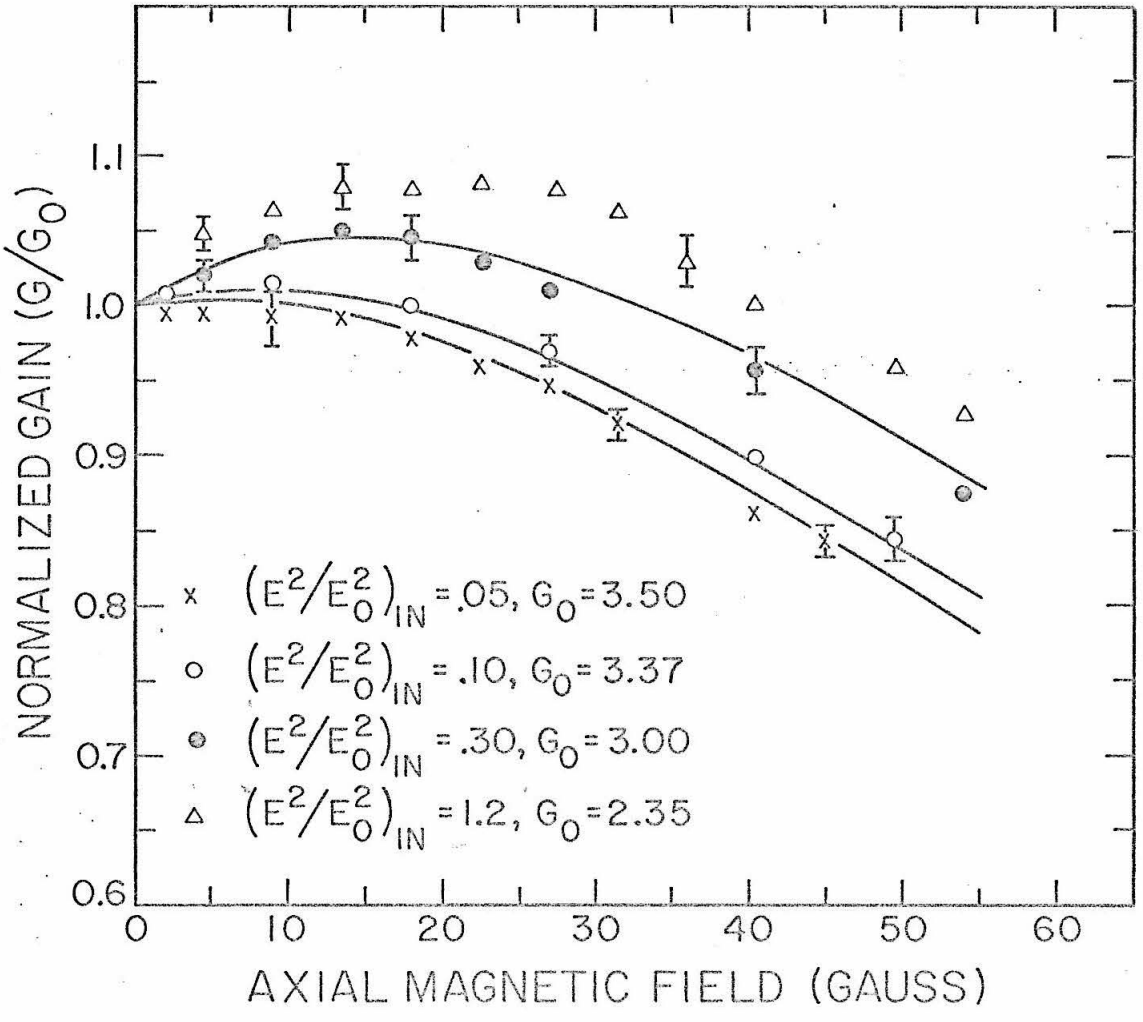

Figure 17

Gain versus Axial Magnetic Field for Various 3.3903-μ (J = 1 to J = 1) Input Signals. $\alpha = 1.76\ m^{-1}$, a = 0.3.

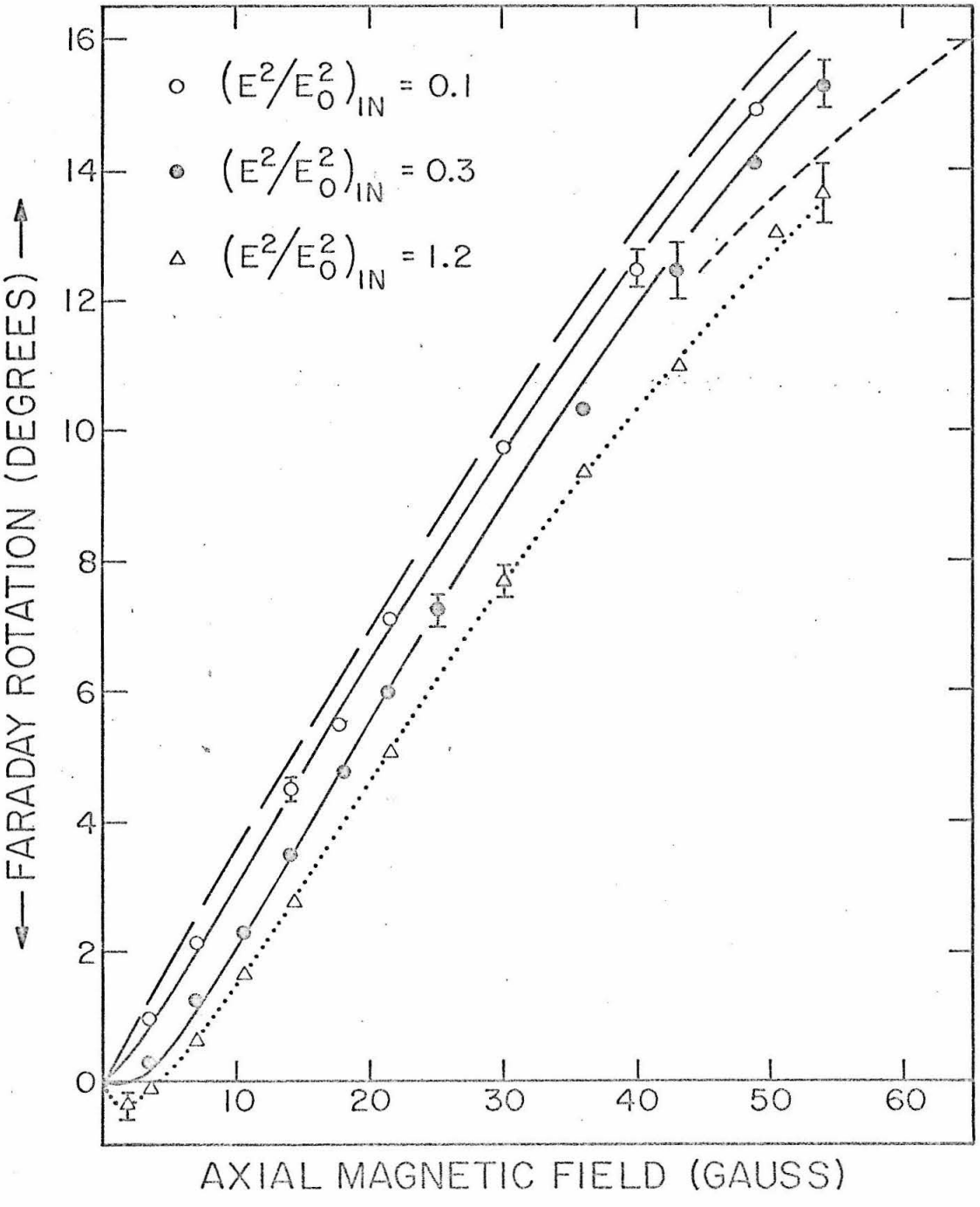

Figure 18

Faraday Rotation for Various 3.3903-μ (J = 1 to J = 1) Input Signals. $\alpha = 1.76\ m^{-1}$, a = 0.3.

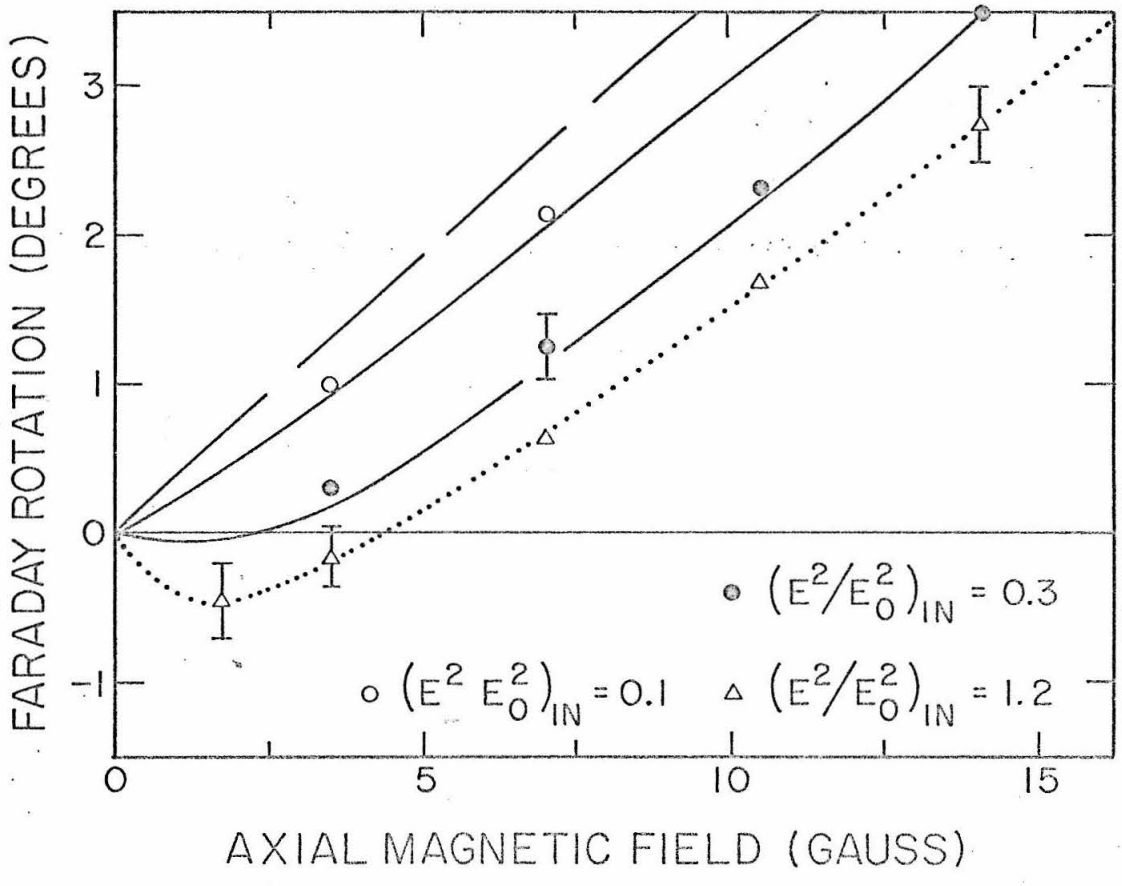

Figure 19

An Enlargement of the Weak Magnetic Field Region of Figure 18.

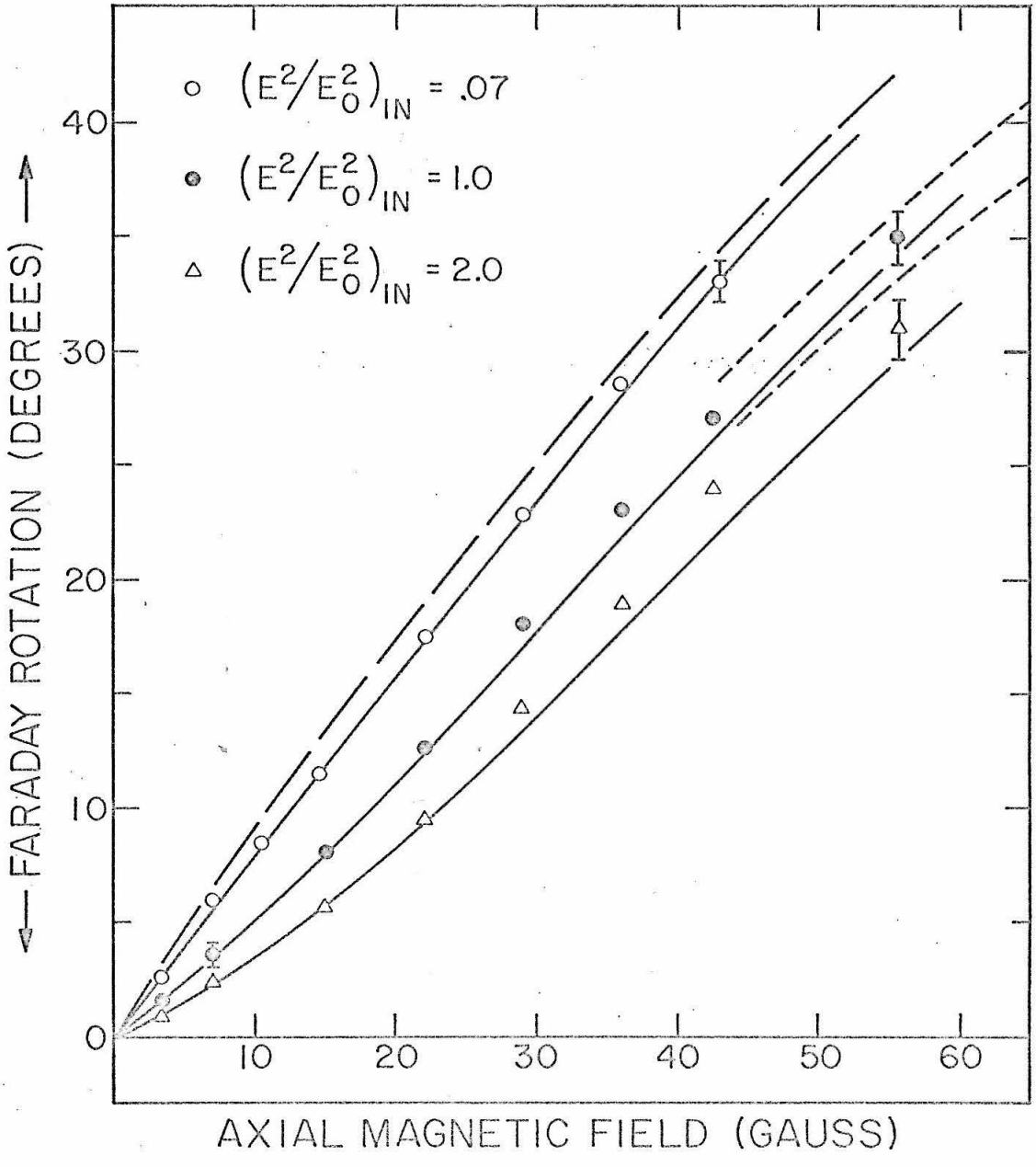

Figure 20

Faraday Rotation for Various 3.3913-μ (J = 1 to J = 2) Input Signals. $\alpha = 4.96\ m^{-1}$, a = 0.3.

Figure 17 shows the traveling wave gain dip at small values of magnetic field for the $J = 1$ to $J = 1$ signal. The solid lines were obtained from equation (3.57), using the isotropic decay limit. According to this theory the dip width depends on the value of A, since it occurs because of the effects of coherence existing among the upper sublevels. This gives a good method of determining the upper level decay constant.

Figure 18 shows the Faraday rotation for the $J = 1$ to $J = 1$ signal, and Figure 19 is a more detailed view of the low magnetic field region of Figure 18. It is obvious that a dip in the Faraday rotation occurs at small values of magnetic field for sufficiently strong signal intensities. The long dashed curve is the unsaturated Faraday rotation obtained by assuming the polarization of the medium to be linearly dependent on signal strength:

$$\Phi_{\ell} = \alpha z \ \mathrm{Im}\ W(y) \tag{6.1}$$

where

$$W(y) = \sum_{M} C^2_{M,M-1}\ w(y_b + M\delta + ia)$$

$$= .5\ w(y_b + ia) + .5\ w(y_a + ia) \tag{6.2}$$

The solid curves in Figures 18 and 19 are theoretical curves obtained by using equation (3.58), assuming isotropic decay. We see that the weakly saturating signal theory gives good fits to experimental points in its region of validity. We observe a <u>reversal</u> of the Faraday

rotation at small magnetic fields when $I_{in} = 1.2$, as predicted in Chapter 3, although the weak signal theory ceases to be quantitatively valid for such signal strengths. (The dotted curve is merely a line joining the experimental points.) Presumably larger signals would produce a larger dip in the rotation; thus our theoretical predictions are qualitatively accurate for strong signals.

The short dashed line in Figure 18 is a theoretical curve using equations (4.12) and (4.13). Since the value of y_a at 50 gauss is 0.55, the condition of validity of (4.12) and (4.13) is not quite satisfied for magnetic fields of this size. The effects of the coherent interactions are not quite negligible in this region, as is assumed in the derivation of (4.12) and (4.13); thus we expect the experimental points to be a little lower than the dashed curve.

Figure 20 shows the Faraday rotation for the $J = 1$ to $J = 2$ signal. The discharge current was 14 ma during the course of these measurements. The long dashed curve is once again the unsaturated or linear rotation, for a value of $\alpha = 4.96\ m^{-1}$ and for $\Omega_b/2\pi = 1.67$ MHz/gauss. Comparison of Figures 18 and 20 supports our argument that the effects of the coherent interaction terms are much stronger for a $J = 1$ to $J = 1$ transition than for a $J = 1$ to $J = 2$ transition. There are no dips in the curves shown in Figure 20, even for large values of input signal strength.

The weak signal theory presented in Chapter 3 was not very useful when applied to this transition. For signal strengths which are low enough such that the perturbational results are valid, the degree of saturation is so small that the difference between unsaturated

and saturated Faraday rotations is within the error limits for the experimental points. The gain for the case $I_{in} = 0.07$ in Figure 20 was 26, which means that near the output end of the amplifier the signal strength was too large for the weak signal theory to be applicable; and the results for this case indicate only a slight decrease in Faraday rotation from that predicted by the linear theory.

The short dashed lines in Figure 20 were obtained from equations (4.22) and (4.23). These equations assume the circular component interactions are negligible, and the comments made for the short dashed line in Figure 18 hold here also.

Equation (4.18) was used to obtain the solid lines of Figure 20. (This involved an extensive numerical integration first over velocities and second over the axial distance z. Thanks go to A. Dienes and M. Sargent III of Bell Telephone Labs for developing the computer programs and performing this numerical integration.) In deriving equation (4.18) we assumed the left and right circular components interact via the upper sublevels only, and that $B = a = 0.3$. Actually B is smaller than this value; since the nonlinear interaction terms are proportional to B, this probably results in predicting too much saturation. We see that the experimental points are slightly higher than the solid curves, but the overall fit is good.

In general, good agreement between experiment and the predictions of the low pressure theories was found. Although there was reason to believe that the assumption $\gamma_a + \gamma_b = 2\gamma_{ab}$, which these theories contain, was not strictly valid for a gas pressure of 1.0 Torr (30), the relaxation of this condition was not necessary for the gain

and Faraday rotation experiments presented in this section. The experimental points for the $J = 1$ to $J = 1$ signal were found also to agree with weak signal theoretical predictions (at signal strengths for which the weak signal theory was valid) assuming $2\gamma_{ab} > \gamma_a + \gamma_b$ and isotropic decay. The values of the homogeneous linewidth parameter for which good fits were made were $0.3 \leq a \leq 0.35$, and the corresponding range for the lower level decay rate parameter was $.25 \geq B \geq .20$. The value of the upper level decay rate parameter, which is given by the dip width, remained at $A = .05$. The values $A = 0.5$, $B = .20$, $a = .35$ are probably closer to the actual decay rates. Thus these experiments yielded an accurate value for A but only approximate values for B and a.

6.3 Elliptically Polarized Input Signal; Nonlinearity-Induced Anisotropy

For measurements of zero field nonlinearity-induced anisotropy, or the change in ellipticity of a signal as it passes through the amplifier when no axial magnetic field is applied, the arrangement in Figure 13 was used, with the exception that the x-axis of the XY recorder was disconnected from the magnetic field solenoid and allowed to sweep at a slow (50 sec./in.) rate. The signal was tuned to line center while the quarter wave plate (QWP) was removed; then the QWP was placed in its position, and measurements of intensity and ellipticity of the output signal were made for various values of input signal intensity. Channel 2 in Figure 13 measured the intensity, while the analyzer in channel 1 was rotated manually to read the maximum and

minimum of the signal polarization ellipse. The slowly sweeping recorder pens plotted this information. In this manner slight fluctuations in output signal intensity could be taken into account when computing the ellipticity of the signal, because the two pieces of information were recorded simultaneously on paper. The accuracy necessary to detect the nonlinearity-induced anisotropy with reasonable error limits required the use of this method of measurement.

When the measurements were complete, the amplifier tube was turned off, and measurements of the ellipticity and the intensity at the same settings of the attenuator were then made. This information was enough to determine gain saturation and ellipticity change at various input signal strengths, which were given in terms of the saturation intensity parameter, E_o^2.

The results for the $J = 1$ to $J = 2$ signal at 3.3913-μ are shown in Figure 21. The small signal gain constant for these results was $\bar{\alpha} = 3.1$ ($\bar{\alpha} = \alpha$ Re $w(0 + i.3)$), which corresponds to a linear gain of 22. The amplifier tube discharge current was 12ma. The input signal ellipticity,

$$r = \left[\frac{E_- - E_+}{E_- + E_+}\right]_{in} ,$$

was set at .600 ± .002. The reading error for the ellipticity measurements was better than ± .002. This kind of accuracy necessitates calibrations of the nonlinearities of the detection equipment responses. These calibrations were performed, and more detailed comments about them are in Chapter 8.

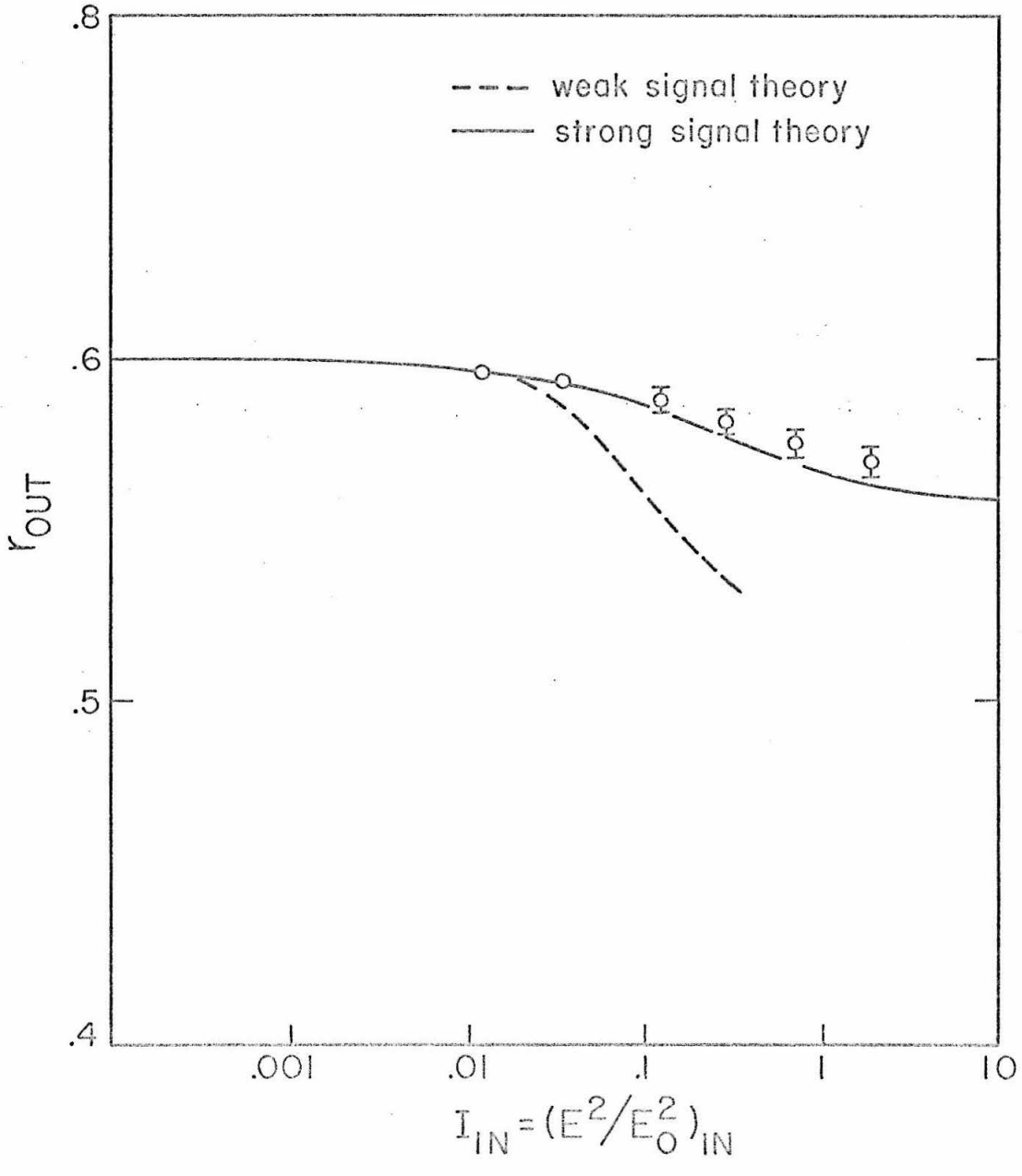

Figure 21

Nonlinearity-Induced Anisotropy for Various 3.3913-μ (J = 1 to J = 2) Input Signals. $r_{in} = 0.60$, $\alpha = 4.25\ m^{-1}$, $a = 0.3$.

The solid curve in Figure 21 was obtained using equations (4.14) and (4.15), and the dashed curve was obtained from the gain equations resulting from (3.63) and its counterpart for the negative helicity component. The atomic parameters used for these theoretical curves were $a = 0.3$, $A = 0.05$, $B = 0.25$, $\frac{1}{\tau}u = 165$ MHz, $\Omega_b/2\pi = 1.67$ MHz/gauss. The figure shows that the weak signal theory predicts too much ellipticity change when the signal strength goes beyond its limits of validity. This type of behavior was first noticed by Dienes (1). However even the strong signal theory seems to predict too much ellipticity change in this case. Since both of these theories are valid only for very low pressures, this deviation is most likely due to pressure effects.

Experiments studying a laser excited Hanle effect in a He-Ne discharge had shown that the decay of the common laser levels was slightly anisotropic at the pressures used in our amplifier tube (45). Tomlinson and Fork (30, 42) first noted that anisotropic decay would influence the coupling strength of the transition, and this, of course, directly affects the nonlinearity induced anisotropy (see the pertinent discussion in Chapter 3). Our results with the sealed-off tube with a gas pressure of 1.0 Torr did not dispel doubts that this deviation could be ascribed to pressure effects - it was plausible to argue that some systematic error could have been the source of our small discrepancy. However further experiments at other gas pressures are presented in the next chapter, and they clearly show the influence of gas pressure on nonlinearity-induced anisotropy.

Since, according to the low pressure theories, the $J = 1$ to

J = 1 transition is a "neutral coupling" transition, there should be no nonlinearity-induced anisotropy for the 3.3903-μ (J = 1 to J = 1) signal. Measurements taken with this signal did not show any evidence of deviation from this theoretical prediction. The small gain of this line, when compared with the gain of the 3.3913-μ line, would reduce the effect of any deviation due to gas pressure to a point such that it would be swamped by the random error brackets. Thus we cannot draw any conclusions based on these results.

6.4 Spontaneous Feeding Effects

The preceeding analysis in this chapter neglects the effects of spontaneous feeding of the lower laser level. Let us return to equations (3.47) through (3.49) in order to evaluate the accuracy of this approximation. The theoretical line strengths for the transitions $3s_2 \rightarrow 3p_4$ and $3s_2 \rightarrow 3p_2$ give values for $(\gamma/2\pi)$ of 2.8 MHz and 1.1 MHz, respectively (85). If we assume that the zero-pressure value for $(\gamma_a/2\pi)$ is 10 MHz (45) and that $\gamma_b = 5\gamma_a$, then we can calculate the effects of the spontaneous feeding terms in (3.48) at the low pressure limit. At higher pressures the effects should be less due to the increases in the value of A_K, B_K.

Assuming the zero pressure values for G, A, and B (zero pressure decay is isotropic), and using Table 1, we calculate a 2% to 3% decrease in the sizes of the coefficients of $f_1(y)$ and $f_2(y)$ for the J = 1 to J = 2 transition; and we calculate a 1% decrease in the corresponding coefficients for the J = 1 to J = 1 transition. The effects on the $f_3(y)$ coefficients are even less. We have been pri-

marily interested in the nonlinear dips at small magnetic field values, which is mainly due to the contribution of the first term inside the square brackets multiplying $f_3(y)$ in (3.48b). For the $J = 1$ to $J = 2$ transition this term is negligibly small to begin with, and the spontaneous emission feeding term decreases its contribution by about 10% in the small magnetic field region. For the $J = 1$ to $J = 1$ transition the dip size is decreased about .5% by the spontaneous emission feeding term. In addition, in the isotropic decay limit there is no effect of the spontaneous emission feeding terms on the zero-field coupling strengths of the transitions. Thus we can safely neglect these terms entirely in our analyses.

CHAPTER SEVEN

PRESSURE EFFECTS ON THE 3.39 MICRON TRANSITIONS

7.1 Introduction

By attaching the laser amplifier tube to a gas-handling station, we were able to study saturation effects for various gas pressures. This chapter discusses the results of these measurements; namely, the dependence on the amplifier gas pressure of gain saturation, nonlinearity induced anisotropy, and gain and Faraday rotation versus axial magnetic field.

The experimental gain saturation curves fit strong-signal theoretical curves quite well when the homogeneous linewidth parameter, $a = \gamma_{ab}/ku$, and the saturation signal intensity, $E_o^2 = 3\hbar^2\gamma_a\gamma_b/|\langle b\|p\|a\rangle|^2$ are allowed to become monotonically increasing functions of pressure. The use of these curves, along with unsaturated Faraday rotation curves for various pressures, allows the determination of the pressure-dependent homogeneous linewidths for both 3.39-μ transitions. The results of these measurements are presented. Another useful result of these measurements is the determination of the ratio of the small signal gain constants for the two transitions. This value is quite close to the theoretical ratio of the line strengths.

The dip width in the gain and Faraday rotation versus axial field curves for the 3.3903-μ (J = 1 to J = 1) signal is observed to increase with increasing gas pressure, as predicted. Resulting values for the neon $3s_2$ level quadrupole moment decay rate are given for a

limited range of pressures.

The nonlinearity-induced anisotropy measurements strongly indicated the presence of anisotropic decay at high gas pressures. The coupling strength of the $J = 1$ to $J = 2$ transition increases with increasing pressure, while no detectable change in the coupling strength of the $J = 1$ to $J = 1$ transition is observed.

7.2 Gain Saturation

When the gas pressure in the laser amplifier tube is increased, the gain saturation curves for the two 3.39-μ signals are affected in two ways. First, the form of the saturation curve changes - the gain decreases faster for increasing signal intensity at higher pressures. This characteristic is consistent with a larger value of the homogeneous linewidth parameter ($a = \gamma_{ab}/ku$) at higher pressures. As the gain line becomes more homogeneously broadened ($a \to \infty$), the gain saturates as $(1 + I)^{-1}$, whereas for small values of a ($a \to 0$ is called inhomogeneous broadening) the gain saturates as $(1 + I)^{-\frac{1}{2}}$. (Discussions of these gain saturation characteristics can be found in references 7,8 and 82.) Second, the saturation signal intensity increases with increasing pressure. According to the strong signal theory of Chapter 4, the saturation signal intensity is E_o^2, and it is proportional to the product of the monopole (population) decay rates of the two levels of the transition. These decay rates do increase with increasing pressure. However the weak signal theory of Chapter 3, which is more capable of handling pressure effects, demonstrates that the increase of the higher moment level decay rates and the dipole moment decay rate also influence

the saturation process; and even if the monopole decay rates increase only very slightly with pressure, the saturation (or the size of the nonlinear contribution to the gain) will become significantly smaller at a given signal strength if the other decay rates increase substantially. Since these decay rates are influenced to a much greater extent by "soft" collisions, they should play a greater role in causing the saturation signal intensity to increase with increasing pressure.

Regardless of the sizes of the level decay rates, the shape of the gain saturation curve depends almost exclusively on the homogeneous linewidth (dipole moment decay rate). Experimental curves were obtained for five total gas pressures, each having a He:Ne ratio of 10:1. (For all of our pressure measurements the ratio of He:Ne was kept at 10:1.) Each curve could be fitted quite well with a theoretical curve based on equation (4.14). Figure 22 depicts the fits for the $J = 1$ to $J = 2$ transitions, for the lowest and highest values of total pressure. The value of E_o^2 was allowed to increase with increasing pressure in order to obtain the best fits. The value of E_o^2 for $P_T = 2.2$ Torr is almost twice the value of E_o^2 for $P_T = 0.6$ Torr. The homogeneous linewidth increases from 0.25 to 0.5 over this pressure interval, according to these fits.

The gain saturation plots in Figure 22 were obtained with a linearly polarized signal. Gain saturation varies with the ellipticity of the signal; according to equations (4.14) and (4.15) a circularly polarized signal saturates more than a linearly polarized signal. Reference 1 discusses this phenomenon and contains an experimental verification. We also plotted gain saturation curves using a signal with

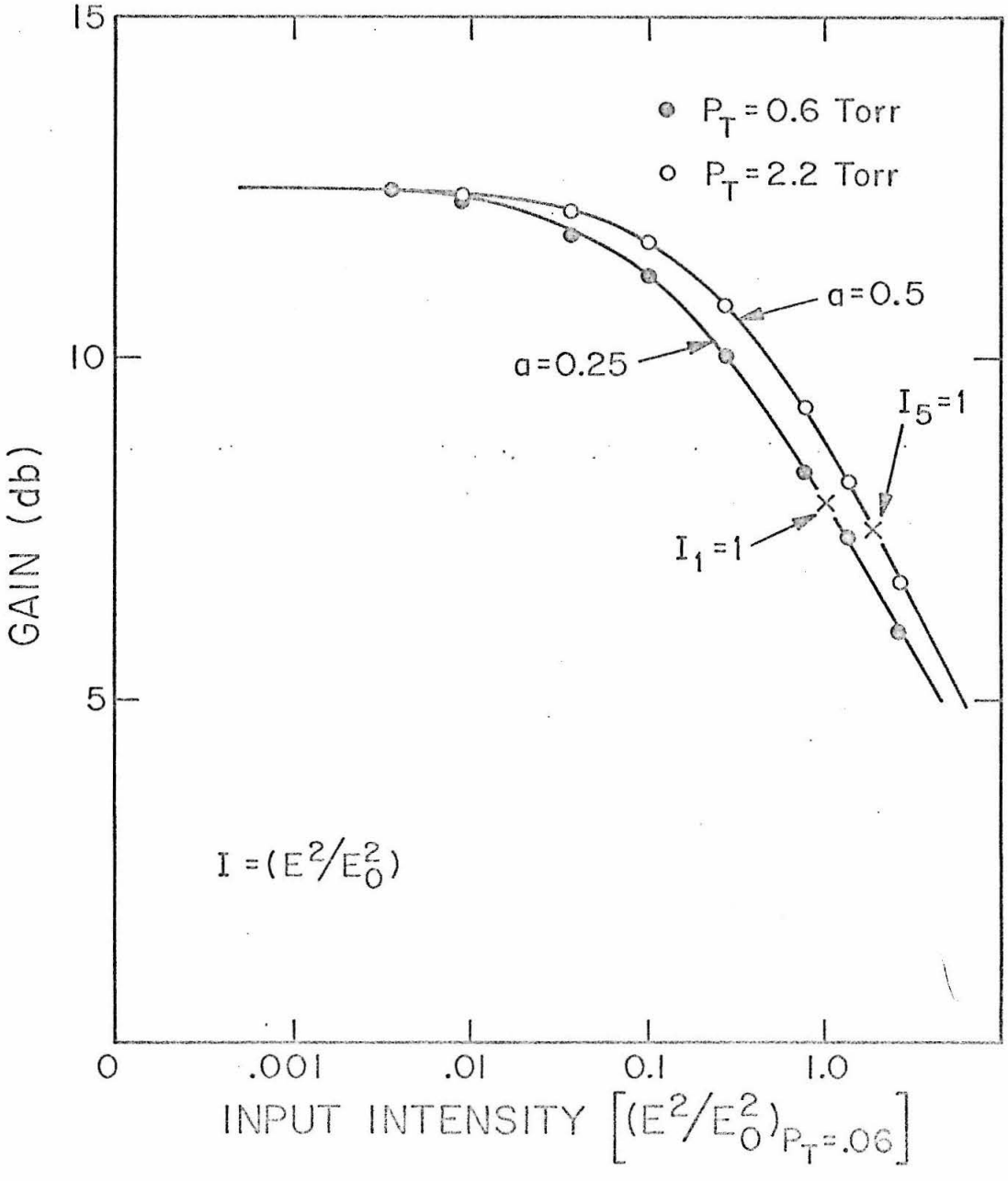

Figure 22

Pressure Dependence of Gain Saturation for 3.3913-μ (J = 1 to J = 2) Input Signals.

r = 0.6, which was also used for a study of nonlinearity-induced anisotropy. The small signal gains were too low for us to observe this polarization effect unambiguously, however.

Gain saturation curves were also plotted for the J = 1 to J = 1 transition. The signal input intensities were not as large, though; only intensities which were about equal to E_o^2 were obtained, due to less power output from the laser oscillator and the greater absolute value of E_o^2 for this transition. This causes some difficulty in assigning proper values of a, the homogeneous linewidth, to the various saturation curves. (Another method, based on Faraday rotation, was used to obtain these values with greater accuracy. This will be discussed in the following section.)

From the gain data for the two 3.39-μ transitions, we obtained the ratio of the two linear gain parameters for various values of discharge current and gas pressure. The ratio did not seem to depend on either gas pressure or discharge current for the ranges in which we operated (P_T = 0.6 Torr to 2.2 Torr, i = 10 ma to 20 ma); any pressure or discharge current dependence would be within our accuracy limits.

Our results are

$$\frac{\alpha_{(3.3913-\mu)}}{\alpha_{(3.3903-\mu)}} = 2.6 \pm .1 \qquad (7.1)$$

This is very close to the theoretical ratio of line strengths, which is 2.55 (85). Since α depends on the pumping and decay rates for each level of the transition (see the definiton following Equation (3.49d)), these results are in accord with the assumption that the upper level

$(3s_2)$ population is much greater than the lower level $(2p_2, 2p_4)$ populations when the amplifying medium is unsaturated and in a steady-state situation. Concomitant with this assumption we can attest to the accuracy of the theoretical calculations in Reference 85.

7.3 Linearly Polarized Signal: Gain and Faraday Rotation

Small signal or "linear" Faraday rotation is useful in determining relative sizes of homogeneous linewidths at various pressures. These measurements must be used in conjunction with gain saturation measurements in order to establish an absolute scale for the linewidths.

It is difficult to determine the value of the homogeneous linewidth of a transition from gain saturation data. In the first place the strong signal theory, which is used to give gain saturation curves for comparison with experimental observations, has been derived assuming $\gamma_a + \gamma_b = 2\gamma_{ab}$; and this is not true for the intermediate and high pressure regions in He-Ne. It was stated previously, however, that the shape of the experimental gain saturation curves seemingly depends only on the homogeneous linewidth and not on the level decay rates, regardless of whether or not the condition $\gamma_a + \gamma_b = 2\gamma_{ab}$ is valid. A more troublesome characteristic of gain saturation is the relative insensitivity of the shape of the curve to changes in the value of a in the region of interest, i.e. $0.2 < a < 0.6$. This can be observed in Figure 22; the shapes of the curves for $a = 0.25$ and for $a = 0.5$ are not much different, although it is noticeable. This characteristic makes it difficult for us to determine values for the homogeneous linewidth, a, which are accurate to less than ± 0.05. It

would probably help matters to have a longer amplifier tube and/or larger input signal strengths available. However added problems with reflection and other instabilities are inherent in this regime.

A novel method of determining relative linewidths involves the unsaturated, or "linear" Faraday rotation of a linearly polarized input signal. Our apparatus was designed to detect this phenomenon with high accuracy. If a signal has a given unsaturated gain as it passes through the tube, its Faraday rotation angle will depend on the homogeneous linewidth of the transition. Recall the appropriate expressions for unsaturated gain and Faraday rotation from Chapter 3 (equations (3.57) and (3.58)):

$$\frac{1}{I}\frac{dI}{dz} = 2\alpha \text{ Re } w(y + ia) \tag{7.2a}$$

$$I(z) = I(0) \exp [2\alpha z \text{Re } w(y + ia)] \tag{7.2b}$$

$$\frac{d\Phi}{dz} = \alpha \text{ Im } w(y + ia) \tag{7.3a}$$

$$\Phi = \alpha z \text{ Im } w(y + ia) \tag{7.3b}$$

These equations are true regardless of the sizes of the level decay rates; hence they are strictly valid over the entire pressure range of interest. Now if the quantity $2\alpha z \text{ Re } w(0 + ia)$ is a known number (known from a gain measurement), the value of the quantity $\alpha z \text{ Im } w(y+ia)$ for a particular value of y will depend on the size of a $(=\gamma_{ab}/ku)$ used. For example, the Faraday rotation for a linewidth $a = 0.2$ is

about 6% higher than the rotation for a linewidth $a = 0.3$ in the range $0 < y < .5$, given the same linear gains. Of course the value of ku must be known in order to determine absolute values for y and a.

Using the $J = 1$ to $J = 2$ transition gain saturation results for $P = 0.6$ Torr, shown in Figure 22, we determined an absolute scale for a. Comparison with the unsaturated Faraday rotation results at the same pressure yielded a value of $(ku/2\pi) = 165$ MHz. Unsaturated Faraday rotation curves for various values of discharge current in the range 10 to 20 ma. were studied to determine a current-dependent change in the value of ku. No variation of ku was observed. Then similar Faraday rotation curves were plotted for various pressures and for both 3.3913-μ ($J = 1$ to $J = 2$) and 3.3903-μ ($J = 1$ to $J = 1$) signals. These measurements yielded homogeneous linewidth values for both transitions. The results are shown in Figure 23. These results indicate that the zero-pressure limiting values of γ_{ab} for the two transitions are

$$\gamma_{ab}/2\pi \ (3s_2 \rightarrow 3p_4) = 28 \text{ MHz}$$

$$\gamma_{ab}/2\pi \ (3s_2 \rightarrow 3p_2) = 21.5 \text{ MHz} \qquad (7.4)$$

Since in the low pressure limit, $2\gamma_{ab} = \gamma_a + \gamma_b$, we conclude that the $2p_2$ level decay rate is lower than the $2p_4$ level decay rate. As stated previously, the accuracy of the numerical values is limited by the gain saturation results.

According to the weak signal theory in Chapter 3, the dip width in the Faraday rotation and gain versus axial magnetic field

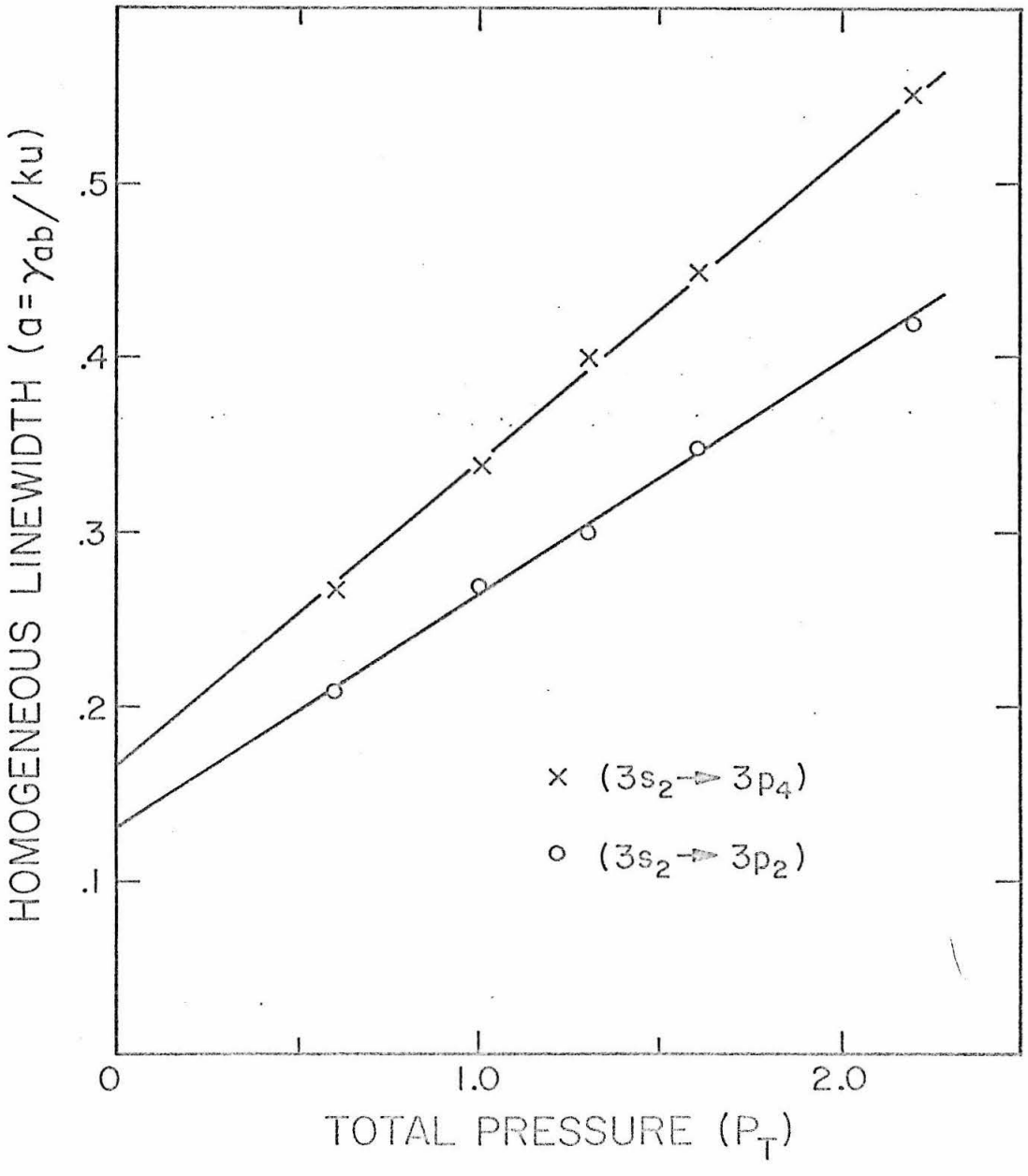

Figure 23

Homogeneous Linewidths for Neon $3s_2 \rightarrow 3p_4$ and $3s_2 \rightarrow 3p_2$ Transitions.

curves is given by A_2, the quadrupole moment or alignment decay rate of the upper (neon $3s_2$) level. The dip can be observed only when using the 3.3903-μ (J = 1 to J = 1) signal, and only for intermediate pressures is the gain of the signal high enough so that a reasonably accurate measurement of the width can be made. Curves similar to those shown in Figure 17 were obtained for three total gas pressures: 1.0 Torr, 1.3 Torr, and 1.6 Torr. The unsaturated gain for each case was fixed at 4.25 ($\bar{\alpha}$ = 1.45 m^{-1}). The results of the dip width measurements are:

$$\gamma_a^2/2\pi \ (P_T = 1.0 \text{ Torr}) = 15 \pm 2.5 \text{ MHz}$$

$$\gamma_a^2/2\pi \ (P_T = 1.3 \text{ Torr}) = 16 \pm 2.5 \text{ MHz} \qquad (7.5)$$

$$\gamma_a^2/2\pi \ (P_T = 1.6 \text{ Torr}) = 17 \pm 2.5 \text{ MHz}$$

These values are about 40% higher than those reported by Decomps and Dumont, who utilized a laser excited Hanle effect experiment in order to determine population and alignment decay rates for certain excited levels of neon (45).

Their results were extrapolations to zero discharge current, and they stated that the observed decay rates increased with increasing discharge current. Since our values for A_2 were determined in the current range of 18-20 ma., this might account for part of the difference. We attempted similar dip width measurements at lower discharge current values; however the accompanying gain decrease precluded an accurate determination of the dependence of A_2 on discharge current. We con-

clude that although this effect probably exists, it is not large enough to fully account for the much larger values for A_2 that we obtained. Further investigations would be helpful in clearing up this matter. We obtained a good fit to the gain versus axial field curve for P_T = 1.6 Torr with the use of the anisotropic decay theory, assuming certain values for the pressure dependent decay rates. This anisotropic decay model will be discussed in the next section.

7.4 Elliptically Polarized Signal: Nonlinearity-Induced Anisotropy

Simultaneous measurements of gain and change in ellipticity were taken for a 3.3913-μ (J = 1 to J = 2) signal which was tuned to line center, with r_{in} = 0.6. These measurements were repeated for various gas pressures. Gain saturation plots similar to those in Figure 22 were obtained, and fits to these points were made with the use of the strong signal theory. The strong signal theory was then applied to the nonlinearity-induced anisotropy results. Figure 24 shows the results for three gas pressures: (a) P_T = 0.6 Torr, (b) P_T = 1.0 Torr, (c) P_T = 2.2 Torr. The linear gains for each case were set at 17.5, or 12.5 db. The accuracy limits due to random fluctuations in signal intensity are about the same size as the circles marking the experimental points. The predictions of strong signal theory are the solid lines; we note that at low pressures the fit is good, but at high pressures the experimental points show much less change in ellipticity than that predicted by theory. Note that the three scales for input intensity are not equivalent; a certain input signal intensity might be equal to E_o^2 for the P_T = 0.6 Torr case, but it would then be

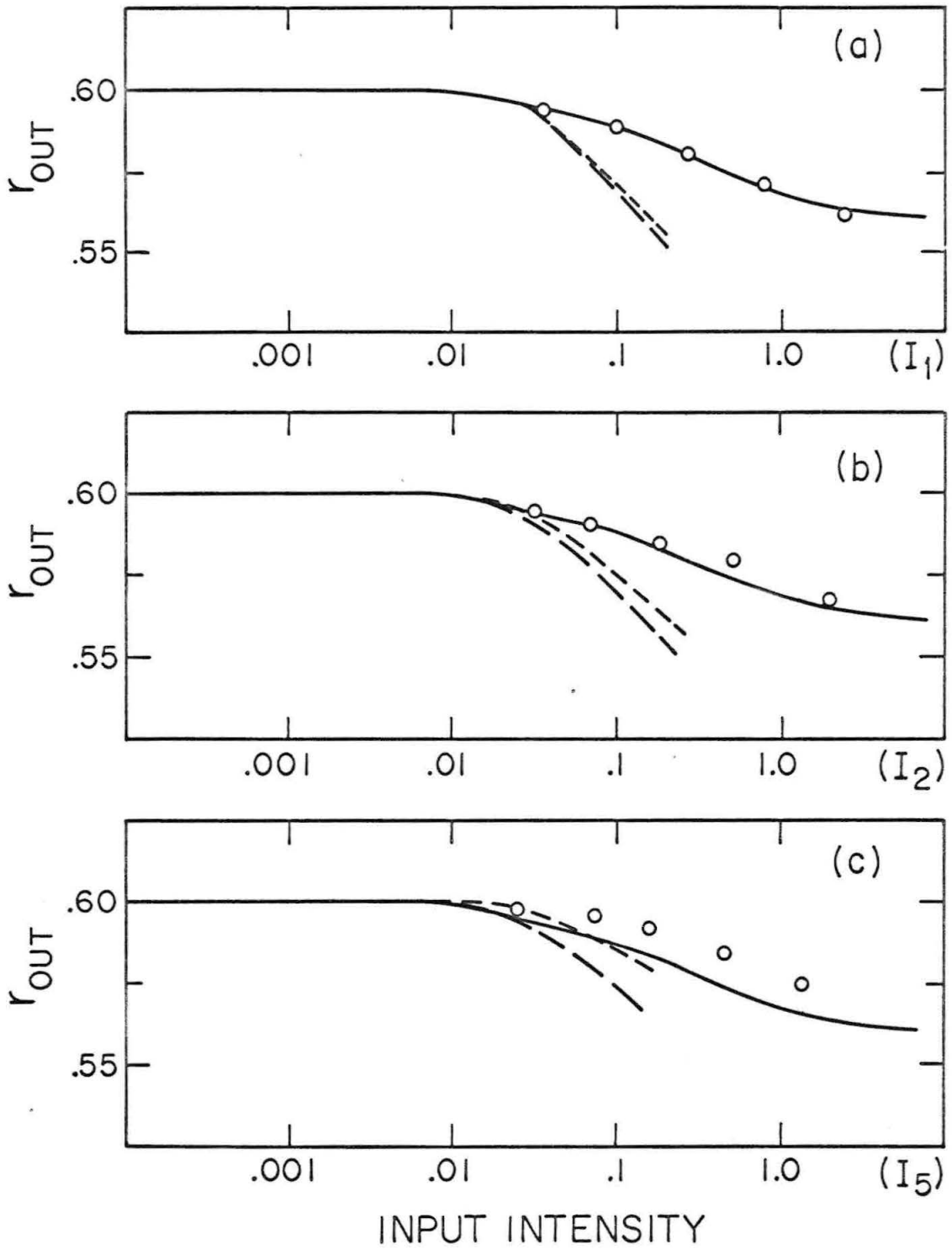

Figure 24
Nonlinearity-Induced Anisotropy for 3.3913-μ (J = 1 to J = 2) Input Signals. r_{in} = .60; $\bar{\alpha}$ = 2.86; (a) P_T = 0.6 Torr, (b) P_T = 1.0 Torr, (c) P_T = 2.2 Torr

equal to $.5E_o^2$ for the $P_T = 2.2$ Torr case. Each scale is given in terms of its own saturation signal intensity; these are obtained from the gain saturation curves.

The observed departure from strong signal theoretical predictions for high pressures suggests the existence of anisotropic decay. From the discussion in Chapter 3 we know that for a J = 1 to J = 2 transition, anisotropic decay tends to make the coupling closer to neutral. This is what is observed in Figure 24. To demonstrate this we have constructed theoretical curves valid for weakly saturating signals - the long dashed curves in Figure 24 are the predictions of weak signal theory assuming isotropic decay, and the short dashed curves are the predictions of weak signal theory assuming anisotropic decay. The values for the decay rate parameters used for these two cases are given in Tables 2 and 3. The linewidths assumed are those obtained from Figure 23. The zero pressure decay rates are assumed to be $a = .175$ ($\gamma_{ab}/2\pi = 29$ MHz), $A = .035$ ($\gamma_a/2\pi = 11$ MHz), $B = .14$ ($\gamma_b/2\pi = 46$ MHz).

The level decay rates for the isotropic decay case were obtained by assuming $B = 4A$, and fixing the values of A and B such that the magnitudes of the saturation terms correspond with the relative saturation signal intensities obtained from the gain saturation curves. For a gas pressure P, the smaller the values assumed for A and B, given a certain value for a, the less saturation occurs at a given signal intensity, according to equations (3.48) and (3.61). This corresponds with larger values for saturation signal intensities $(E_o^2)_P$. At a pressure of 2.2 Torr, the saturation signal intensity,

$(E_o^2)_{2.2\ \text{Torr}}$ is slightly more than twice the zero-pressure saturation signal intensity, E_o^2. This means that $A + B < \frac{1}{2} a$ for $P_T = 2.2$ Torr.

The level decay rates in Table 3, exhibiting anisotropic decay, were chosen on the basis of several other results. The neon $3s_2$ level decay rates of population and alignment have been studied by Decomps and Dumont (45), while we have studied the pressure dependence of the alignment decay rate over a limited range of pressure. We have assumed a much larger pressure dependence for the population decay rate (A_o) than that assumed in Reference 45. Our values for this quantity are more consistent with the results of Bennett and Kindlmann (86), who measured pressure dependences of 2p level decay rates. The ratios of $(A_1 - A_o)/(A_2 - A_o)$ and $(B_1 - B_o)/(B_2 - B_o)$ are roughly the same as the theoretical values derived in Reference 43, namely 5/3 and .88 respectively.

P_T = 0.6 Torr	P_T = 1.0 Torr	P_T = 2.2 Torr
a = .27	a = .34	a = .55
A = .04, B = .16	A = .045, B = .18	A = .055, B = .22

Table 2

Neon $3s_2 \rightarrow 3p_4$ Transition Isotropic Decay Rates for Various Total Gas Pressures, P_T. ($P_{He}:P_{Ne}$ = 10:1 in all cases.)

P_T = 0.6 Torr	P_T = 1.0 Torr	P_T = 2.2 Torr
a = .27	a = .34	a = .55
A_o=.036, B_o=.15	A_o=.037, B_o=.16	A_o=.04, B_o=.18
A_1=.044, B_1=.164	A_1=.050, B_1=.187	A_1=.07, B_1=.25
A_2=.041, B_2=.167	A_2=.045, B_2=.193	A_2=.06, B_2=.26

Table 3

Neon $3s_2 \rightarrow 3p_4$ Transition Anisotropic Decay Rates for Various Total Gas Pressures, P_T. (P_{He}:P_{Ne} = 10:1 in all cases.).

The level structure of the J = 1 to J = 2 transition is too complex for us to individually determine the various level decay rates with much accuracy. The primary consideration here is the fact that experimentally observed nonlinearity-induced anisotropy strongly suggests the existence of anisotropic decay at high pressure. It is obvious from Figure 24 that the weak signal theory is valid only for a limited range of signal strengths; yet this theory does account for the pressure effects which we have observed when it is valid, and it gives a qualitative indication of these phenomena when higher signal strengths are used. The combination of the generalized weak signal theory and the low pressure strong signal theory can be used to predict saturation phenomena over a wide range of conditions.

Similar experiments were performed on the 3.3903-μ (J = 1 to J = 1) signal. The strong and weak signal isotropic decay theories

predict no change in ellipticity of a $J = 1$ to $J = 1$ signal which is tuned to line center when it passes through the amplifying medium. According to the generalized weak signal theory, the coupling will remain neutral if the decay rates for orientation and alignment remain equal to each other while becoming larger than the population decay rate. However if the orientation and alignment decay rates for each level become unequal, the coupling will become either strong or weak, depending on which of the decay rates is larger. The observation of strong coupling in a 1.52-μ ($J = 1$ to $J = 0$) He-Ne laser led Tomlinson and Fork to postulate the existence of a larger cross section for $|\Delta m| = 2$ transitions (orientation decay transitions) than for $|\Delta m| = 1$ transitions (alignment decay transitions) in order to account for this effect (30, 42). More recently Wang and Tomlinson developed theoretical expressions for collision induced anisotropic relaxation in gases which verified this postulate for a $J = 1$ level (43).

The results of our measurements on the 3.3903-μ ($J = 1$ to $J = 1$) signal for two gas pressures are shown in Figure 25. The linear gains for each case were set at 3.65, or 5.6 db. Along with the strong signal predictions shown in Figure 25, we have demonstrated the prediction of the generalized weak signal theory in which the decay rate parameters are those given in Table 4. In keeping with the theoretical results of Wang and Tomlinson (43), we have set $(A_1 - A_o)/(A_2 - A_o) = (B_1 - B_o)/(B_2 - B_o) \simeq 5/3$. This changes the coupling for the transition from neutral to strong at high pressures. Our experimental results do not indicate unambiguously any departure from neutral coupling at $P_T = 2.2$ Torr. Thus we cannot state that nonlinearity-

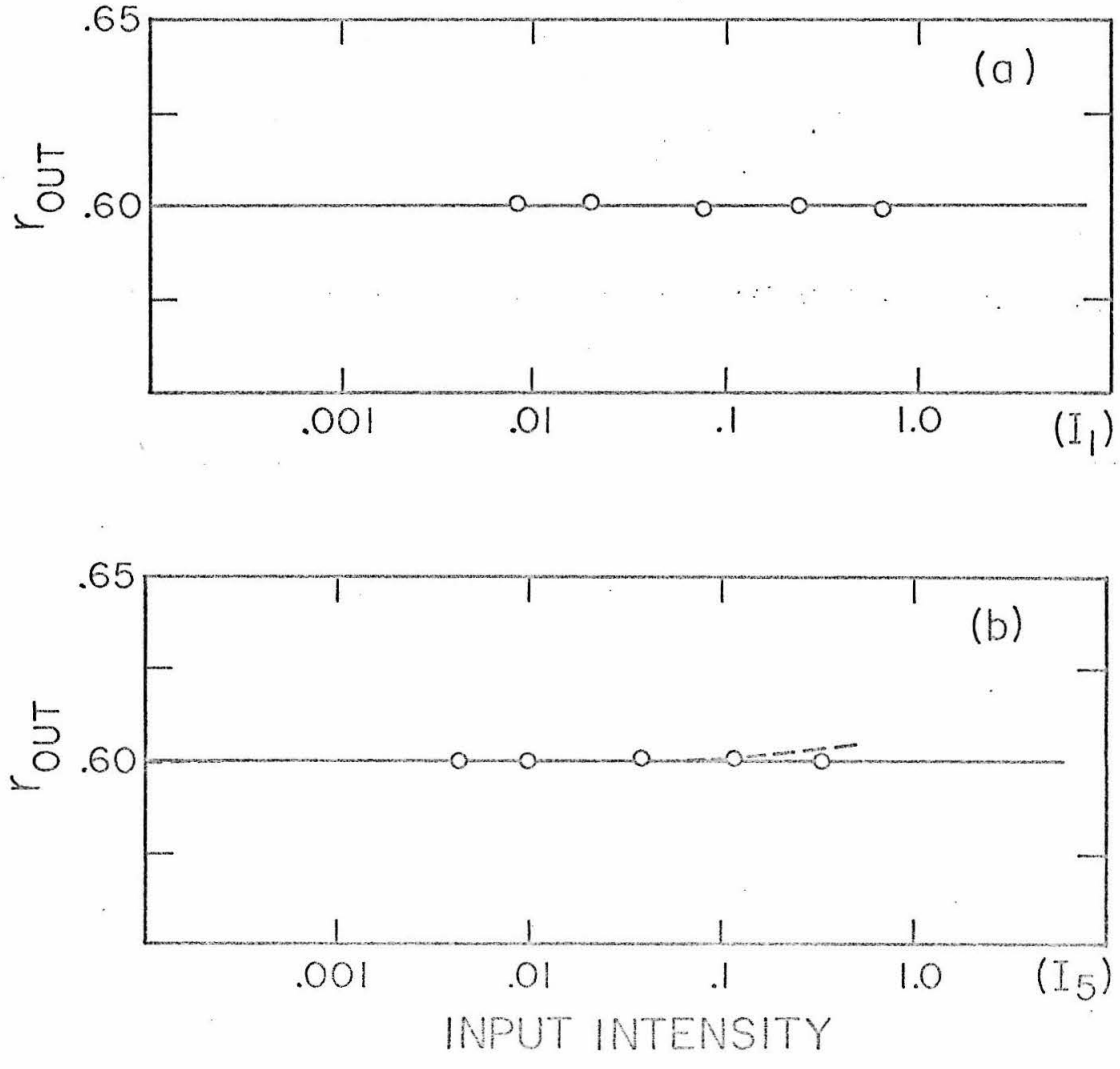

Figure 25

Nonlinearity-Induced Anisotropy for 3.3903-μ (J = 1 to J = 1) Input Signals. r_{in} = .60; $\bar{\alpha}$ = 1.30; (a) P_T = 0.6 Torr, (b) P_T = 2.2 Torr.

induced anisotropy exists for this transition. Since the weak signal theory loses validity for input signals stronger than $I_{in} = 0.1$, we would not expect the experimental points to follow the short-dashed line past this point in any case. A longer amplifier tube would be necessary in order to detect the existence of strong coupling unambiguously.

P_T = 2.2 Torr
a = .45
A_o = .04, B_o = .12
A_1 = .07, B_1 = .18
A_2 = .06, B_2 = .155

Table 4

Neon $3s_2 \rightarrow 3p_2$ Transition Anisotropic Decay Rates for P_T = 2.2 Torr. (P_{He}:P_{Ne} = 10:1).

CHAPTER EIGHT

DISCUSSION OF SOURCES OF SYSTEMATIC ERROR

8.1 Introduction

In this chapter we discuss the effects of systematic departure from theoretical perfection on our experimental results. Four systematic error sources are discussed here: residual and inhomogeneous magnetic fields, deviations of the 3.39-μ signals from their respective line centers, nonlinearity of photodetector response, and possible inaccuracies in pressure gauge readings. The effects of the first three of these sources of systematic error are well understood for our experiments, and we will show that they either have negligible effects on our results or are taken into account in a satisfactory manner. The pressure gauge readings represent an unknown source of error, since the Pirani type gauge tube which we used has not been recently calibrated against a standard gauge; but there is reason to believe that the possible gauge inaccuracies are small and do not affect our overall results.

8.2 Residual Fields and Inhomogeneities

Magnetic field measurements were made using a Bell 120 Gauss-meter with an axial probe, which was capable of measuring fields as small as .01 gauss. The probe was made of InAs, and its operation was based on the Hall effect. A zero-gauss chamber, capable of reducing the ambient magnetic field by a factor of 10^{-4}, was used in order to correctly establish the zero field value for the probe and meter.

Effects of the steel table on the magnetic field produced at the position of the amplifier tube were found to be negligible. The earth's magnetic field produced an axial (horizontal) component of .25 gauss and a transverse (vertical) component of nearly .4 gauss. The axial component could be balanced by the solenoid; the remaining transverse component is a residual field, whose effects we must consider.

When the total axial field is zero, we can consider the effect of the transverse field on Faraday rotation as follows. The polarization of the linearly polarized input signal lies in the horizontal plane, due to the orientation of the laser oscillator tube and the attenuator polarizers. We shall state that the input signal is polarized in the x-direction. We know that the transverse field is in the vertical, or y-direction. Then the x-polarized signal operates from $\Delta m = \pm 1$ transitions only. Assuming the signal to be tuned to line center, when the Doppler gain curves for the $\Delta m = \pm 1$ transitions are split due to the field, the total gain of the signal is reduced slightly. This could cause a slight error in the determination of the linear gain constant. We can write the linear gains of the x and y polarizations of a signal (assuming the g-factors g_a, g_b are equal) as

$$\frac{dE_y}{dz} = \alpha \, \mathrm{Re}\, w(0 + ia) \tag{8.1a}$$

$$\frac{dE_x}{dz} = .5\alpha \, \mathrm{Re}[w(-y + ia) + w(y + ia)]. \tag{8.1b}$$

If the transverse field equals 0.4 gauss, $y = \Omega/ku \simeq .004$. A look at

the real parts of the complex error functions (71) for various values of $a = \gamma_{ab}/ku$ will demonstrate that the difference in gains in this case is about .1% of the total gain of either component. This is much smaller than our experimental accuracy.

The effect on nonlinearity-induced anisotropy is also negligibly small. If the difference in gains of the x and y polarization components is only .1%, the change in r ($r_{out} - r_{in}$) due to this residual field would be much less than the experimental accuracy limits. Likewise for the phase shifts in the x and y polarization components.

When the axial field is not zero, we can treat the total field (axial plus transverse residual component) as being slightly misaligned. Borrowing some notation from the paper by Sargent, Lamb, and Fork (26), we define the laser coordinate system as ($\underline{i}$, $\underline{j}$, $\underline{k}$), and the magnetic field (or atomic) basis as ($\underline{i}$, $\underline{j}'$, $\underline{k}'$), as shown in Figure 26.

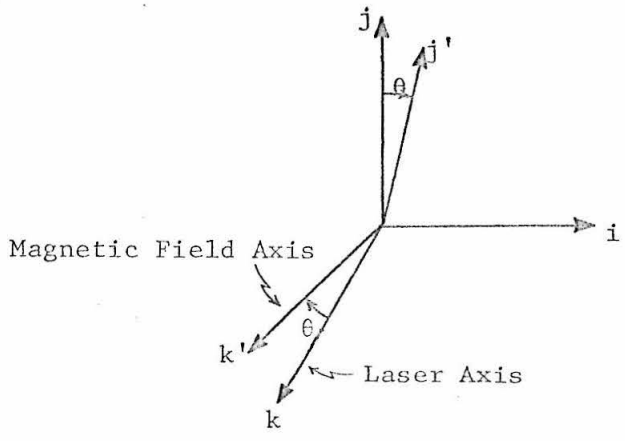

Figure 26

The Coordinate Systems for a Misaligned Magnetic Field

If we write the electric field of the signal in terms of the vector basis ($\underline{i}$, $\underline{j}$, $\underline{k}$), as in equation (2.4) we can define "direction cosines" $f_g(m)$, given by

$$f_{\pm}(m) = \mp \hat{e}_m \cdot (\hat{e}_x \pm i\hat{e}'_y) \frac{1}{\sqrt{2}}, \quad f_o(m) = \hat{e}_m \cdot \hat{e}'_z \tag{8.2}$$

Then we can write the linear gain of a signal of polarization i as

$$\frac{dE_i}{dz} = \text{Re } \alpha E_i \sum_k f_k(i)^* f_k(i) \sum_{a',b'} \delta_{a',b'+k} C^2_{a'b'} w\left(\frac{\omega_{a'b'}-\omega}{ku} + ia\right), \tag{8.3}$$

where a',b' denote the sublevels of levels a, b, $\omega_{a'b'}=(E_{a'}-E_{b'})/\hbar$, and ω = line center frequency. For a positive helicity component and a $J = 1$ to $J = 0$ transition,

$$\frac{dE_+}{dz} = \text{Re } \alpha E_+ \left\{\frac{1}{4}(1 + \cos\theta)^2 w(y + ia) + \frac{1}{4}(1 - \cos\theta)^2 w(-y + ia) + \frac{1}{4}\sin^2\theta\, w(0 + ia)\right\} \tag{8.4}$$

The coefficients of the "undesirable" nonlinear (third-order) terms are like

$$(1 - \cos\theta)^4, \quad \sin^4\theta, \quad (1 + \cos\theta)^2(1 - \cos\theta)^2, (1 + \cos\theta)^2\sin^2\theta,$$

as compared with the "desired" coefficients,

$$(1 + \cos\theta)^4 .$$

The experimental points at small values of axial magnetic field were taken in order to observe the nonlinear "dips", which have a half-width of $y = A$. The axial magnetic field strengths used to observe these dips ranged from about 2.5 gauss to 10 gauss. For an axial field of 2 gauss, $\tan\theta = .2$, $\sin^2\theta \sim .04$, $(1 - \cos\theta)^2 \sim 4 \times 10^{-4}$. Thus the largest of the undesirable terms are only a few percent of the normal terms, so that we are not being led astray by ignoring these terms.

The axial magnetic field produced by the solenoid was slightly inhomogeneous. The field at the input end of the amplifier was about 25% low and rose to the average field value at $z \simeq 2.5$ cm. The inhomogeneity along the rest of the axial distance was only about 5% of the average field value. These slight inhomogeneities produced an error which was quite small compared with experimental accuracy limits due to random instabilities. This was determined by numerically integrating equations (3.55) and (3.56) for the $J = 1$ to $J = 1$ transition, using appropriate sets of input and atomic parameters, and letting the magentic field strength vary with distance in the axial direction to closely correspond with the inhomogeneous axial field. The results were compared with corresponding results obtained by assuming a uniform average value of field along the axial direction, an assumption we have made for all our theoretical fits. The correspondence was very close.

8.3 Deviations From Line Center

The unsaturated Faraday rotation is not critically dependent on the signal being tuned to line center. It can be seen by looking at the dispersion curve in Figure 2, that for $y < ku$ the dispersion

curve is nearly linear; hence when the signal is not on line center, the unsaturated Faraday rotation,

$$\frac{d\Phi}{dz} = \frac{1}{2}\,\alpha\left\{\text{Im } w(x_o + y + ia) - \text{Im } w(x_o - y + ia)\right\}, \qquad (8.5)$$

does not change much for small values of y until $x_o = (\nu-\omega)/ku$ is nearly equal to unity. The output signal will be elliptically polarized with its major axis direction at an angle Φ with respect to the original input signal polarization direction.

The third-order polarization functions b and c, defined in Chapter 3, become asymmetric about $y = 0$ when $x_o \neq 0$, and the interaction function c becomes smaller for all values of y. According to the weak signal theory, the Faraday rotation for a $J = 1$ to $J = 1$ signal is

$$\frac{d\Phi}{dz} \simeq \frac{1}{2}\,\alpha \text{Im}\left\{\left[.5(w(x_o+y_a+ia) - w(x_o-y_a+ia) + w(x_o+y_b+ia)\right.\right.$$

$$\left. - w(x_o-y_b+ia))\right] - (E^2/4E_o^2)\left[.25(b(x_o+y_a) - b(x_o-y_a)\right.$$

$$+ b(x_o+y_b) - b(x_o-y_b) + c(x_o+y_a) - c(x_o-y_a) + c'(x_o+y_b)$$

$$\left.\left. - c'(x_o-y_b))\right]\right\}, \qquad (8.6)$$

for values of x_o which are small enough such that $(E_+)_{out} \simeq (E_-)_{out}$.

In our experiments the magnitude of the deviations of the signal frequency from line center was about $\pm$ 3 MHz. This gives a

value for x_o of $x_o \simeq .02$. For this value of x_o the sizes of the nonlinear polarization functions are less than .5% smaller than at $x_o = 0$. (This was determined by computer-calculating the sizes of these functions for various values of x_o.) Thus the saturated Faraday rotation is hardly affected.

The nonlinearity-induced anisotropy experiments were performed at zero axial magnetic field. Slight deviations from line center will not affect the ellipticity of the signal if just the linear polarization terms are included. The overall gain of the signal will decrease, but this will be less than a 1% decrease if $x_o = .02$. When the third order terms are included, the ellipticity will change depending on the ratio of the sizes of the self-saturation and interaction terms. Each of these terms decreases slightly in magnitude when $x_o = .02$, so that the ratio changes by less than a few tenths of a percent. Compared with pressure-induced changes in this ratio of from 25% to 50% for the J = 1 J = 2 transition, the deviations from line center produce a negligible effect on nonlinearity-induced anisotropy.

8.4 Nonlinearity of Detector Response

The InAs p-n junction type photodiodes do not respond linearly to 3.39-μ signal strengths of the order of a milliwatt. Below this region of signal strengths the response is linear; however the photodiode output voltage is only 2 mv. or less at this point. It is difficult in our experimental setup (see Figure 13) to cover a wide range of signal strengths without entering the nonlinear region, unless two phase-lock detectors are used to extend the lower limit of detection.

Then a fixed attenuator could be placed in front of each photodetector in order to reduce the incoming signal strengths, and a wide range of signal strengths could still be detected. Attenuators other than pairs of calcite polarizers are not very reliable at 3.4-μ, however.

Due to the lack of this additional equipment, we calibrated the nonlinearity of each photodiode response. The nonlinearity curves were found to depend somewhat on the diode bias voltage; for this region it was necessary to take all readings at the proper bias voltage. We placed a calcite analyzer in front of the photodiode in order to obtain the nonlinearity response curves, taking readings of I_o and $I_o \cos^2\theta$, at a particular value of θ, for various values of signal strength I_o. Departures from the correct ratio for these two quantities at high signal strengths could be ascribed to the nonlinear photodiode response.

The diode nonlinearity curves obtained are most susceptible to error at large values of signal strength. For this reason possible errors in the gain saturation and nonlinearity-induced anisotropy curves could result. However these curves seem to agree quite well with theoretical predictions at high signal strengths and low gas pressures, where the strong-signal theory is applicable.

8.5 Pressure Gauge Readings

The pressure readings were taken with a C.V.C. Autovac gauge, using a Pirani-type gauge tube. The Pirani gauge works well in the region of pressures 10^{-3} Torr to 2 Torr for the common gases. At higher pressures the sensitivity to pressure variations is low.

The gauge which we used was originally calibrated at the factory. It can be partially calibrated by setting the meter deflection appropriately at low pressures (less than 10^{-4} Torr) and at atmospheric pressure. However aging might have a slight effect on the response at intermediate pressures.

The gauge has been used in processing He-Ne laser tubes, and the pressure dependences on output power agree quite well with those reported in the literature. There is no reason to believe that the readings are grossly inaccurate. In any case, for most of the pressure effects which we studied, only qualitative comparisons between theory and experiment were made. Due to other sources of error or uncertainty in the gain saturation, Faraday rotation and gain versus axial field data, the uncertainties involved in the determinations of pressure dependent decay rates are substantial. If these other sources of uncertainty could be reduced, then it would be necessary to calibrate the pressure gauge carefully in order to obtain valid numerical results. The absorption coefficient of the methane line at 3.3913-μ should be measured again with a carefully calibrated gauge; our method of measurement has very high inherent accuracy, and our results are quite different from the results obtained by Gerritsen and Heller (82) with another technique.

CHAPTER NINE

CONCLUSIONS

We have investigated the interaction between a gas laser amplifier and a monochromatic resonant traveling wave, including effects which occur because the intensity of the wave is strong enough to saturate the population inversion of the amplifying medium. When this occurs, we view the problem as a classical electromagnetic wave interacting with a nonlinear medium. The application of an external axial magnetic field splits the degenerate energy levels of the gas atoms and allows us to obtain more information about the characteristics of the nonlinear interactions.

A considerable amount of theoretical effort has been devoted to this topic by many authors; yet a theory which satisfactorily describes the effects of nonlinear interactions for arbitrarily strong electromagnetic signals, and the influences of gas pressure on these interactions, does not exist at present. Experiments which carefully test the validity of the existing theories in their regions of applicability are generally complex; most of the work has been done on He-Ne laser oscillators, which necessitates the inclusion of cavity effects in the theoretical treatments. The study of a resonant traveling wave passing through a laser amplifier is less complicated and portrays the interaction of the signal with the atomic medium without the presence of cavity effects. We have carefully performed some straightforward amplifier experiments which exhibit some effects of the complex nonlinear interactions and we have developed

a theory which explains the results quite well for weakly saturating signals.

The nonlinear phenomena which we have studied both theoretically and experimentally are gain saturation, the coupling between circularly polarized components of a signal, nonlinear Faraday rotation and gain as a function of axial magnetic field for a linearly polarized signal, and the nonlinearity-induced anisotropy of the medium when it is amplifying an elliptically polarized signal. The results of this study give increased understanding to the effects of a saturated medium on an interacting laser signal.

The character of the nonlinear effects has been observed to be critically dependent on the total angular momenta (J values) of the atomic laser levels. For example the importance of double quantum interactions, which establish coherence between sublevels involved in the laser process, decreases markedly as one passes from consideration of a $J = 1$ to $J = 0$ transition to a $J = 1$ to $J = 1$ transition and then to a $J = 1$ to $J = 2$ transition. This has been observed in the Faraday rotation and corresponding gain of linearly polarized 3.39-μ signals which interact with one of two He-Ne transitions; the neon $3s_2 \rightarrow 3p_4$ ($J = 1$ to $J = 2$) and $3s_2 \rightarrow 3p_2$ ($J = 1$ to $J = 1$) transitions. For the $J = 1$ to $J = 1$ signal, the double quantum interactions produce sizeable nonlinear dips in the rotation and gain for small values of axial field. The size of the dip is large enough in this region to produce a <u>reversal</u> of Faraday rotation from the direction normally expected, if the incoming signal strength is high. For the $J = 1$ to $J = 2$ signal, the corresponding dips are so small that they are unobservable. Another example

involves the nonlinearity-induced anisotropy of the medium. The ellipticity of an elliptically polarized $J = 1$ to $J = 2$ signal is affected much differently from that of a $J = 1$ to $J = 1$ signal as they pass through a saturated amplifying medium.

We have demonstrated that a theory which analyzes nonlinear effects in a gas laser amplifier, such as the He-Ne example, must pay attention to possible influences of gas pressure on the interaction of the light with the medium. The theories which assume $\gamma_a + \gamma_b = 2\gamma_{ab}$, where γ_a, γ_b are the laser level decay rates and γ_{ab} is the homogeneous linewidth of the transition, and do not include pressure effects which cause this relation to become invalid or which cause sublevel mixing, are adequate in predicting saturation phenomena only at low gas pressures. For higher pressures, such as the pressures at which He-Ne lasers usually operate, a more generalized theory is needed to account for observed phenomena. We have developed a generalized theory which is applicable to weakly saturating signals passing through an amplifier in which the gas pressure effects are significant. It has proven to be successful, especially in predicting nonlinearity-induced anisotropy, in its range of validity. The combination of this theory and the low pressure strong signal theory previously developed by A. Dienes can qualitatively explain all the experimentally observed phenomena discussed in this work. Presumably other effects, such as combination tone generation, can be explained as well.

On the basis of a firmer understanding of the pressure effects on various gas laser transitions, further experimentation should yield absolute values for quantities such as the low pressure saturation

signal intensity, E_o^2, which depends on the matrix element $|\langle a\|p\|b\rangle|^2$ and the spontaneous decay rates, γ_a and γ_b. It should also be possible to determine various cross sections for excitation and decay of the atoms involved in laser processes. This has already been done in certain cases; however there is certainly much more work to be done, even with the He-Ne laser discharge, which has received the greatest amount of attention thus far.

Additional improvements in the gas laser theories would be valuable. The most glaring weaknesses in the present theories are: (1) the inability to treat arbitrarily strong signals in a theory which includes the nonlinear coherence effects and also allows for pressure effects; (2) the approximate manner in which radiation trapping is taken into account in a laser interaction model. Advances in these areas would allow theory and observation to be compared quantitatively for a wider range of experimental conditions.

REFERENCES

1. A. Dienes, "Polarization Dependent Gain Saturation and Nonlinearity Induced Anisotropy in the 3.39-μ He-Ne Laser Amplifier," IEEE J. Quantum Electronics QE-5, 162 (1969).

2. H. A. Kramers, Quantum Mechanics, North Holland Publishing Company (1958), pp. 480-489.

3. W. E. Lamb, Jr., "Theory of an Optical Maser," Phys. Rev. 134, A1429 (1964).

4. J. A. Armstrong, N. Bloembergen, J. Ducuing, and P. S. Pershan, "Interactions Between Light Waves in a Nonlinear Dielectric," Phys. Rev. 127, 1918 (1962).

5. N. Bloembergen and Y. R. Shen, "Quantum-Theoretical Comparison of Nonlinear Susceptibilities in Parametric Media, Lasers, and Raman Lasers," Phys. Rev. 133, A37 (1964).

6. W. R. Bennett, Jr., "Hole Burning Effects in a He-Ne Optical Maser," Phys. Rev. 126, 580 (1962).

7. E. I. Gordon, A. D. White, and J. D. Rigden, "Gain Saturation at 3.39 Microns in the He-Ne Maser," Proc. of the Symposium on Optical Masers, Polytechnic Institute of Brooklyn (1963), pp. 309-318.

8. D. H. Close, "Nonlinear Effects in Traveling Wave Laser Amplifiers," Ph.D. dissertation, California Institute of Technology, Pasadena, Calif.; Scientific Report 5, AF 49(638) - 1322, 1965.

9. D. H. Close, "Strong Field Saturation Effects in Laser Media," Phys. Rev. 153, 360 (1967).

10. W. Culshaw and J. Kannelaud, "Zeeman and Coherence Effects in the He-Ne Laser," Phys. Rev. 133, A691 (1963).

11. W. Culshaw and J. Kannelaud, "Hanle Effect in the He-Ne Laser," Phys. Rev. 136, A1209 (1964).

12. R. L. Fork and M. Sargent III, "Mode Competition and Frequency Splitting in Magnetic-Field-Tuned Optical Masers," Phys. Rev. 139, A617 (1965); also "Multiple Quantum Processes in Magnetic Field Tuned Optical Masers," Proc. of the Conference on Quantum Electronics, Puerto Rico, McGraw-Hill (1965), p. 611.

13. W. Culshaw and J. Kannelaud, "Coherence Effects in Gaseous Lasers with Axial Magnetic Fields. I. Theoretical," Phys. Rev. 141, 228 (1965).

14. J. Kannelaud and W. Culshaw, "Coherence Effects in Gaseous Lasers with Axial Magnetic Fields. II. Experimental," Phys. Rev. 141, 237 (1965).

15. W. Culshaw and J. Kannelaud, "Effects of Transverse and Axial Magnetic Fields on Gaseous Lasers," Phys. Rev. 145, 257 (1966).

16. C. V. Heer and R. D. Graft, "Theory of Magnetic Effects in Optical Maser Amplifiers and Oscillators," Phys. Rev. 140, A1088 (1965).

17. C. V. Heer, "Theory for the Polarization of Cosmic OH 18-cm Radiation," Phys. Rev. Letters 17, 774 (1966).

18. C. V. Heer and J. R. Bupp, "Polarization of an Amplifying Medium and of Cosmic OH Radiation," Phys. Letters 26A, 354 (1968).

19. C. V. Heer and R. A. Settles, "Theory for the Anomalous Polarization of Cosmic OH-18-cm Radiation and for Hyperfine Lasers," J. Molecular Spectroscopy 23, 448 (1967).

20. M. I. D'yakonov, "On the Theory of the Gas Laser in a Weak Longitudinal Magnetic Field," [English translation]: Sov. Phys.-JETP 22, 812 (1966).

21. M. I. D'yakonov and V. I. Perel', "On the Theory of a Gas Laser in a Magnetic Field," [English translation]: Optics and Spectroscopy 20, 257 (1966).

22. M. I. D'yakonov and V. I. Perel', Dependence of the Radiation Intensity of a Gas Laser on the Magnetic Field," [English translation]: Sov. Phys.-JETP 23, 298 (1966).

23. H. de Lang and G. Bouwhuis, "Quasi-Stationary Polarization of a Single Mode Gas Laser in a Magnetic Field," Phys. Letters 19, 481 (1965).

24. D. Polder and W. Van Haeringen, "The Effect of Saturation on the Ellipticity of Modes in Gas Lasers," Phys. Letters 19, 380 (1965).

25. W. M. Doyle and M. B. White, "Effects of Atomic Degeneracy and Cavity Anisotropy on the Behavior of a Gas Laser," Phys. Rev. 147, 359 (1966).

26. M. Sargent III, W. E. Lamb, Jr., and R. L. Fork, "Theory of a Zeeman Laser I. and II.," Phys. Rev. 164, 436 (1967).

27. A. Dienes, "Nonlinear and Anisotropic Effects in Magnetically Tuned Laser Amplifiers," Ph.D. dissertation, California Institute of Technology, Pasadena, Calif.; Scientific Report 6, AF49(638) - 1322, 1967.

28. A. Dienes, "Theory of Nonlinear Effects in a Gas Laser Amplifier. I. Weak Signals," Phys. Rev. 174, 400 (1968).

29. A Dienes, "Theory of Nonlinear Effects in a Gas Laser Amplifier. II. Strong Signals," Phys. Rev. 174, 414 (1968).

30. W. J. Tomlinson and R. L. Fork, "Properties of Gaseous Optical Masers in Weak Axial Magnetic Fields," Phys. Rev. 164, 466 (1967).

31. R. A. Settles and C. V. Heer, "Polarization of a Single-Mode Laser in a Transverse Magnetic Field," Appl. Phys. Letters 12, 350 (1968).

32. W. van Haeringen, "Polarization Properties of a Single-Mode Operating Gas Laser in a Small Axial Magnetic Field," Phys. Rev. 158, 256 (1967).

33. W. van Haeringen and H. de Lang, "Role of Linear Phase Anisotropy in a Zeeman Laser," Phys. Rev. 180, 624 (1969).

34. W. J. Tomlinson and R. L. Fork, "Anisotropy Effects in a Zeeman Laser," Phys. Rev. 180, 628 (1969).

35. H. Greenstein, "Some Properties of a Zeeman Laser with Anisotropic Mirrors," Phys. Rev. 178, 585 (1969).

36. R. L. Fork and M. A. Pollack, "Mode Competition and Collision Effects in Gaseous Optical Masers," Phys. Rev. 139, A1408 (1965).

37. R. A. McFarlane, W. R. Bennett, and W. E. Lamb, "Single Mode Tuning Dip in the Power Output of a He-Ne Optical Maser," Appl. Phys. Letters 2, 189 (1963).

38. A. Szöke and A. Javan, "Effects of Collisions on Saturation Behavior of the 1.15-μ Transition of Ne Studied with He-Ne Laser," Phys. Rev. 145, 137 (1966).

39. S. G. Rautian, "The Effect of Collisions on Spectral Characteristics of Gas Lasers," [English translation]: Sov. Phys.-JETP 24, 788 (1967).

40. S. Rautian and I. Sobel'man, "The Theory of Doppler and Impact Broadening of Spectral Lines and Pressive Effects on the Power Output of a Gas Laser," IEEE J. Quantum Electronics QE-2, 446 (1966).

41. B. L. Gyorffy, M. Borenstein, and W. E. Lamb, Jr., "Pressure Broadening Effects on the Output of a Gas Laser," Phys. Rev. 169, 340 (1968).

42. W. J. Tomlinson and R. L. Fork, "Use of Nonlinear Optical Interactions to Measure Relaxation Rates of Atomic Multipole Moments," Phys. Rev. Letters 20, 647 (1968).

43. C. H. Wang and W. J. Tomlinson, "Collision Induced Anisotropic Relaxation in Gases," Phys. Rev. 181, 115 (1969).

44. C. H. Wang, W. J. Tomlinson, and R. T. George, Jr., "Collision Induced Anisotropic Relaxation in a Gas Laser," Phys. Rev. 181, 125 (1969).

45. B. Decomps and M. Dumont, "Polarization of the Fluorescent Light of Ne Atoms Interacting with a Laser Beam--Measurement of Several Relaxation Times," IEEE J. Quantum Electronics QE-4, 916 (1968).

46. P. R. Berman and W. E. Lamb, Jr., "Influence of Resonant and Foreign Gas Collisions on Line Shapes," Phys. Rev. 187, 221 (1969).

47. V. Weisskopf and E. Wigner, "Berechnung der Natürlichen Linienbreite auf Grund der Diracshen Lichttheorie," Z. Physik 63, 54 (1930).

48. W. Heitler, The Quantum Theory of Radiation, Oxford U. Press (1954).

49. R. P. Feynman, R. B. Leighton, and M. Sands, The Feynman Lectures on Physics, volume III, Addison-Wesley Publishing Co., Inc. (1962).

50. J. D. Jackson, Classical Electrodynamics, John Wiley and Sons, Inc. (1962).

51. E. F. Labuda and E. I. Gordon, "Mircowave Determination of Average Electron Energy and Density in He-Ne Discharges [Positive Column]," J. Appl. Phys. 35, 1647 (1964).

52. A. von Engel, Ionized Gases, Oxford U. Press (1965), pp. 122-124.

53. C. H. Papas, Theory of Electromagnetic Wave Propagation, McGraw-Hill Book Co. (1965), Chapter 6.

54. J. Yoh, "Gas Laser Discharge Noise and Its Effects on the Laser Output," Ph.D. dissertation, California Institute of Technology, Pasadena, Calif.; Scientific Report 9, AFOSR-68-1492, project number (9768-02), 1969.

55. J. Fiutak, "The Multipole Expansion in Quantum Theory," Can. J. Phys. 41, 12 (1963).

56. W. E. Lamb, Jr. and T. M. Sanders, Jr., "Fine Structure of Short-Lived States of Hydrogen by a Microwave-Optical Method. I," Phys. Rev. 119, 1901 (1960).

57. R. G. Breene, Jr., The Shift and Shape of Spectral Lines, Pergamon Press (1961).

58. T. P. Sosnowski and W. B. Johnson, "Frequency Shifts of the Lamb Dip Minimum in the He-Ne Laser," IEEE J. Quantum Electronics QE-5, 151 (1969).

59. F. W. Byron, Jr. and H. M. Foley, "Theory of Collision Broadening in the Sudden Approximation," Phys. Rev. 134, A625 (1964).

60. W. Happer and E. B. Soloman, "Resonant Collision Broadening of the $(6s^2 6p7s)\ ^3P_1^\circ$ State in Lead," Phys. Rev. 160, 23 (1967).

61. W. R. Bennett, Jr., "Gaseous Optical Masers," Appl. Opt. Suppl. 1, 24 (1962).

62. R. Bernheim, Optical Pumping, W. A. Benjamin Inc. (1965).

63. G. Breit, "Quantum Theory of Dispersion," Rev. Mod. Phys. 5, 91 (1933).

64. M. I. D'yakonov and V. I. Perel', "Coherence Relaxation during Diffusion of Resonance Radiation," [English translation]: Sov. Phys.-JETP 20, 997 (1965).

65. M. I. D'yakonov, "Theory of Resonance Scattering of Light by a Gas in the Presence of a Magnetic Field," [English translation]: Sov. Phys.-JETP 20, 1484 (1965).

66. M. I. D'yakonov and V. I. Perel', "Coherence Relaxation of Excited Atoms in Collisions," [English translation]: Sov. Phys.-JETP 21, 227 (1965).

67. A. Omont, "Relaxation par Collisions des États Excités d'un Atome," J. de Phys. 26, 26 (1965).

68. A. Messiah, Quantum Mechanics II, John Wiley and Sons, Inc. (1961).

69. M. E. Rose, Elementary Theory of Angular Momentum, John Wiley and Sons, Inc. (1957).

70. M. Rotenberg, R. Bivins, N. Metropolis, and J. K. Wooten, Jr., The 3-j and 6-j Symbols, Technology Press (1959).

71. M. Abramowitz and I. A. Stegun, Eds. Handbook of Mathematical Functions, Nat. Bureau of Standards Applied Math. Series - 55 (1964), pp. 297-304, 325-328.

72. E. U. Condon and G. H. Shortley, The Theory of Atomic Spectra, Cambridge University Press (1967).

73. C. E. Moore, Atomic Energy Levels, N.B.S. Circ. No. 467 (U.S. Government Printing Office, Washington, D.C., 1949), Vol. 1.

74. A. Javan, W. R. Bennett, Jr., and D. R. Herriott, "Population Inversion and Continuous Optical Maser Oscillation in a Gas Discharge Containing a He-Ne Mixture," Phys. Rev. Letters 6, 106 (1961).

75. W. L. Faust and R. A. McFarlane, "Line Strengths for Noble-Gas Maser Transitions," J. Appl. Phys. 35, 2010 (1964).

76. G. Racah, "On a New Type of Vector Coupling in Complex Spectra," Phys. Rev. 61, 537 (L) (1942).

77. D. R. Bates and A. Damgaard, "The Calculation of the Absolute Strengths of Spectral Lines," Phil. Trans., Roy. Soc. of London A242, 101 (1950).

78. P. W. Smith, "Linewidth and Saturation Parameters for the 6328-Å Transition in a He-Ne Laser," J. Appl. Phys. 37, 2089 (1966).

79. W. E. Bell and A. L. Bloom, "Zeeman Effect at 3.39 Microns in a Helium-Neon Laser," Applied Optics 3, 413 (1964).

80. C. B. Moore, "Gas-Laser Frequency Selection by Molecular Absorption," Applied Optics 4, 252 (1965).

81. E. K. Plyler, L. R. Blaine, and M. Nowak, "Reference Wavelengths for Calibrating Prism Spectrometers," J. Res., U.S. Natl. Bur. Std. 58, 195 (1957).

82. H. J. Gerritsen and M. E. Heller, "High-Resolution Tuned-Laser Spectroscope," Appl. Opt. Suppl. 2, 73 (1965).

83. H. Goldring, A. Szöke, E. Zamir, and A. Ben-Reuven, "Pressure Broadening and Shift of 3.39-μ Absorption in Methane Perturbed by Noble Gases," J. Chem. Phys. 49, 4253 (1968).

84. R. L. Barger and J. L. Hall, "Pressure Shift and Broadening of Methane Line at 3.39-μ Studied by Laser-Saturated Molecular Absorption," Phys. Rev. Letters 22, 4 (1969).

85. P. W. Murphy, "Transition Probabilities in the Spectra of NeI, ArI, and KrI," J. Opt. Soc. Am. 58, 1200 (1968).

86. W. R. Bennett, Jr. and P. J. Kindlmann, "Radiation and Collision-Induced Relaxation of Atomic States in the $2p^5 3p$ Configuration of Neon," Phys. Rev. 149, 38 (1966).

87. S. E. Schwarz, "Plasma Diagnosis by Means of Photon-Electron Scattering," Ph.D. dissertation, California Institute of Technology, 1964.